UNIVERITÀ DEGLI STUDI DI PADOVA

FACOLTÀ DI INGEGNERIA

Corso di laurea magistrale in Ingegneria dei Materiali

TESI DI LAUREA

TAILORING THE ARCHITECTURE OF 3D POROUS SCAFFOLDS MADE OF PLLA FOR REGENERATIVE MEDICINE

PROGETTAZIONE DELLA MICROSTRUTTURA DI SCAFFOLD POROSI TRIDIMENSIONALI PER MEDICINA RIGENERATIVA

Relatore
Prof. PAOLO COLOMBO

Correlatore
Prof. ENRICO TRAVERSA

Laureando
FABIO TURELLA

ANNO ACCADEMICO 2010 / 2011

Abstract

Tuning the pore architecture in 3-D polymeric scaffolds for tissue engineering is crucial for providing optimal frameworks for the seeded cells to organize into a functional tissue.

Directional thermally induced phase separation (dTIPS) is a versatile and cost effective self assembly method for fabricating highly porous scaffolds of different materials, having fully tailorable porosity, and strongly anisotropic pore architectures. Consequently, dTIPS scaffolds represent an ideal support for the growth of biological tissues that exhibit gradient morphology, such as bone, tendons, ligaments, nerves, liver, pancreas, and in particular blood vessels. The reconstruction of vascular grafts is in fact a prerequisite when the growth of thick tissues is needed.

In the present work, we investigated the effect of the process parameters, such as cooling temperature (-30°C $\leq T_c \leq$ +5°C), cooling time (2.5 h $\leq t_c \leq$ 32 h), and polymer concentration (1.5 to 6.5 wt%), on the pore microstructure of poly(L-lactic acid) (PLLA) 3-D scaffolds made by dTIPS. The scaffolds exhibited highly ordered dendritic domains, which are expected to act as guiding patterns for blood vessel sprouting. The same showed overall porosities up to 95%, and a degree of interconnectivity over 90%. By controlling the cooling regime, and polymer concentration we were able to tune the pore diameter up to 260 μm, while keeping the peculiar pore hierarchy unaltered. Specifically, pores of few tenths of microns were obtained at the largest t_c, PLLA concentrations, and smallest T_c. On the other side, at the smallest t_c and polymer concentrations, and keeping the system at T_c slightly below the solution freezing point, we managed to push the pore diameter up to 260 μm. Scaffold compression modulus ranged between 1 to 8 MPa, with largest values recorded for samples with the smallest pore diameter, as expected. Finally, scaffolds were seeded with mesenchymal stem cells (MSCs) by means of vacuum-aided

method. The biological validation assessed after 7 days of culture *in vitro* evidenced massive scaffold colonization.

In summary, we showed the possibility to scale up and down the pore architecture in dTIPS scaffold by one order of magnitude, by simple adjustments of the process parameters. This may allow creating a gradient porosity for in-growth of vascular tissue at any length scale (from macro to micro vessels) in one single construct.

Sommario

In ingegneria tissutale, regolare l'architettura dei pori in scaffold tridimensionali polimerici è un fattore cruciale per fornire una struttura ottimale alle cellule seminate in modo tale che queste si organizzino in un tessuto funzionale.
La directional thermally induced phase separation (dTIPS) è un metodo di self assembly versatile ed economico per la fabbricazione di scaffold ad alta porosità a partire da diversi materiali, avente la possibilità di regolare completamente la porosità ed di ottenere strutture porose fortemente anisotropiche.
Di conseguenza, scaffold ottenuti tramite dTIPS rappresentano un supporto ideale per la crescita di tessuti biologici che mostrano morfologia anisotropia, come ossa, tendini, legamenti, nervi, fegato, pancreas ed in particolare vasi sanguigni. La ricostruzione di innesti vascolari è infatti un prerequisito quando l'obiettivo è la crescita di tessuti spessi.
Nel presente lavoro, abbiamo investigato gli effetti delle variabili di processo, come la temperatura di raffreddamento (-30°C ≤ T_c ≤ +5°C), tempo di raffreddamento (2.5 h ≤ t_c ≤ 32 h), e la concentrazione del polimero (da 1.5 a 6.5 wt%), sulla microstruttura dei pori di scaffold tridimesionali in poly(L-lactic acid) (PLLA) ottenuti per dTIPS. Gli scaffold hanno mostrato zone dendritiche ad elevato ordine, alle quali spetta il compito di fungere da struttura guida per i vasi sanguigni in crescita. Gli stessi hanno mostrato porosità totale fino al 95%, ed un grado di interconnessione maggiore del 90%. Controllando il regime di raffreddamento, e la concentrazione del polimero siamo stati in grado di regolare il diametro dei pori fino ad un massimo di 260 μm, mantenendo inalterata la sovrastruttura dei pori. Nello specifico, pori di poche decine di micron sono stati ottenuti con la maggiore t_c, concentrazione di PLLA, e la minor T_c. Dall'altro lato, alla minore t_c e concentrazione di polimero, e mantenendo il sistema alla T_c appena al di sotto della temperatura di congelamento, siamo riusciti a spingere il diametro dei pori fino a 260 μm. Il modulo di compressione degli scaffold è variato

tra gli 1 e 8 MPa, con i valori maggiori registrati, come da previsione, per i campioni con il diametro dei pori minore. Infine, gli scaffold sono stati seminati con cellule staminali mesenchimali (MSCs) tramite il metodo di vacuum-aided. La validazione biologica valutata dopo 7 giorni di cultura *in vitro* ha evidenziato una massiccia colonizzazione dello scaffold.

Riassumendo, abbiamo mostrato la possibilità di aumentare o diminuire la struttura dei pori di un ordine di grandezza in scaffold ottenuti tramite dTIPS, tramite semplici variazioni dei parametri di processo. Questo può permettere la realizzazione di porosità lungo un gradiente per la crescita di tessuto vascolare a qualsiasi scala di grandezza (da vasi micro a macro) in una sola struttura.

Summary of contents

Chapter 1

Introduction

1.1 Regenerative medicine and tissue engineering

Recent advances in the knowledge of molecular and cellular mechanisms of diseases allowed the application of new efficient treatments against organ damage. Nevertheless, none of these treatments demonstrated to be decisive. The finding that a few stem cells are resident within each organ and can be activated when cell death occurs opened unexpected perspectives to highly innovative cell treatments potentially able to induce the reconstruction of the injured areas, rescuing the organ function. First attempts to inject stem cells within damaged organs confirmed only in part experimental data showing that several problems are still open in these so called cellular and molecular therapies. A new exciting and promising field, complementary to these therapeutic strategies, is represented by *tissue engineering*.

Tissue engineering and regenerative medicine are often (and imprecisely) interchanged. They both share some of the knowledge and methods at the base of tissue science, but the second also includes self-healing through endogenous recruitment or exogenous delivery of appropriate cells, bio-molecules, and supporting structures.

Since the term tissue engineering was firstly introduced in the late eighties, enormous progresses have been made, from the better understanding and harnessing of structure-function correlations in living organisms until the commercialization of a first-generation tissue-engineered medical products.

1.2 The tissue engineering approach

Officially coined at a National Science Foundation (NSF) workshop in the fall of 1987, the term tissue engineering (TE), refers to "the application of principles and methods of engineering and life sciences toward fundamental understanding of structure-function relationships in normal and pathological mammalian tissues and the development of biological substitutes to restore, maintain or improve tissue function" [1].

The goal of tissue engineering is to repair or replace damaged organs or tissues by delivering functional cells, supporting scaffolds, growth promoting and signal molecules or their encoding DNA to areas in need.

Tissue engineering has evolved from the use of biomaterials, which may repair or replace diseased or damaged tissue, to the use of controlled three-dimensional constructs, usually denominated *scaffolds*, in which cells can be seeded before implantation. These living tissue structures must tend to be functionally, structurally and mechanically equal to the tissue that must be replaced. The classic tissue engineering strategy is to isolate specific cells through a biopsy from a patient, to grow them on a bi-dimensional (2D) or three-dimensional (3D) bio-mimetic scaffold, under precisely controlled culture conditions, to deliver the construct to the desired site in the patient's body and to direct new tissue formation into the scaffold that can be degraded over time [2]. In order to achieve successful regeneration of damaged organs or tissues based on tissue engineering concepts, several critical elements should be considered, including the biomaterial scaffold that serves as a mechanical and biological support for cell growth and differentiation [2-4].

Strategies of TE can be classified as *in vivo* and *in vitro*. The first approach (also referred to as *in situ* generation), aims to create replacement tissue in the natural milieu. The goal can be accomplished by either cell transplantation [5-7], implantation or catheter-based injection of cell seeded/unseeded scaffold [8-12], or through self-repair and healing promotion by delivery of or active molecules [13,14]. It is feasible and simpler but can be limited by poor control on graft development and outcome.

Among the three pillars (scaffold, cells, bioactive molecules) which sustain tissue engineering, the function of the *scaffold* is crucial. This role is even

fundamental in the *in vitro* approach, where the resolution of problems related to the availability of suitable "biologized" scaffolds is preliminary to any further advance in the reconstruction of functionally efficient strips of tissue destined to be engrafted in damaged organs.

1.3 The Scaffold

As seen, the scaffold plays a key role in the strategies dictated by TE. It is not surprising, at this point, to notice how much attention and expectations are put into scaffold design and characterization, from the choice of the material to the biological testing.

Scaffolds may be composed of polymers, metals, ceramics or composites. Scaffold characteristics include high porosity, large surface area, structural strength, specific two or three-dimensional shape and biodegradability, if needed. Scaffolds can be manufactured in many forms to give the required characteristics for a variety of applications [15]. They can be tubular and flexible for nerves, blood vessels and intestine; stiff and opportunely shaped to match different types of bones and cartilage; jelly, in order to perfectly fit the wound that needs to be healed, and so on.

Regardless its physical characteristics, a supporting scaffold has the main function to physically entrap cells into the specific area to be repaired, direct the spatial orientation of the extra-cellular matrix (ECM) components, sustain and guide the growth of cells, and eventually provide part or all of the signals that are needed for cell proliferation, differentiation and cell-to-cell interaction [2,15]. An ideal device should mimic the extracellular matrix and, when biodegradable, it must be resorbed once the new tissue has formed around it [16].

It must be designed by considering that the composition, structure and, therefore, the mechanical properties of the extracellular matrix can be specific to each organ or tissue [17,18]. In this optics, the adoption of decellularized ECM constructs can, better than any other support, fit this requirements.

In summary, the term scaffold is usually referred to a 3D construct that must fulfill several requirements:

- it must be biocompatible.
- it must be able to bond with the host tissue without leaving any scar or non-

adherent tissue, which means to be a class A bioactive material.

- it should exhibit surface textures able to facilitate such bonds allowing a strong adhesion with cells and eventually the adsorption of biological metabolites.

- its spatial structure (i.e., the scaffold architecture) must act as a template for tissue 3D growing up and it should consist of a thick web of interconnections and present a suitable porosity. Interconnections and porosities diameters ranging from 30 to 80 μm and 50 to 300 μm respectively are sufficient for cells settlement to take place as well as for tissue development and vascularization and for nutrients/drugs delivering [24].

- its rate of degradation (if occurring) should ideally equal that of tissue regeneration. The degradation products should be non-toxic and easily ejectable from the body.

- eventually, the dissolution process should stimulate the biochemical activity of the regenerating tissue in order to promote an efficient cells proliferation and differentiation (bioactivity).

- scaffold mechanical properties should guarantee tissue regeneration even for regions subdued to static or dynamic loads.

- scaffolds processing should allow their fabrication in different shapes in order to fit the damaged regions.

- finally, the materials must possess the requirements imposed by the International Standards Organization (ISO) and from the Food and Drug Administration (FDA).

An impressive number of different scaffolding philosophies for organogenesis have emerged to face the challenge of creating a biologized scaffold, and they can be enclosed in four main categories: (i) *ex-novo* fabrication of 3D bio-mimetic scaffolds, (ii) cell-sheet engineering, (iii) encapsulation devices, (iv) decellularization of pre-existing organic constructs and organ templating.

A brief introduction to these approaches is now presented. The scaffolding methodology adopted in the current work belongs to first, and wider of the mentioned categories, and will be discussed in detail in §1.4.

1.3.1 Cell sheet engineering

Cell-sheet engineering is centered on the use 2D support made of biocompatible thermo-responsive polymers like poly (N-isopropyl acrilamide) (PNIPAM), that can change their physical properties once they are subjected to a temperature change. These materials are biocompatible but non-biodegradable and thus serve as pure support for the constitution of 2D cell sheets. In particular, their temperature-driven water affinity is exploited for culturing and assembling cellular mono-layers to create a thick tissue (cell-sheet® engineering) [18]. This pioneering technology has been systemically applied to several of applications such as cornea [19] in clinical trials and myocardium [20] in preclinical trials. The main advantages of the cell-sheet engineering include the non damaging nature of the cultured cell/tissue harvesting method, the possibility to obtain homogeneous and cell dense tissues, and to perform suture-less implantations. The difficulty to pre-assemby thicker tissues *in vitro* represent the main limitation of this method. Beside the time consumption (each cell layer is about 30 μm thick), cell death was demonstrated to take place in the core layers, due to poor perfusion. [21] On the other side, *in situ* approach would require multiple surery which is unlikely for the recipients.

1.3.2 Cell encapsulation

Encapsulation devices have been experimented for over several decades and principally served as immune-isolating vectors during allogenic or xenogenic cell transplantation [22,23] without the need for immunosuppression and its accompanying effects, or for drug delivery and controlled-release purposes [24]. Encapsulation is a process through which cell or factors are physically entrapped within a semi-permeable membrane or within a homogenous solid mass [22,24,25]. The biomaterials typically used for encapsulation are hydrogels, which are formed by covalent or ionic crosslinking of water-soluble polymers. One important feature of encapsulation is the possibility of scaffold self-assembling from liquid monomers to solid polymer meshwork upon initiation, upon ionic strength, temperature, light, or pH. Provided that the conditions inducing the hydrogel formation or the polymerization are compatible with living cells, encapsulation allows to perform

scaffold fabrication and cell seeding at once, since cells and liquid biomaterials can be mixed before initiation of polymerization. Other relevant advances are the homogeneity of cell distribution in the hydrogel and excellent cell viability. Moreover, this self-assembled approach enables injectable application where the polymerization can be initiated after injection, thus allowing scaffold shaping to fit the wound. However, a great limit of this technique is related to the lack of adequate mechanical properties which prevent this scaffolds from being used in load bearing tissue repair/reconstruction.

1.3.3 Organ templating

A cellular extra-cellular matrices (ECMs) can be collected from allogenic or xenogenic tissues to act as template for addressing cell growth and differentiation. This approach has recently emerged as revolutionary and powerful and tool for TE. It has been used for the reconstruction of many tissues, such as heart valves [26], vessels [27], nerves [28], tendon and ligament [29]. This scaffolding method consists in removing the allogenic or xenogenic cellular antigens from the tissues which may provoke immunogenicity upon implantation, while preserving the ECM components, which are common among species and therefore immunologically tolerated. The major advantage of this scaffolding approach is surely resides in the excellent mimetic mechanical and biological properties of the decellularized ECM.

Moreover, the presence of residual growth factors in the decellularized matrix may further facilitate cell growth and remodeling [30]. Concerns about this method include *in primis*, the risk of immunogenic reaction and rejection of the implant, due to incomplete removal of cellular components [31]. In addition, many of the issues related to synthesized porous scaffold continue to persist for this approach. Cell non-uniform distribution within the decellularized ECM, and in some cases, the need of vascular networks, may lead to the constitution of inhomogeneous tissues.

1.4 Fabricating novel 3D bio-mimetic porous scaffolds

1.4.1 Introduction

Ex-novo fabrication of 3D scaffolds is probably the more challenging but extensively investigated area of TE.

The principal advantage of this approach relies in the possibility to fully design the supporting device, thus conferring to the scaffold predictable shapes, mechanical properties, compartmentalization, surface topologies and functionalities for any given application.

If, on one side, the all-around tailoring ability makes this approach potentially suitable for reconstructing every type of tissue, it also undiscloses thousands of new question about which the correct paradigm should be.

Another issue is related to the integration of the engineered scaffolds with the cellular systems. The *in vitro* scaffold passive culturing is generally a time-consuming and poorly efficient practice, and tends to produce inhomogeneous cell engraftments and tissues.

The adoption of dynamic bioreactors and perfusion chambers (§1.6) can only partially meet the need of higher cell seeding efficiency, while introducing new problems related to the cost of the apparatuses, as well as the low cell viability. Furthermore, cell death can occur in the core region of the synthesized tissue, due to the lack of a vascular net and poor perfusion. This hurdle, which also afflicts the other scaffolding approaches, is what mostly prevents 3D scaffolds to be systematical used in organ repair.

1.4.2 Scaffold fabrication methods

The scaffold suitability for a given clinical application is not only determined by the choice of the material with the proper physico-chemical and mechanical properties, but also strongly depends on the processing routes applied to the chosen materials [2, 32-35]

Materials processing can be performed by a multitude of techniques. The extent to which new materials can be created, engineered and shaped is only limited

by imagination.

Some of the most currently in vogue routes for scaffold manufacturing, which can be easily found in literature, are: *foaming* techniques (solvent casting and particulate leaching [36], phase separation [37], gas foaming [38], etc.); *bottom-up* strategies like *rapid prototyping* (3D printing [39], pressure assisted micro-syringe [40], etc.), *soft-lithography* (micro-molding [41], micro-fabrication [42], spin casting and membrane lamination [41,43], etc.), and *self-assembly* (pneumatic [44] and electrical fiber spinning [45], emulsification/freeze-drying processes [46], fiber bonding [47], etc.); *top-down* approaches (selective laser sintering [48], etc.), and so on. Some of the mentioned techniques represent the core subject of this work, and will be later and more in depth discussed.

1.4.3 Degradation

Once implanted, the biodegradable material-based device should maintain its mechanical properties until it is no longer needed and then be absorbed and excreted by the body [49]. Controllable degradation of substrate scaffold is important to the ultimate clearance of the synthetic implant materials within an engineered tissue [50,51]. Simple chemical hydrolysis of the hydrolytically unstable backbone is the prevailing mechanism for the polymer's degradation. This occurs in two phases. In the first phase, water penetrates the bulk of the device, preferentially attacking the chemical bonds in the amorphous phase and converting long polymer chains into shorter water-soluble fragments. Since this takes place in the amorphous phase initially, there is a reduction in molecular weight without a loss in physical properties, being the device matrix is still held together by the crystalline regions. The degradation of the physical properties occurs as water begins to fragment the device.

In the second phase, enzymatic attack and metabolization of the fragments occurs, resulting in a rapid loss of polymer mass. This type of degradation, i.e., when the rate at which water penetrates the device exceeds that at which the polymer is converted into water-soluble materials, resulting in erosion throughout the device, is called *bulk erosion*. All of the commercially available synthetic devices and sutures degrade by bulk erosion.

A second type of biodegradation, known as *surface erosion*, occurs when the rate at which the water penetrates the device is slower than the rate of conversion of the polymer into water-soluble materials. Surface erosion results in the device thinning over time while maintaining its bulk integrity. Polyanhydrides and polyorthoesters are examples of materials that undergo this type of erosion, i.e., when the polymer is hydrophobic, but the chemical bonds are highly susceptible to hydrolysis. In general, this process is referred to in the literature as bio-erosion rather than biodegradation [52].

Generally, the degradation-absorption mechanism is the result of many correlated factors, including:

- the chemical stability of the polymer backbone.
- the presence of catalysts, additives, impurities, or plasticizers.
- the geometry of the device.

Balancing these factors by tailoring an implant to slowly degrade and transfer stress at the appropriate rate to surrounding tissues as they heal is one of the major challenges facing researchers today.

1.5 Cell sources for tissue engineering

1.5.1 Introduction

The reconstruction of a given tissue type needs several aspects to be considered, including, the function of the tissue, the mechanical requirements, such as load and flexibility, the specific environment in which the tissue is located, etc. Among them, the identification of a suitable cell source for obtaining the specialized cell types within the tissue, is priority.

The ideal cell required for tissue engineering must show good self-regenerative potential, the ability to functionally replace the damaged tissue and must be readily available in desired quantity.

The versatility of TE provides for addition of cells sourced from the same recipient (*autologous* cells), from a genetically non-identical individual of the same species, (*allogeneic* cells), and from an individual belonging to another specie (*xenogeneic* cells, e.g., from pigs to human [53]), to the produced devices.

Safety issues to recipients of autologous cells implants (*autografts*) are generally limited to acquisition of adventitious agents (microbial, viral, etc.). On the other hand, the possibility of allogeneic or xenogeneic cells implants (*allografts* and *xenografts*, respectively) opens to the risk of transmission of pathogens from nonautologous donors (§1.7).

Among others, the use of stem cells (§1.5.2) has catalyzed enormous attention in TE, due to the unique properties which characterize these cells respect to differentiated cell models. In particular, the possibility to derive different tissue types from one single stem type, offers unprecedented possibilities in the optics of organ reconstruction. Stem cells for TE include adult stem cells, such as bone marrow stromal (mesenchymal) stem cells, embryonic stem (ES) cells or germ (EG) [54]. However, the most appropriate mixture of growth factors and physical stimuli to be combined to lead undifferentiated cells to a specific phenotype is still under debate.

1.5.2 Stem cells: definition and classification

Stem cells are a population of immature tissue precursor cells which are capable of self-renewal or proliferation as well as of differentiation into a spectrum of different cell types, under specific conditions [55]. In general, they possess the following characteristics: i) high capacity for self-regeneration, and ii) the highest potential for differentiation, iii) the ability to be cultured *ex vivo* and used for tissue engineering, and iv) plasticity (the ability to trans-differentiate [56].

On the basis of their potential towards differentiation , stem cells may be classified into four categories: 1) *totipotent*, 2) *pluripotent*, 3) *multipotent* and 4) *monopotent* or *oligopotent*.

Totipotent stem cells have the potential to differentiate into cells of all three embryonic layers: endoderm (interior stomach lining, gastrointestinal tract, the lungs), mesoderm (muscle, bone, blood, urogenital), or ectoderm (epidermal tissues and nervous system). If implanted in a functional uterus, a totipotent cell can generate an entire body, provided with a central and peripheral nervous system. In mammals, the only totipotent stem are zygotes at an early stage of cell division (blastomeres). With the progression of differentiation, zygotes tend to form cell layers inside and outside of the embryo.

The cells belonging to the inner layers are called *pluripotent* Pluripotent stem cells can give rise to any fetal or adult cell type. However, alone they cannot develop into a fetal or adult animal because they lack the potential to contribute to extra-embryonic tissue, such as the placenta [57]. As they continue to divide and to further specialize, they become the specific-tissue progenitors. At this stage, they are *multipotent* cells, since they can differentiate into different cell types within a given organ. For example, blood stem cells or multipotent hematopoietic stem cells can differentiate into red cells, white cells or platelets.

Finally, *monopotent* or *oligopotent* stem cells, can only lead to one or a few types of specialized cells. However, they have the property of self-renewal which distinguishes them from non-stem cells (e.g. muscle stem cells).

1.5.3 Stem cell sources: embryonic and adult stem cells

On the basis of their origin and biological properties, stem cells can be also classified into *embryonic* stem cells and *adult* stem cells

Embryonic stem cells derive from the internal layer of the blastocyst (a post-zygotic early embryonic stage) [58]. These cells possess the ability to proliferate in an undifferentiated state for long culturing periods. Moreover, a single ESC can develop in more than 200 cell types and, therefore, in different tissues or organs, under favorable conditions, due to their powerful differentiation capacity [59]. ESCs can be harvested from three sources: aborted fetuses, embryos discarded after in vitro fertilization and embryos specifically created in laboratory for stem cells production. In vitro differentiation of human embryonic stem cells in cardiomyocites was demonstrated by Kehat et al [60].

Adult stem cells are undifferentiated cells that reside in a specialized tissue or a developed body and are able to specialize into any of the cells of the tissue or body from which they originate. Due to their ability to self-regenerate, these cells constitute a repair system which allows tissues to maintain their stability and function, by replenishing specialized cells, but also maintaining the normal turnover of regenerative organs (such as blood, skin or intestinal tissues, etc.). Sources of adult stem cells include self-regenerating tissues such as bone marrow, blood, epidermis, but even tissues such as brain or liver.

1.5.4 Humans stem cells: ethical and clinical issues

There exist several ethical problems associated with the collection of human embryonic stem cells (hESCs), mainly related to the inevitable destruction of the originary source (i.e., the embryo) [54]. The *tout court* equalization of the human *embryo* state to the *adult* state, has raised a controversial dispute within the scientific (and not) community, leaving unresolved fundamental moral and legal issues related to the usage of hESCs, beside affecting either the liberty of research and religious beliefs of the individual researcher. The decision to carry out experimentation on hESCs is delegated to the single countries. It's worthy to mention US recent change of policy, with the settlement of the new democratic government. The US adoption of a regulated liberalization in the use hESC could serve as a guide model and hopefully have resonance in other countries, including Italy. Other potential barriers to the use of these cells relate to the need for the receivers to undergo immunosuppressive therapies, due to embryonic stem cells to be potentially allogeneic. The uncontrolled differentiation of these cells may also represent a hurdle to their extensive use [61].

Adult stem cells do not involve the previously mentioned ethical or immunological concerns, as, in this case, donor and recipient coincide and none of them has to (or at least shouldn't) be sacrificed. However, respect to their embryonic counterpart, the capacity for proliferation and differentiation is lower. Furthermore, they are often difficult to identify, isolate and purify and are often not sufficiently numerous for clinical transplantation without *in vitro* expansion. This also may represents a problem since adult stem cells do not replicate indefinitely in culture [62].

1.6 Bioreactors

A widely supported finding is that the three-dimensional architecture of a tissue is not only determined by the scaffold structural and chemical stimuli, but also depends on subjecting the cells to physiological stress during cultivation. Growing blood vessels, for example, must be exposed to compression, shear stresses and a pulsated flow of the culture medium to acquire their mechanical properties [16,63].

In order to match most of these requirements, cell seeded scaffolds are often treated in bioreactors until the tissue or organ is fully developed. To improve the results of the *in vitro* approach and manage to grow three-dimensional living constructs that contain more than a few layers of cells, researchers have implemented various types of bioreactors, each one simulating a different fluido-dynamical state and thus characterized by a different geometry of the container. A typical and largely diffused container for dynamic culturing is the *spinner flask*, which is nothing but a shaken flask (usually at 50 rpm). In such containers, the cell constructs are subjected to turbulent mixing in presence of proper fluids that provide a well-homogenized environment around the cells, thus minimizing the settling of stagnant layer nearby

Fig. 1.6.1: A diffused design of dynamic bioreactor: Spinner flask

the surface. It been shown that the cultivation of cardiac cell constructs in spinner flask produces engineered tissues that are superior in almost every aspect (aerobic metabolism of cells, DNA content, metabolic activity and morphological appearance) compared to tissues grown in static conditions [64]. The spinner flask, however, may not be the best device for the cultivation cells. The turbulent flow of fluid to the surface of the cell constructs is usually characterized by local vortexes
that can destroy the implanted cells.

More complex bioreactors combined with mechanical signals such as stretching or compression, have proven to their effectiveness in enhancing the proliferation and distribution of seeded human cardiac cells through the entire volume of the scaffold, by further stimulating the formation and organization of ECM graft [65,66]. These encouraging achievements, however, must face some difficulty. Many bioreactors are unable to provide sufficient oxygen and nutrients to tissue growth. The growth in a bioreactor typically stops once the tissue has reached a thickness of 100μm,

corresponding to about 6-10 layers cellular [21,67]. Beyond this thickness, the cells of the central layers are too far away because the addition of fresh medium can take hold there. Therefore future bioreactors for tissue engineering should combine perfusion and mechanical stimulation, for example allowing adjustable movement pulsatile and variable levels of pressure.

1.7 Safety concerns and regulatory issues: the role of FDA

Multidisciplinary character of TE raised intrinsic concerns about validity and safety of TE therapies. In fact, although acellular biomaterials or drugs have many predicates, virtually all TE therapies have no predicates. Consequently, no standards exist by which these strategies may be assessed for safety and effectiveness prior to their application.

Despite the lack of standards for assessment, the responsibility of U.S. Food and Drug Administration (FDA) to protect the public from health risks associated with investigational therapies remains unchanged.

FDA's responsibility requires that new therapies approved for use in the United States be *safe* and *effective*.

Safety criteria for medical devices require that probable benefits to health outweigh probable risks of the therapy itself, or the untreated diseases. For example, many systems for cell culture contain animal-derived components, and other biological or chemical contaminants may derive from the scaffold material or result from the combined cell-scaffold action upon interaction. In addition, if allogenic or xenogenic cells are included, transmission of adventitious agents may occur. Both the patient and the working staff must be protected from possible pathogens.

In the effort to guarantee as much as possible the safety of TE therapies, FDA has applied several standards, principally from the Center of Biological Evaluation and Research (CBER) [68], which establish precise regulatory respect to media components, tissue acquisition, implant handling and storage, and safety validation of the final products.

For non-autologous therapies, safety standards have been established for conventional banking of human and non-human tissues or tissue extracts. For allogeneic tissues, these standards are similar to blood banking, and require the screening of donors for multiple pathogens like HIV, and hepatitis type B and C [68-70].

In addition to safety issues regarding pathogen transmission, in the case of xenogeneic tissues, immunogenicity and stability of transgenic vectors must be assessed [71]. This subject deserves great attention, since the use of xenogeneic tissues holds potentials of enormous supply of tissues from many different species or transgenic animals.

Effectiveness criteria for devices should demonstrate that use of the device for its meant uses, and conditions for use, restore as much as possible of the physiological deficiency caused by the disease in a significant portion of the target population [72]. Tissue-engineered devices may require assessments different from those for nonliving, non-resorbable implants (ceramic or metallic hip and knee joints, polymeric vascular grafts, etc.) These kind of prosthetic devices are meant to remain and interface indefinitely with the host tissue and their efficacy is typically stable, and durable. On the other hand, most tissue-engineered implants are constituted by a resorbable and a cellular component. Although well-characterized standards exist for the breakdown of acellular biodegradable polymers (e.g., poly(L-lactic acid) [73], addition of cells to either FDA approved or non approved polymers may require both preclinical and clinical assessments.

These regulatory standards apply to tissue-engineered therapies just as for conventional medical devices, drugs, or biologics. However, the composite nature of most TE therapies complicates FDA's evaluation of their safety and effectiveness. For this reason, FDA will be asked to provide new approaches for establishing standards and regulatory protocols for TE.

1.8 Aim of the present work

Background

The emergence of TE as an academic discipline and global industry, has opened unprecedented possibilities for the development of advanced therapies in the

treatment of congenital and acquired diseases [1,2,3,4,74]. Up to date, encouraging results have been obtained in fully reconstructing hard tissues, such as bone [75] and cartilage [76], and flat soft tissues, such as cornea [77] and skin [78], while more complicated soft tissues (heart, as an example) are far more challenging to be replicated *in vitro*. Several TE strategies have been successfully proposed for tissue reconstruction (§1.3), such as the overlaying of several bi-dimensional sheets of differentiated cells, cell entrapment in self-assembling hydrogels, and cell engraftment on pre-constituted decellularized templates. The other approach, as said, relies in the use of biodegradable bio-mimetic 3D scaffolds, and constitutes the subject of this work.

Set in this scenery, my research proposed to tailor and to test biocompatible polymer based constructs, destined to host, address and sustain the proliferation of human cellular colonies *in vitro*.

Description of the work

The work has been done at National Institute for Material Science (NIMS) in Tsukuba City, Japan.

Preliminary experiments aimed at reproducing and mastering the scaffold fabrication techniques: *thermally induced phase separation*.

The work carried out after this initial period was focused on the further development and optimization of the fabrication technique as well as to the overcoming of the several problems related to the fabrication routes. These scaffolds were subjected to deeper characterizations (mechanical and biological viability) while ameliorations were brought to the synthesis protocols.

Scaffolds by thermally induced phase separation (TIPS)

One of the main unresolved problems of TE is the difficulty in reconstructing healthy thick tissues. Usually, if constructs do not allow oxygen perfusion, no more than three cell layer can grow *in vitro* without occurring of necrosis in the core layers [21]. As a result, while a number of bio-supports processed by many different techniques have been successful in hosting a multitude of cell systems, while only few of them have proven their potential capability in maintaining cell cultures over time [79,80].

No flourishing civilization could exist far from a river. For these same reasons,

beside the capability of supporting cell growth, expansion, and differentiation, the scaffold should primarily guarantee perfusion, vascularization, growth factor delivery, and all those processes responsible for cellular long term retention [81,82].

This convictions animated my research on 3D scaffolds for TE, in the effort to incorporate in a single construct the information able to trigger the specific tissue reproduction. Such a scaffold should be able to exhibit hierarchical porosities, at the millimetre scale to help nutrition and vascularization, at the micrometer scale to accommodate cells, and at the nanometre scale to favour the expression of extra-cellular matrix components, with the desired chemical and mechanical functions [83]. Most of these requirements were matched with the adoption of directional Thermally Induced Phase Separation as synthesis method.

Chapter 2

Materials and methods

2.1 TIPS

The main limiting factor of 3D scaffolds for growing *in vivo* healthy thick tissues is represented by the lack of perfusion into the core regions of the construct, resulting in poor colonization and cells confinement on the cortical layers of the scaffold. The lack of a suitable pore arrangement able to facilitate capillary diffusion of growth factors and nutrients, is among the principal causes, together with the scaffold inability to host more organized structures like blood vessels [15,81].

In this research, a multitude of attempts were done, all aimed at the implementation of original solutions to the optimal architecture dilemma [83]. With respect to poly(lactic acid) (PLLA) a large number of processing techniques have been reported, including gas foaming [84], solvent casting and particulate leaching [85], fiber bonding [47], electrospinning [86,87], soft-lithography [41], and phase separation [88]. In particular, lactide-based scaffolds made by thermally induced phase separation (TIPS) have demonstrated their suitability to host cell systems. Their multi-scale porosity is potentially capable of supporting cell-matrix interaction at any biological level (Fig. 2.1.1) [83,89].

As schematically shown in Fig. 2.1.2, TIPS is basically a three step process in which a homogeneous polymer-solvent solution is brought to phase separate upon the application of a thermal gradient into a polymer-rich phase and a solvent-rich phase. Porosity is obtained by leaching out the solvent phase by exposing to a second specific solvent that acts as a non-solvent for the polymer. The driving force of the process relies in the alteration of the thermodynamic equilibrium imposed by the under cooling that causes polymer solubility to decrease within the solvent phase undergoing solidification.

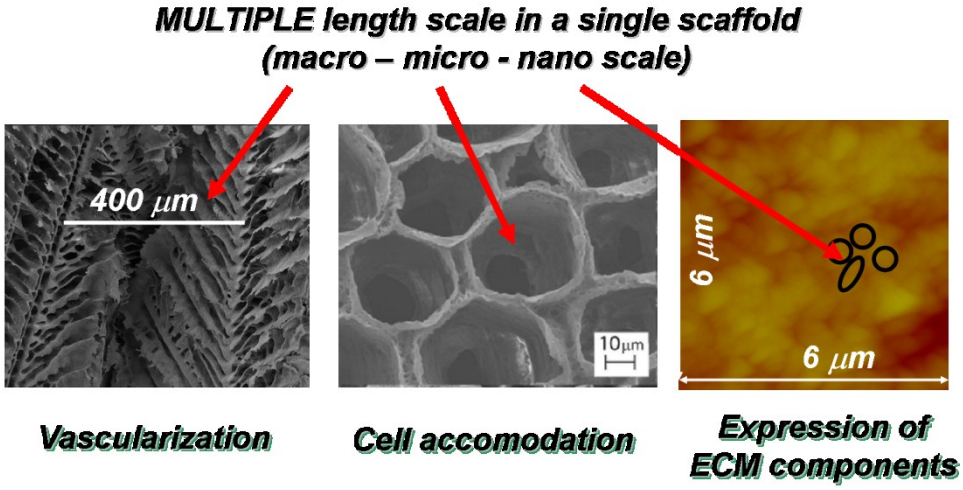

Fig. 2.1.1: Scaffolds made by thermally induced phase separation provide for a multi-scale porosity in a single construct, which make them suitable for supporting a variety of biological functionalities

A number of ternary systems have been investigated for producing polymeric structures by TIPS [90,91]. In particular, for PLA-based systems, the use of dioxane as the polymer solvent turned out to be the election choice, due to its relatively high melting temperature (T = 11.8°C) and ease of removal. Moreover, it has been demonstrated that dioxane can crystallize into different geometries depending on its concentration within the polymer solution and quenching conditions [89]. The ability to control solvent shaping under solidification is crucial because crystallite geometry and order act as template for porosity. It has been observed that the imposition of an anisotropic thermal gradient to the polymeric solution can force dioxane crystallization along specific directions, thus conferring a higher degree of order to the whole system at a macroscopic level [92]. Several research groups managed to obtain densely packed arrays of parallel micro channels by applying uni-directional TIPS to mixed PLA and PLGA solutions in dioxane [93-95].

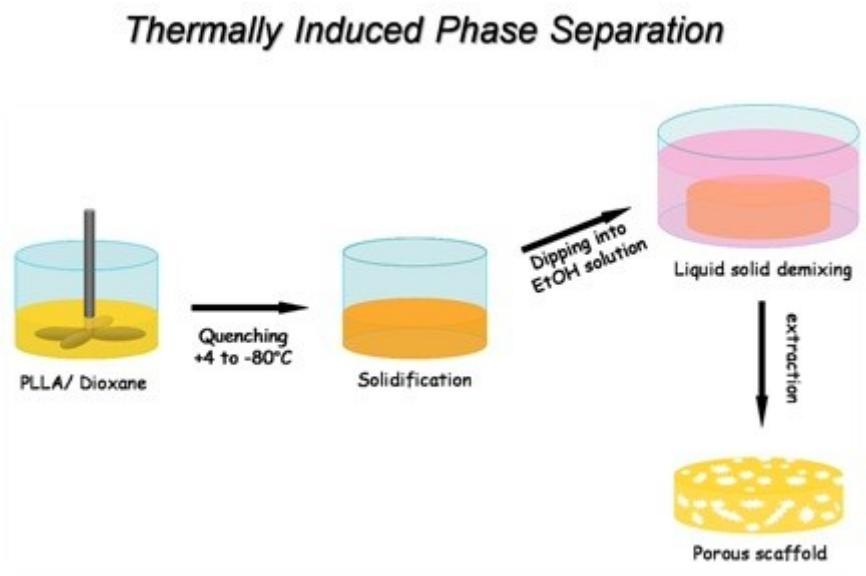

Fig 2.1.2: Step-preparation of PLLA porous scaffold by thermally induced phase separation.

However, this configuration may represent an obstacle for intense cell-to-cell signalling between adjacent channels, or even result in short-term cells viability in the case of inadequate nutrient supply/diffusion through the micro-cavities of the inner walls. In addition, cells constriction to a mono-dimensionally ordered displacement may impede cells arrangement into more complex structures or prevent vessels capillary sprouting.

In this optics, the set of TIPS conditions identified and adopted in the present work, corresponds to a porosity arrangement that more than others would better support diffusive phenomena as well as suit blood vessels accommodation, thus easing angiogenesis promotion.

2.2 *Scanning Electron Microscopy* (S.E.M.)

Essential components of all SEMs include the following:

- Electron Source ("Gun")
- Electron Lenses
- Sample Stage
- Detectors for all signals of interest
- Display / Data output devices
- Infrastructure Requirements:

- Power Supply
- Vacuum System
- Cooling system
- Vibration-free floor
- Room free of ambient magnetic and electric fields

SEMs always have at least one detector (usually a secondary electron detector)

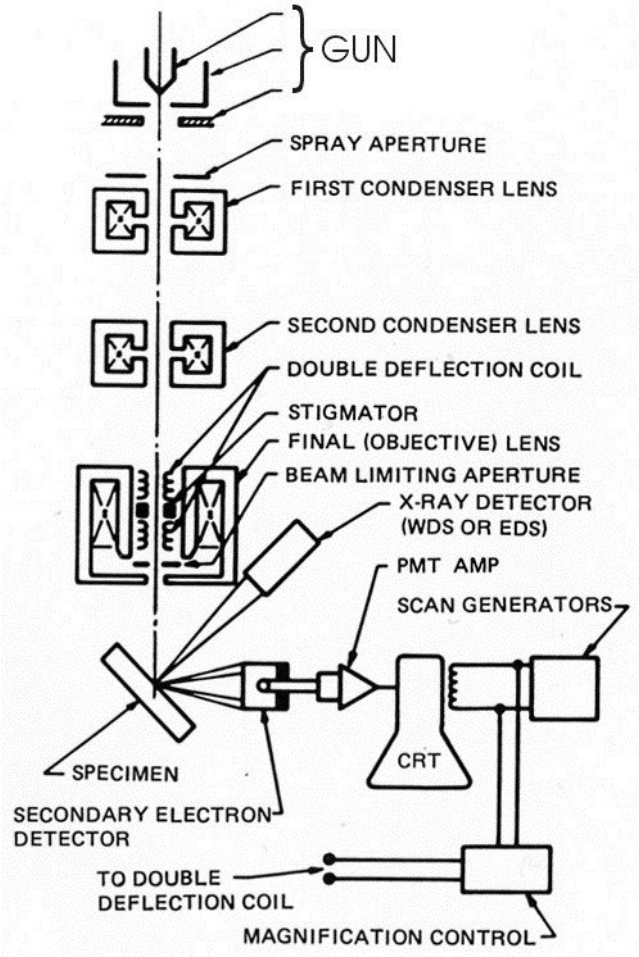

Fig 2.2.1: Schematic drawing of the electron and x-ray optics of a combined SEM-EMPA

In a typical SEM, an electron beam is thermionically emitted from an electron gun fitted with a tungsten filament cathode. Tungsten is normally used in thermionic electron guns because it has the highest melting point and lowest vapour pressure of all metals, thereby allowing it to be heated for electron emission, and because of its low cost. Other types of electron emitters include lanthanum hexaboride (LaB6) cathodes, which can be used in a standard tungsten filament SEM if the vacuum

system is upgraded and field emission guns (FEG), which may be of the cold-cathode type using tungsten single crystal emitters or the thermally-assisted Schottky type, using emitters of zirconium oxide.

The electron beam, which typically has an energy ranging from 0.5 keV to 40 keV, is focused by one or two condenser lenses to a spot about 0.4 nm to 5 nm in diameter. The beam passes through pairs of scanning coils or pairs of deflector plates in the electron column, typically in the final lens, which deflect the beam in the x and y axes so that it scans in a raster fashion over a rectangular area of the sample surface.

When the primary electron beam interacts with the sample, the electrons lose energy by repeated random scattering and absorption within a teardrop-shaped volume of the specimen known as the interaction volume, which extends from less than 100 nm to around 5 μm into the surface. The size of the interaction volume depends on the electron's landing energy, the atomic number of the specimen and the specimen's density. The energy exchange between the electron beam and the sample results in the reflection of high-energy electrons by elastic scattering, emission of secondary electrons by inelastic scattering and the emission of electromagnetic radiation, each of which can be detected by specialized detectors. The beam current absorbed by the specimen can also be detected and used to create images of the distribution of specimen current.

These signals include secondary electrons (that produce SEM images), backscattered electrons (BSE), diffracted backscattered electrons (EBSD that are used to determine crystal structures and orientations of minerals), photons (characteristic X-rays that are used for elemental analysis and continuum X-rays), visible light (cathodoluminescence--CL), and heat. Secondary electrons and backscattered electrons are commonly used for imaging samples: secondary electrons are most valuable for showing morphology and topography on samples and backscattered electrons are most valuable for illustrating contrasts in composition in multiphase samples (i.e. for rapid phase discrimination). X-ray generation is produced by inelastic collisions of the incident electrons with electrons in discrete ortitals (shells) of atoms in the sample. As the excited electrons return to lower energy states, they yield X-rays that are of a fixed wavelength (that is related to the difference in energy levels of electrons in different shells for a given element). Thus, characteristic X-rays are produced for each element in a mineral that is "excited" by the electron beam.

Electronic amplifiers of various types are used to amplify the signals which are displayed as variations in brightness on a cathode ray tube. The raster scanning of the CRT display is synchronized with that of the beam on the specimen in the microscope, and the resulting image is therefore a distribution map of the intensity of the signal being emitted from the scanned area of the specimen. The image may be captured by photography from a high resolution cathode ray tube, but in modern machines is digitally captured and displayed on a computer monitor and saved to a computer's hard disk.

The SEM is also capable of performing analyses of selected point locations on the sample; this approach is especially useful in qualitatively or semi-quantitatively determining chemical compositions (using EDS), crystalline structure, and crystal orientations (using EBSD). The design and function of the SEM is very similar to the EPMA and considerable overlap in capabilities exists between the two instruments.

SEM analysis is considered to be "non-destructive"; that is, x-rays generated by electron interactions do not lead to volume loss of the sample, so it is possible to analyze the same materials repeatedly.

The SEM is routinely used to generate high-resolution images of shapes of objects (SEI) and to show spatial variations in chemical compositions: 1) acquiring elemental maps or spot chemical analyses using EDS, 2)discrimination of phases based on mean atomic number (commonly related to relative density) using BSE, and 3) compositional maps based on differences in trace element "activitors" (typically transition metal and Rare Earth elements) using CL. The SEM is also widely used to identify phases based on qualitative chemical analysis and/or crystalline structure. Precise measurement of very small features and objects down to 50 nm in size is also accomplished using the SEM. Backescattered electron images (BSE) can be used for rapid discrimination of phases in multiphase samples. SEMs equipped with diffracted backscattered electron detectors (EBSD) can be used to examine microfabric and crystallographic orientation in many materials. [96-99]

2.3 Materials for scaffold synthesis

The choice of the material destined to 3D scaffold *ex-novo* fabrication for TE is a crucial issue and mainly depends on the kind of application required, i.e. the type of tissue to mimic. The past several years have witnessed the explosion of the

material science applied to tissue engineering [96]. Many natural substances are proving valuable, while the world of synthetic materials, mostly polymeric, has completely opened up.

In comparison to attachment of adherent cells to a rigid and smooth surface, greater extent of attachment, survival, and function can be achieved by cell adhesion on and porous (either soft or stiff) and roughness-controlled substrates, that resemble the macro-molecular structure of extra-cellular matrix [97-99]. Base materials used as substrates in TE may be divided into *natural* (collagen, albumin, hyaluronic acid, fibrin, chitosan, silk, alginate, ecc.), *synthetic* (poly-lactide acid, poly-glycolide, poly- caprolactone, poly-N-isopropyl acrilamide, hydroxyapathite, ceramic glasses, ecc.), and *semi-synthetic* or *hybrid materials*.

Each material is accompanied by a series of pros and cons which determine its usage or not for a specific application. The advantage of naturally derived polymers resides in their close compatibility with ECM environments, thus providing better supports for *ex-vivo* cultures of cells. However, they typically lack the necessary mechanical integrity for fabrication into scaffolds or other differently shaped polymer structures. They also suffer from the limitation of sufficient supply and source variation, which limits their use for TE. Some naturally derived polymers might also be immunogenic. Synthetic biocompatible and/or biodegradable polymers are widely used in surgical sutures and constructs for *ex-vivo* cell culturing, expansion and transplantation [100-102]. The most widely used synthetic bio-polymers belong to the poly (α-hydroxy acid) family of polymers, including poly(lactic acid) (PLA), poly(glycolic acid) (PGA), poly(D,L-lactide-*co*-glycolide) (PLGA), and their modified derivatives. Because of the wide range of the desirable physical properties, synthetic polymers can be precisely constructed in various formats of defined shape, morphology, and composition [103,104]. Their bio-degradation can be controlled by their design and fabrication [105]. However, initial interaction between degradable scaffolds and seeded cells, as well as initial host response to tissue engineering devices, presents a critical challenge in the design of the synthetic polymers [99,106-108]. Finally, hybrid polymers are generally designed to achieve the desirable physical properties of synthetic polymers and the biocompatibility of natural bio-polymers. This may be achieved by chemically coupling bio-active components of natural substrates with synthetic polymers or chemically modifying bio-polymers to introduce desired physical properties

[99,109,110].

As for the present work, it was almost entirely based on the use and engineering of lactide derived biodegradable polymers as base materials.

The reasons underlying this choice are not to be enclosed in a simple imitative model related to the widespread usage of these materials, at least not directly. Inevitably, the adoption of a "trendy" technological standard allows, more than others, to have at one's disposal a vast and readily available source of knowledge and tools that only experience could provide otherwise. In this optics, the access to a consolidated technological apparatus, like that of lactide-based polymers industry, is a necessary prerequisite for granting a solid starting base for any further advancement and contribution to the existing knowhow.

Poly(lactic acid) (PLA)

Poly(lactic acid), or polylactide, is a biodegradable, thermoplastic, aliphatic polyester. It is obtained by the ring-opening polymerization of lactide, the dimer of lactic acid (Fig. 2.3.1), which is produced from the bacterial fermentation of agricultural products and by-products.

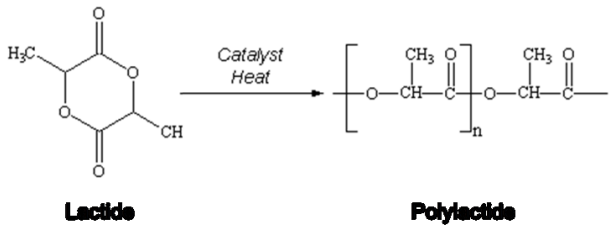

Fig 2.3.1: Synthesis of poly(lactic acid) (PLA) [111].

Lactide exists as two optical isomers, D and L. L-lactide is the naturally occurring isomer, and DL-lactide is the synthetic blend of D-lactide and L-lactide. The homo-polymer of L-lactide (PLLA) is a semi-crystalline polymer. These types of materials exhibit high tensile strenght and low elongation, and consequently have a high modulus that makes them more suitable for load bearing applications, such as in orthopedic fixation and sutures [102]. Poly(D,L-lactide) (PDLA) is an amorphous polymer exhibiting a random distribution of both isomeric forms of lactic acid, and accordingly is unable to arrange into an organized crystalline structure. This material has lower tensile strength, higher elongation, and a much more rapid degradation

time, making it more attractive as a drug delivery system[112-114].

PLA is about 37% crystalline, with a melting point of 175-178°C and a glass transition temperature of 60-65°C [49,115]. The degradation time of PLLA is much slower than that of PDLA, requiring more than a years to be completely adsorbed [116]. Co-polimers of L-lactide and DL-lactide have been prepared to disrupt the crystallinity of L-lactide and accelerate the degradation process [117,50].

With respect to soft and hard tissue repair, PLA has always been one of the most diffused biomaterials [118-121]. Until the late 1980s, application of PLA was limited to medical uses due to its high price. However, decreases in the production cost of lactic acid together with the improvements in the polymerization process, have led its commercial-scale production. Due to its chemical and mechanical stability, PLA is currently used in several biomedical and foodservice applications, while its "green" nature makes it a promising replacement for plastics like polyethylene terephthalate (PET) and polyvinyl chloride (PVC) for the sustainable packaging market [120]. Unlike most commercial polymers, the cost of PLA is not dependent on the production and price of oil, and is only determined by that of agricultural products like corn, tapioca, sugar cane and sugar beet. PLA is biodegradable in vivo, in the environment and in compost. Finally, high molecular weight PLA is rarely effected by fungi, mold, or other microbes at ordinary temperatures.

Poly (lactic-co-glycolic acid) (PLGA)

Poly(lactic-*co*-glycolic acid) is obtained by the co-polymerization of the PLA and PGA monomers (see Fig. 2.3.2), through which it is possible to extend the range of homo-polymer properties of the starting materials [121].

Copolymers of glycolide with both L-lactide and DL-lactide have been developed for both device and drug delivery applications [102,113]. It is important to note that there is not a linear relationship between copolymer composition and the mechanical and degradation properties of the materials. As an example, a 50:50 lactide-co-glycolide copolimer degrades faster than the base homopolymers [122].

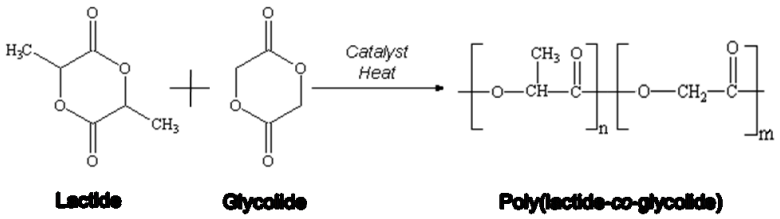

Fig 2.3.2: Synthesis of poly(lactic-co-glycolic acid) (PLGA) [111].

This phenomenon is due to the disruptive activity exerted by the glycolic monomer which alters the regularity of the PLA polymer chain [117], resulting in a globally amorphous copolymer, i.e. PLGA.

PLGA shows important advantages and drawback respect to PLLA. It's much softer, easier to be degraded and re-adsorbed by cells, with a much lower inflammatory response. Unfortunately, as the scaffold is required to be mechanically self-sustainable, even in the biological environments, in this work PLLA was generally preferred respect to pure PLGA for scaffold fabrication.

In this work, the use of PLGA was limited to smooth film production or as base material for producing composite scaffolds, due to the possibility to enhance its weaker mechanical properties *in vitro* by nano-ceramics addition, while still preserving its higher suitability towards cellular systems.

2.4 Porosity measurements

Porosity measurements were performed onto round samples obtained from collected scaffold. Samples average thickness was measured by means of a dial micrometer (Rambold, Germany). The weight of each sample W_s was first measured using an analytical balance in order to get polymer's effective volume V_o :

$$V_0 = \frac{W_s}{\rho_0} \qquad (1)$$

being ρ_0 the measured density of the purchased polymer, equal to 1.27 g*cm^{-3}.

Scaffold open porosity, the only relevant for cell viability considerations, was derived by subtracting the value for scaffold closed porosity from that of the total porosity, both calculated using a density balance and applying Archimedes' principle, through the following relationship:

$$\varepsilon = (1 - \rho/\rho_0) \cdot 100 \qquad (2)$$

where ρ is the density calculated as the ratio of the weight and the volume of PLLA samples.

The high hydrophobicity of PLLA added to capillary forces deriving from the sub-100 μm pore size make it impossible for water to spontaneously penetrate into the scaffold.

If we consider the extremely low weight to apparent volume ratio for these structures it's easy to imagine how they would receive a strong up thrust once immersed in the fluid, proportional to $V_{tot,}$, i.e., the volume occupied by the polymer and the total air (scaffold's total porosity):

$$UT_{tot} \equiv V_{tot} \cdot \rho'' = W'' - V_0 \cdot \rho'' + W_s \qquad (3)$$

and:

$$\varepsilon_{tot} = \frac{V_{tot}}{V_{tot} + V_0} \cdot 100 \qquad (4)$$

where W'' *is* the measured net up thrust, UT_{tot} the total air contribution and ρ" is the fluid density, equal to 1.0 g*cm^{-3},in this case water. The samples were then immersed into absolute ethanol where they sank after around 30 minutes. the samples ware left soaking for 2 hours in order to ensure complete ethanol permeation

into the scaffolds. The difference between the expected scaffold weight in ethanol ($W_s - V_0 \cdot \rho'$) with respect to that measured after scaffold sinking in ethanol, W' was due to the up-thrust exerted by ethanol on the air trapped inside the scaffold (UT_{closed}), and thus is directly proportional to the scaffold closed porosity V_{closed}, being:

$$UT_{closed} \equiv V_{closed} \cdot \rho' = W_s - V_0 \cdot \rho' - W' \quad (5)$$

And:

$$\varepsilon_{closed} = \frac{V_{closed}}{V_{tot} + V_0} \cdot 100 \quad (6)$$

In which W' is the soaked scaffold weight in ethanol and ρ'= 0.8 g/cm^3 is ethanol density. The interconnected porosity was calculated as:

$$\varepsilon_{open} = \varepsilon_{tot} - \varepsilon_{closed} \quad (7)$$

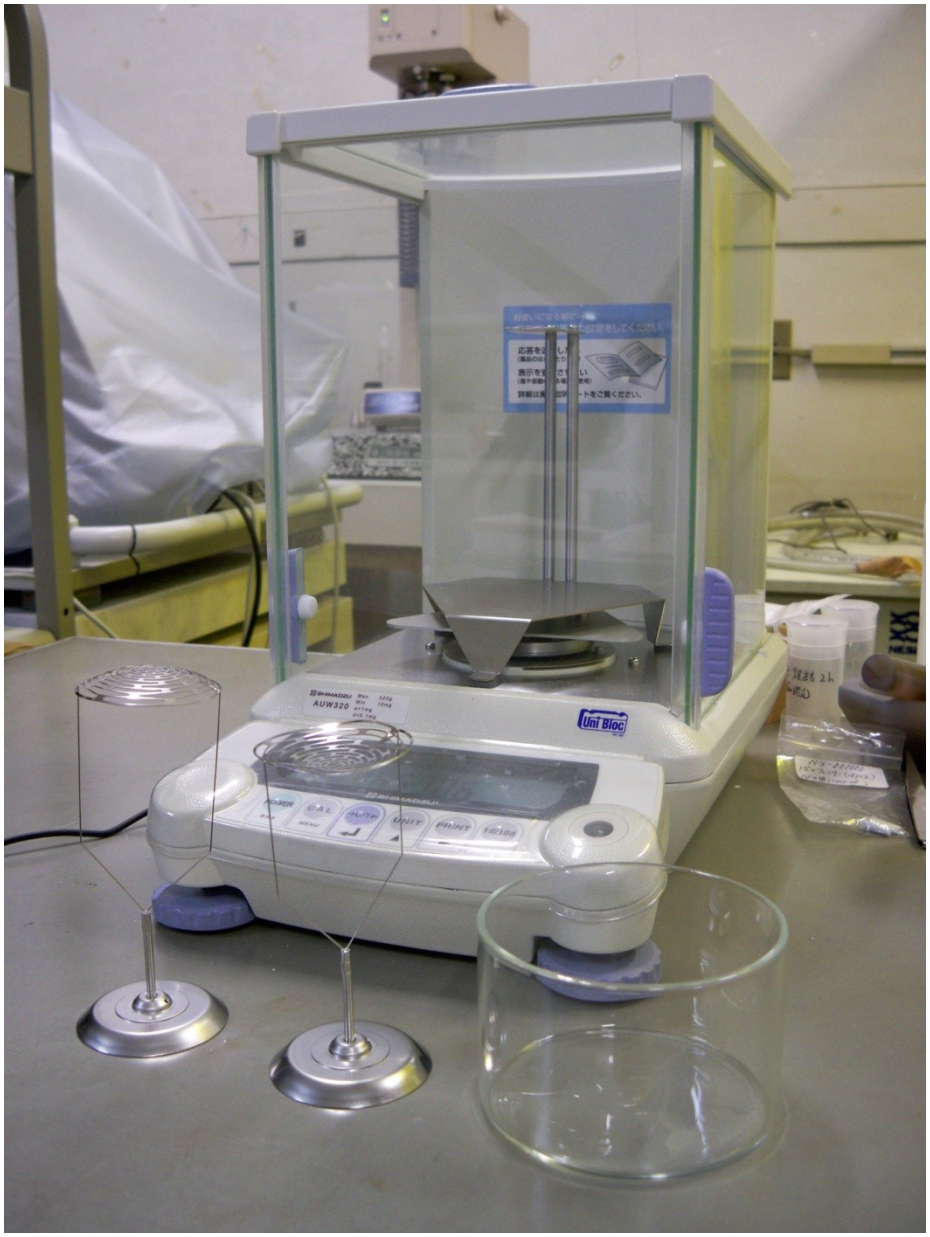

Fig 2.4.1: Analitical balance for porosity measurements

2.5 Lithography

Photolithography (or "optical lithography") is a process used in microfabrication to selectively remove parts of a thin film or the bulk of a substrate. It uses light to transfer a geometric pattern from a photo mask to a light-sensitive chemical "photoresist", or simply "resist," on the substrate. A series of chemical treatments then either engraves the exposure pattern into, or enables deposition of a new material in the desired pattern upon, the material underneath the photo resist. In complex

integrated circuits, for example a modern CMOS, a wafer will go through the photolithographic cycle up to 50 times.

Photolithography shares some fundamental principles with photography in that the pattern in the etching resist is created by exposing it to light, either directly (without using a mask) or with a projected image using an optical mask. This procedure is comparable to a high precision version of the method used to make printed circuit boards. Subsequent stages in the process have more in common with etching than to lithographic printing. It is used because it can create extremely small patterns (down to a few tens of nanometers in size), it affords exact control over the shape and size of the objects it creates, and because it can create patterns over an entire surface cost-effectively. Its main disadvantages are that it requires a flat substrate to start with, it is not very effective at creating shapes that are not flat, and it can require extremely clean operating conditions.
The steps involved in the photolithographic process are wafer cleaning; barrier layer formation; photoresist application; soft baking; mask alignment; exposure and development; and hard-baking.

2.5.1 Wafer cleaning, barrier formation and photoresist application

In the first step, the wafers are chemically cleaned to remove particulate matter on the surface as well as any traces of organic, ionic, and metallic impurities. After cleaning, silicon dioxide, which serves as a barrier layer, is deposited on the surface of the wafer. After the formation of the SiO2 layer, photoresist is applied to the surface of the wafer. High-speed centrifugal whirling of silicon wafers is the standard method for applying photoresist coatings in IC manufacturing. This technique, known as "Spin Coating", produces a thin uniform layer of photoresist on the wafer surface.

2.5.2 Positive and negative photoresist

There are two types of photoresist: positive and negative. For positive resists, the resist is exposed with UV light wherever the underlying material is to be removed. In these resists, exposure to the UV light changes the chemical structure of the resist so that it becomes more soluble in the developer. The exposed resist is then washed away by the developer solution, leaving windows of the bare underlying material. In

other words, "whatever shows, goes." The mask, therefore, contains an exact copy of the pattern which is to remain on the wafer.

Negative resists behave in just the opposite manner. Exposure to the UV light causes the negative resist to become polymerized, and more difficult to dissolve. Therefore, the negative resist remains on the surface wherever it is exposed, and the developer solution removes only the unexposed portions. Masks used for negative photoresists, therefore, contain the inverse (or photographic "negative") of the pattern to be transferred. The figure below shows the pattern differences generated from the use of positive and negative resist.

Negative resists were popular in the early history of integrated circuit processing, but positive resist gradually became more widely used since they offer better process controllability for small geometry features. Positive resists are now the dominant type of resist used in VLSI fabrication processes.

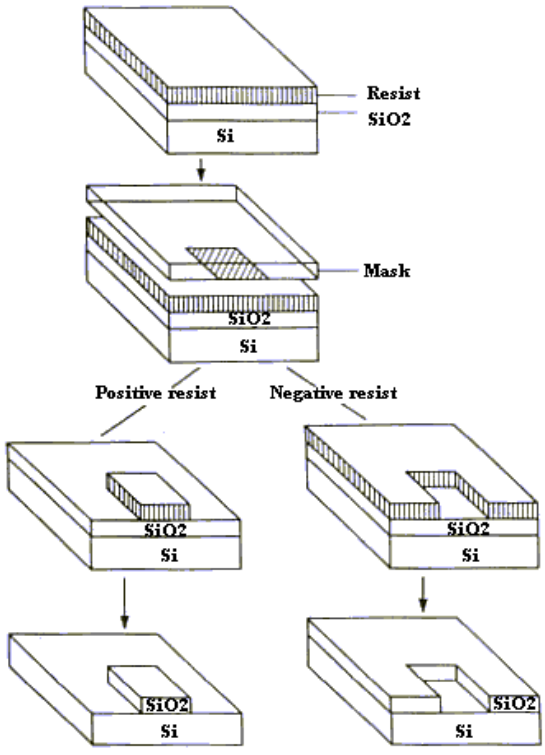

Fig. 2.5.2.1: Example of working process for positive and negative photo-resist

2.5.3 Soft-baking

Soft-baking is the step during which almost all of the solvents are removed from the photoresist coating. Soft-baking plays a very critical role in photo-imaging. The photoresist coatings become photosensitive, or imageable, only after softbaking. Oversoft-baking will degrade the photosensitivity of resists by either reducing the developer solubility or actually destroying a portion of the sensitizer. Undersoft-baking will prevent light from reaching the sensitizer. Positive resists are incompletely exposed if considerable solvent remains in the coating. This undersoft-baked positive resists is then readily attacked by the developer in both exposed and unexposed areas, causing less etching resistance.

2.5.4 Mask alignment and exposure

One of the most important steps in the photolithography process is mask alignment.
A mask or "photomask" is a square quartz plate with a patterned emulsion of metal film on one side. The mask is aligned with the wafer, so that the pattern can be transferred onto the wafer surface. Each mask after the first one must be aligned to the previous pattern.
Once the mask has been accurately aligned with the pattern on the wafer's surface, the photoresist is exposed through the pattern on the mask with a high intensity ultraviolet light. There are three primary exposure methods: contact, proximity, and projection. They are shown in the figure below.

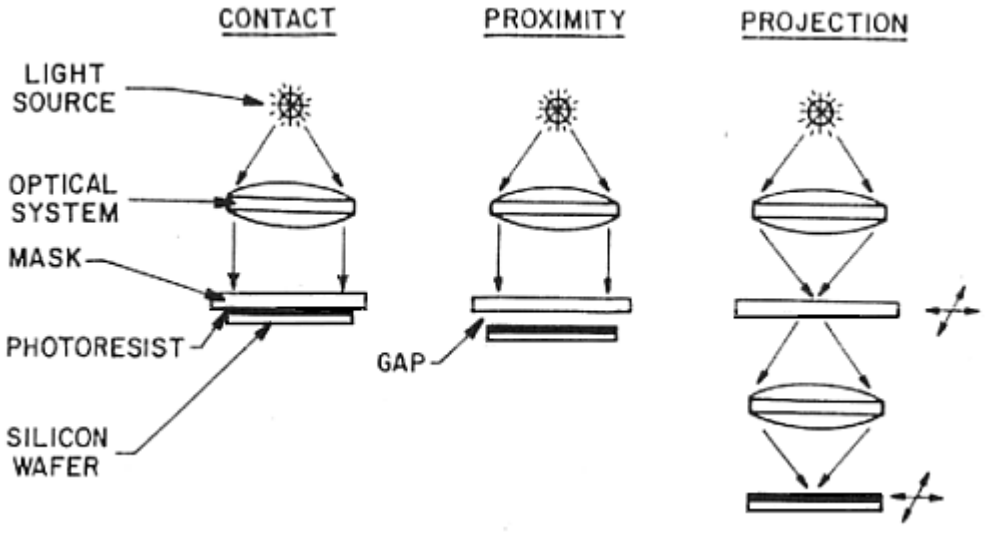

Fig.2.5.4.1: Three principal methods of exposure: (from left to right) Contact, Proximity, Projection

2.5.4.1 Contact printing

In contact printing, the resist-coated silicon wafer is brought into physical contact with the glass photomask. The wafer is held on a vacuum chuck, and the whole assembly rises until the wafer and mask contact each other. The photoresist is exposed with UV light while the wafer is in contact position with the mask. Because of the contact between the resist and mask, very high resolution is possible in contact printing (e.g. 1-micron features in 0.5 microns of positive resist). The problem with contact printing is that debris, trapped between the resist and the mask, can damage the mask and cause defects in the pattern.

2.5.4.2 Proximity printing

The proximity exposure method is similar to contact printing except that a small gap, 10 to 25 microns wide, is maintained between the wafer and the mask during exposure. This gap minimizes (but may not eliminate) mask damage. Approximately 2- to 4-micron resolution is possible with proximity printing.

2.5.4.3 Projection printing

Projection printing, avoids mask damage entirely. An image of the patterns on the mask is projected onto the resist-coated wafer, which is many centimeters away. In order to achieve high resolution, only a small portion of the mask is imaged. This small image field is scanned or stepped over the surface of the wafer. Projection printers that step the mask image over the wafer surface are called step-and-repeat systems. Step-and-repeat projection printers are capable of approximately 1-micron resolution.

2.5.5 Development

One of the last steps in the photolithographic process is development. Fig.2.5.5.1 below, shows response curves for negative and positive resist after exposure and development.

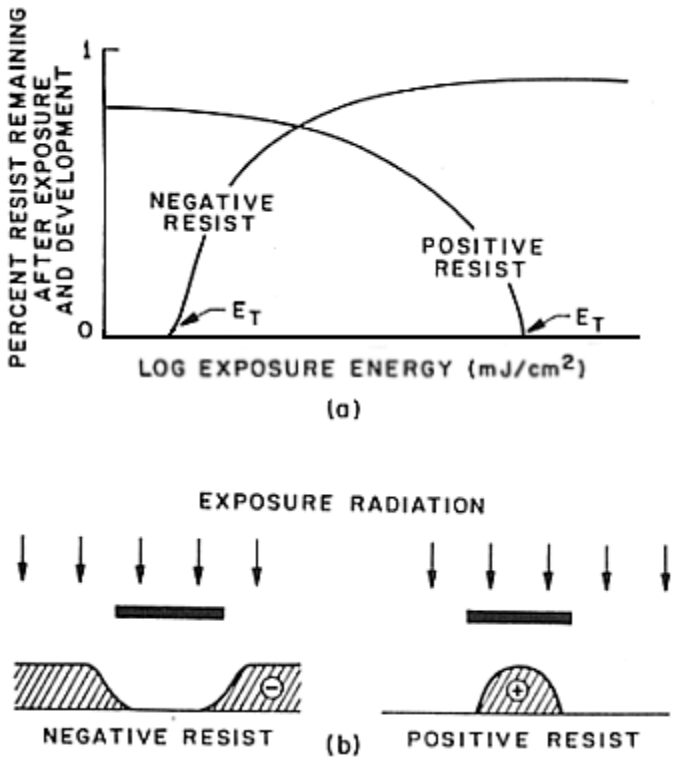

Fig.2.5.5.1: (a) Resist exposure characteristics (b) Resist after development

At low-exposure energies, the negative resist remains completely soluble in the developer solution. As the exposure is increased above a threshold energy Et, more of the resist film remains after development. At exposures two or three times the threshold energy, very little of the resist film is dissolved. For positive resists, the resist solubility in its developer is finite even at zero-exposure energy. The solubility gradually increases until, at some threshold, it becomes completely soluble. These curves are affected by all the resist processing variables: initial resist thickness, prebake conditions, developer chemistry, developing time, and others.

2.5.6 Hard-baking

Hard-baking is the final step in the photolithographic process. This step is necessary in order to harden the photoresist and improve adhesion of the photoresist to the wafer surface.

2.5.7 Soft-lithography for tissue engineering

Photolithographic technologies offer a broad and unique tool for scaffolds the

design and fabrication of complex geometries and working devices operating at the micro and nano-scales [123,124]. The recent years have witnessed an impressive explosion and growth of photolithography even in the area of TE, usually referred to as soft-lithography [40], since it also deals with materials, generally plastics, softer than silicon and others. In particular, soft-lithography comprises a set of techniques (spin casting and lamination [43], replica moulding [48], microfabrication [42], capillary micromoulding [41], etc.), which rely on the use of an elastomeric stamp or replica for transferring a particular pattern over a suitable biocompatible or biodegradable polymer. The replica can be prepared by casting the liquid pre-polymer of an elastomer (like PDMS) over a master exhibiting a pre-designed patterned decoration on its surface. In this way, multiple copies of the highly complex structures in the master can be promptly obtained with nanometer resolution. A complex 3D architecture can be finally achieved by stacking the produced membranes in different orientations [48,43].

The incredible spatial resolution that can be achieved by these techniques (down to 100 nm) are such to confer to the engineered scaffold the highest aspect ratio which characterize living organs, below which only self assembly processes can arrive.

2.6 Cell culture

Human Mesenchymal Stem Cells (hMSC) were purchased from LONZA Group Ltd (Basel, CH) and cultured in Mesenchymal Stem Cell Basal Medium (MSCBM) according to manufacturer instructions. Human Umbilical Vein Endothelial Cells (HUVEC) were purchased from LONZA Group Ltd (Basel, CH) and cultured in Endothelial Basal Medium (EBM-2) according to manufacturer instructions. Before the setting up of hMSC-HUVEC co-culture, hMSC were stained with a vital dye to distinguish them from HUVEC. For this reason, hMSC were washed in sterile phosphate buffer saline (PBS) and incubated for 30 minutes in complete growth medium with Vybrant™ Red vital dye (concentration: 4 ml/ml). After two washings in PBS, stem cells were cultured for 24 hours in complete growth medium.

2.7 Cryostat

Cryostat are used in medicine to cut histological slides. They are usually used in a process called frozen section histology.

The cryostat is essentially an ultrafine "deli-slicer", called a microtome, placed in a freezer. The cryostat is usually a stationary upright freezer, with an external wheel for rotating the microtome.

The temperature can be varied, depending on the tissue being cut - usually from minus 20 to minus 30 degree Celsius. The freezer is either powered by electricity, or by a refrigerant like liquid nitrogen. Small portable cryostats are available and can run off generators or vehicle inverters. To minimize unnecessary warming all necessary mechanical movements of the microtome can be achieved by hand via a wheel mounted outside the chamber. Newer microtomes have electric push button advancement of the tissue. The precision of the cutting is in micrometres. Tissue are sectioned as thin as 1 micrometre. Usual histology slides are mounted with a thickness of about 7 micrometres. Specimens that are soft at room temperature are mounted on a cutting medium (often made of egg white) on a metal "chuck", and frozen to cutting temperature (for example at -20 degrees C). Once frozen, the specimen on the chuck is mounted on the microtome. The crank is rotated and the specimen advances toward the cutting blade. Once the specimen is cut to a satisfactory quality, it is mounted on a warm (room temperature) clear glass slide, where it will instantaneously melt and adhere. The glass slide and specimen is dried with a dryer or air dried, and stained. The entire process from mounting to reading the slide takes from 10 to 20 minutes, allowing rapid diagnosis in the operating room. The cryostat can be used to cut histology and tissue slide outside of medicine, but the quality of the section is poor compared to standard fixed section wax mounted histology.

Chapter 3

Experimental

3.1 Sample realization

3.1.1 Scaffold synthesis by thermally induced phase separation

At the beginning of this work, the initial setup consisted of:

- A chiller (Thomas® TRL107SLC)
- A dewar
- An aluminum holder (hollow cylinder)

The heat exchanger part of the chiller is a circular serpentine connected to the compressor by a bendable tube. This serpentine is placed inside the dewar. Ethanol has been used as heat exchange liquid.

Commercial PLLA (Mw_a = 100,000 ÷ 150,000, Aldrich, USA) was dissolved in 1,4 dioxane (Aldrich, USA) at the fixed concentration of 4 wt%. The solution was cast into a circular teflon mold and left freezing for 4 days in a cold room at temperatures of -50°C. For directional gradient induced TIPS, the solution-containing mold was placed on top of the aluminum holder set at -30°C. After solidification, the sample was immersed into an 80% wt ethanol aqueous solution to leach out the solvent. It is worth to mention that, as the congealed solution was removed from the freezing chamber, its internal structure was completely formed and fixed in the solid state so that the ethanol bath temperature can only influence the speed of the dioxane extraction process. Nevertheless, under too high extracting temperatures, e.g. room temperature, dioxane change of state may occur, leading to localized polymer re-dissolution and loss of the pre-formed scaffold architecture. To avoid an excessively slow process while still preserving scaffold features, the extraction temperature was set -18°C for four days. Ethanol solution was finally removed by letting the scaffold in air for one day at room temperature.

One of the critical factor to obtain a good structured scaffold is the perfect perpendicularity between the polymer solution surface and the applied thermal gradient.

To obtain this condition then, the aluminum holder must be accurately horizontally positioned.

The need of manually positioning the sample mold, other operations and most of all the round shaped internal bottom of the dewar makes this task not easy.

As said before, the time between the mold positioning and the start of freezing is really short, so it's not possible to check the horizontality after positioning the mold.

Moreover, removing the cap for too long leads to a rise of the bath temperature and increase of humidity, resulting in water condensation on the metal holder and alteration of the thermal interface.

It is clear then, why some efforts have been made to researched a method to fix the holder in a horizontal position.

A first option was to weld a thin metal plate on the internal bottom surface of the dewar. This solution was put aside because of the high probability of damaging the dewar, in fact the heat of the welding can easily pierce the bottom of the dewar.

A second, mechanical, solution is represented in fig.3.1.1.1.

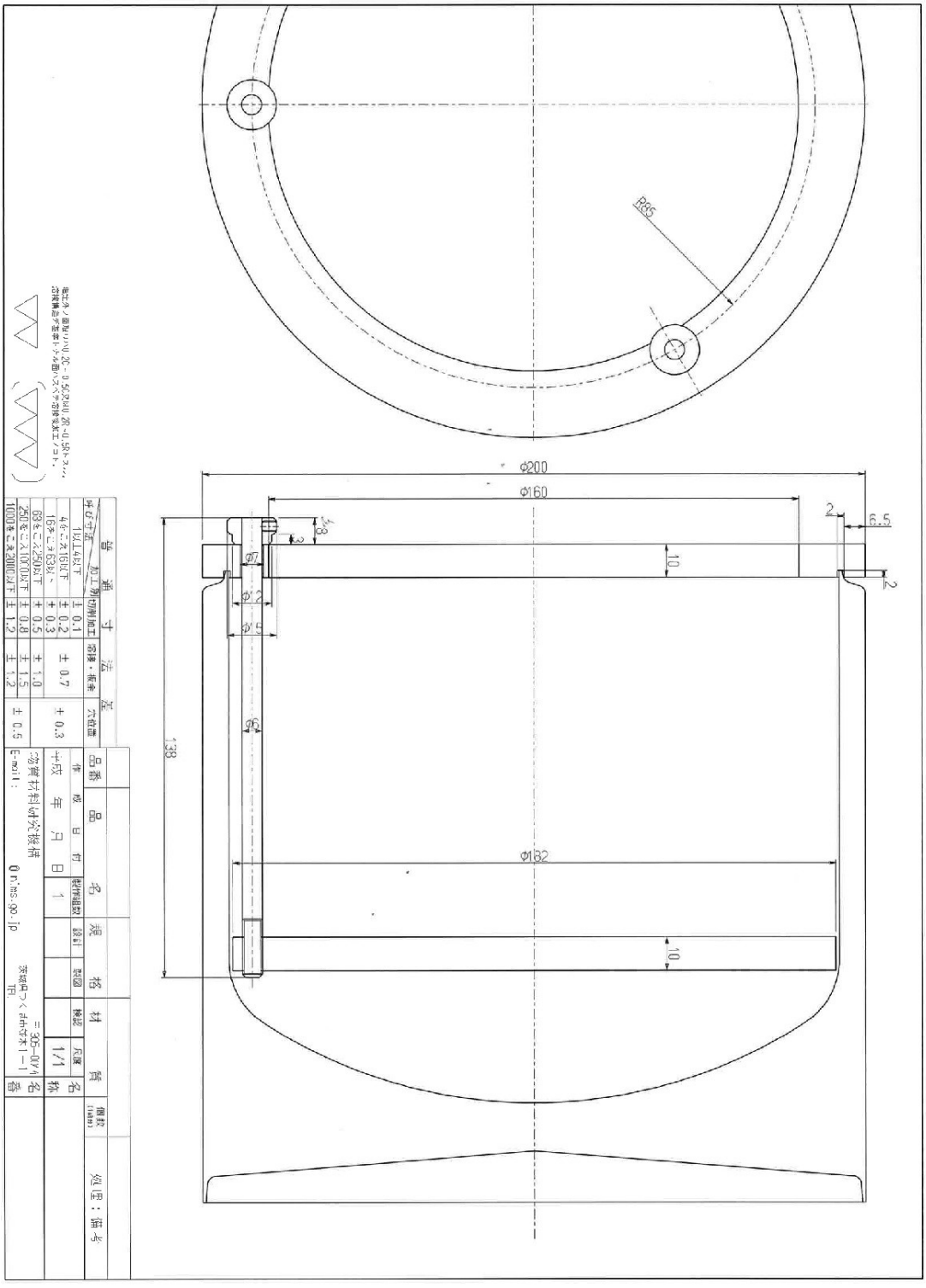

Fig.3.1.1.1: Scheme of the first device designed, aimed to obtain a horizontal plane inside the dewar

Three screws are used to aid the regulation of the horizontality of the support for the aluminum holder.

Despite the easiness of the regulation this method wasn't free from issues. To permit the escape of the three screws it would have been needed a radical modification of the dewar cap, additionally the structure was not stiff enough to support the combined chiller serpentine and aluminum holder weight without some uncontrollable displacements.

Finally the method that has been chosen is represented in fig.3.1.1.2.

An aluminum ring is conjunct on top of an inox steel ring of the same diameter through the use of screws. Both plates were perforated in several points to create a pattern able to permit the diffusion of convectional flows inside the ethanol bath.

The so composed structure is fixed in horizontal position by a three-point-anchorage.

Three inox steel spheres are pushed against the internal wall of the dewar by lowering the screws making the whole system fixed to the dewar.

The role of the steel ring is of giving weight and thus stability.

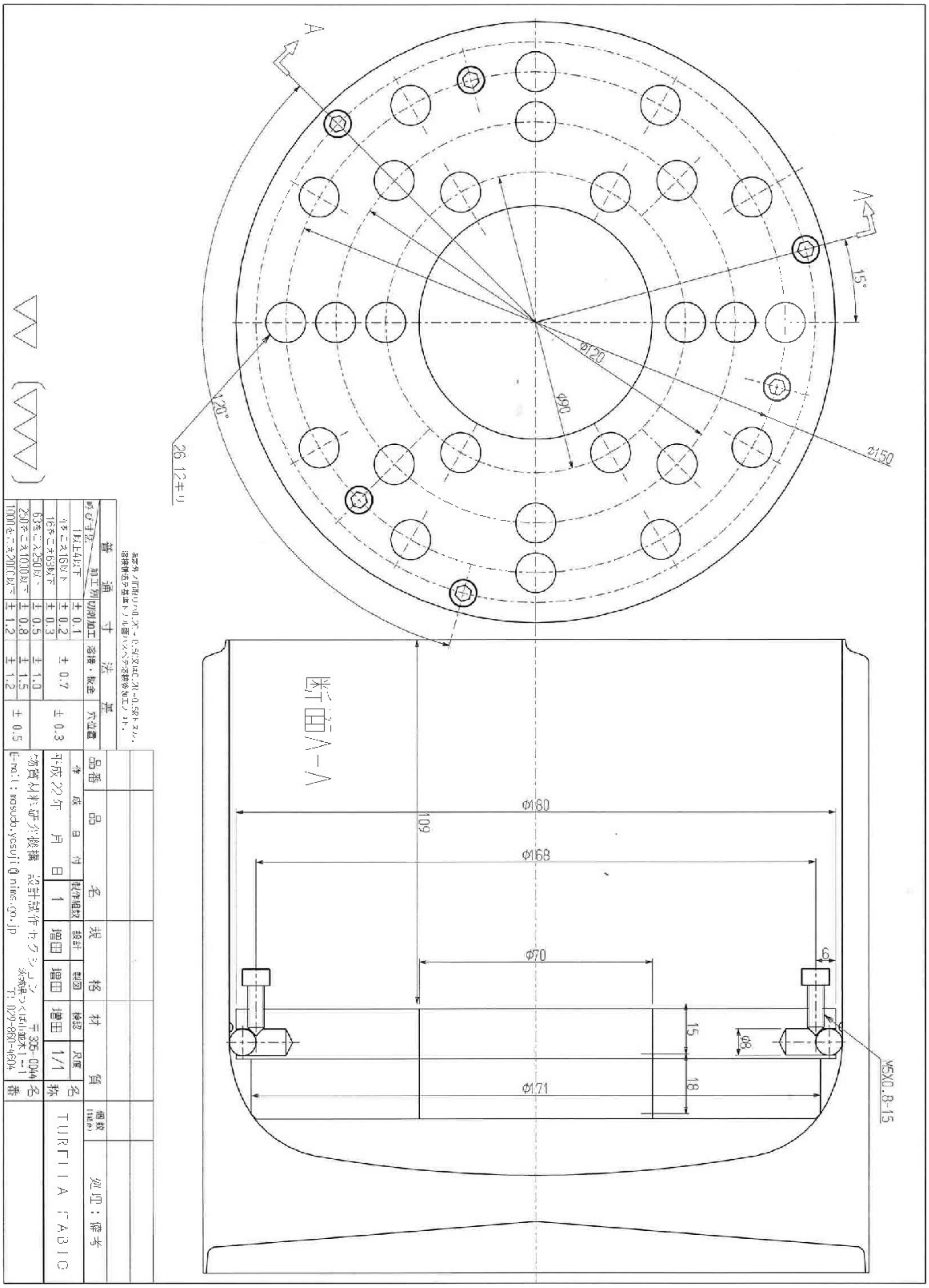

Fig.3.1.1.2: Scheme of the device utilized to flatten the bottom of the dewar

3.1.2 Used molds

In this work three types of molds have been used:

- a small beaker-like Teflon mold
- three Teflon molds of different geometrical shape
- a new Teflon reactor (described in § 3.1.3)

The small beaker molds were used at the beginning of the work and they also resulted convenient during the optimization of the process because of the possibility of utilize more than one per time thanks to their limited size and amount of chemicals required.

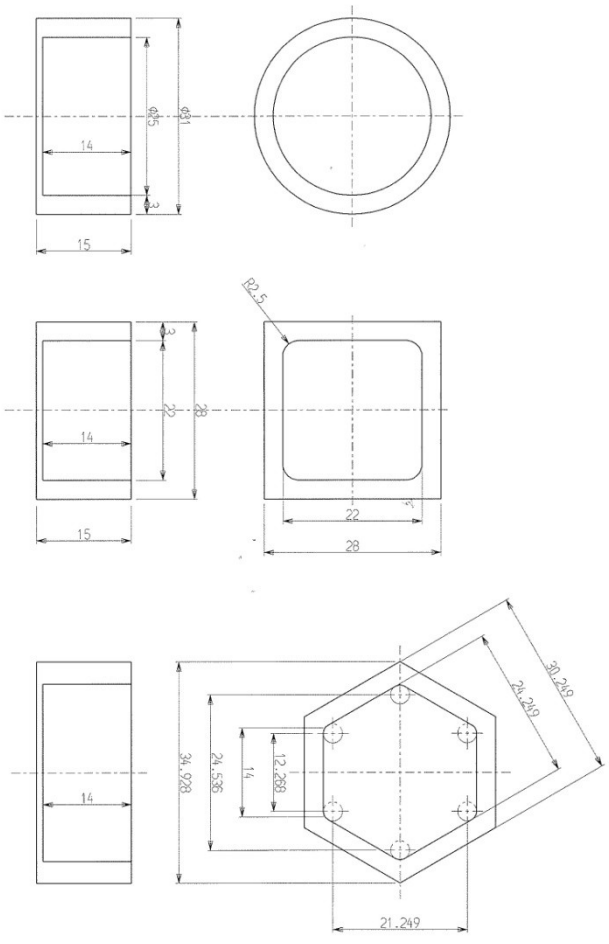

Fig. 3.1.2.1: Scheme of the three different Teflon molds

When the mold is putted inside the chiller, the solution in contact with the cold walls of the mold solidifies in a first amorphous layer and then in an ordered structure.

This amorphous layer reduces the amount of the sample that can be used so it was decided to try using new molds (Fig.3.1.2.1) to increase the ordered area.
These new molds share the same base area and maintain the same bottom and wall thickness of the beaker-like molds to prevent uncontrolled behavior changes of the system.
Furthermore we investigated any possible influence of the mold geometry respect of the order/disorder of the structure of the scaffolds.

3.1.3 Design of a new reactor

Due to the non significant differences between the previous mold types, it was designed a new reactor utilizing a different approach.

The concept was to maximize the thermal insulation of the walls and the conductivity of the bottom, improving the control of the system by direct temperature measurement of the bottom.
Since the working temperatures were quite low, it was decided to maintain the structure of the reactor as simple as possible, thus with the minimum of different materials to avoid thermal deformation problems.
Another parameter that influenced the design was the small amount of available materials.
The final solution was to utilize a Teflon rod and silicon wafers.
The device has completely been realized by machining the Teflon rod.

As shown in Fig.3.1.3.1, the reactor has a cylindrical geometry to reduce the loss of material during the machining and because a circular shape of the mold seemed the one with the best results.
The reactor is composed of five components:

- the Teflon body:
    - bottom part
    - middle part
    - cap
- a poly-carbonate O-ring
- a silicon wafer

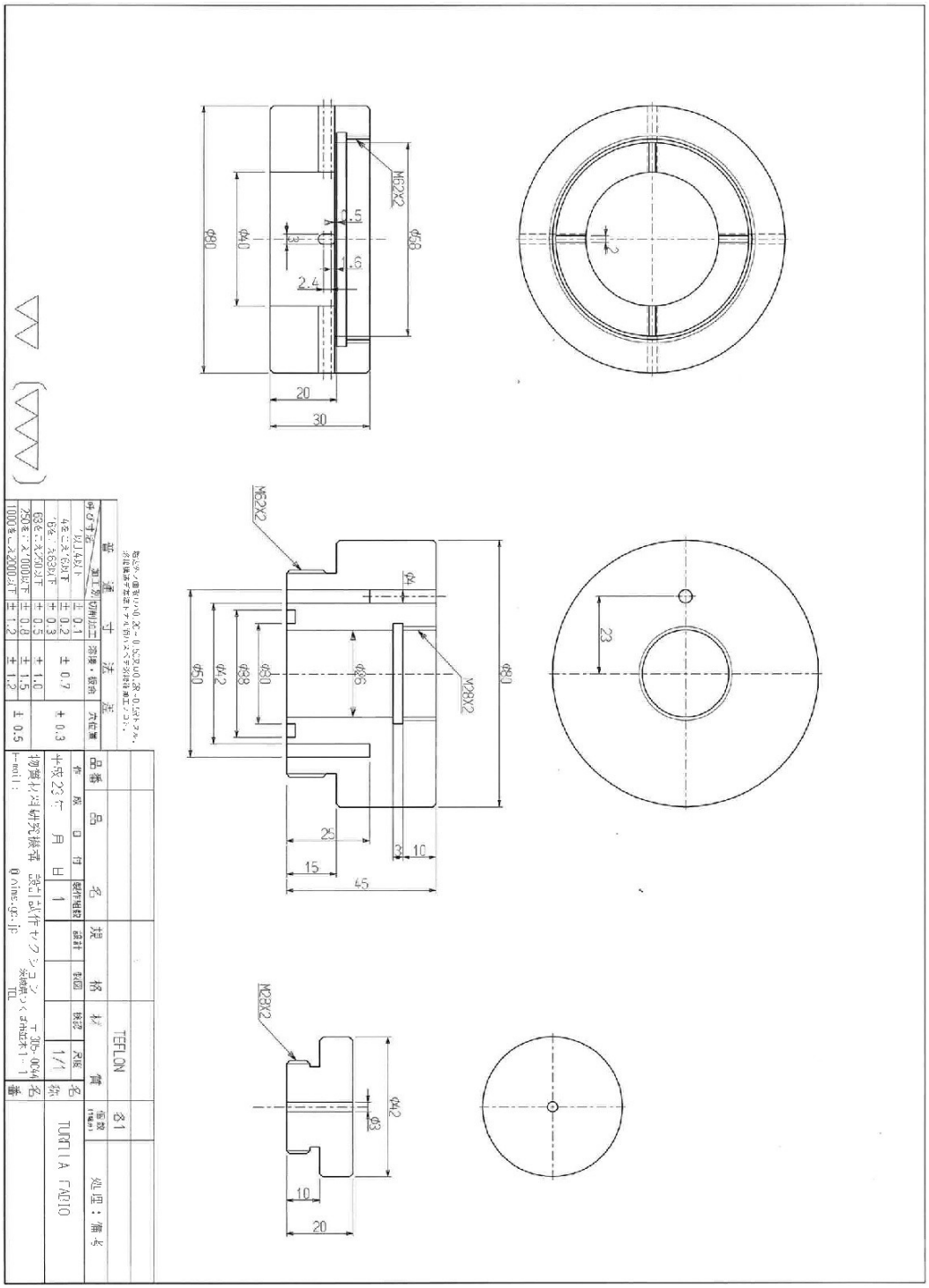

Fig. 3.1.3.1: Scheme of the three parts of the Teflon reactor

The bottom part presents a lower half composed of many foot stands and an upper half with a lodging in which the silicon wafer allocates.

The hole through the entire piece, combined with the many small foot stands, allow a good circulation of the liquid that acts as heat exchanger.

Right under the level of the wafer there are four holes, which go through all the length of the wall, permitting the escape of air during the immersion of the reactor in the dewar, avoiding bubbles and a low efficiency in the extraction of heat.

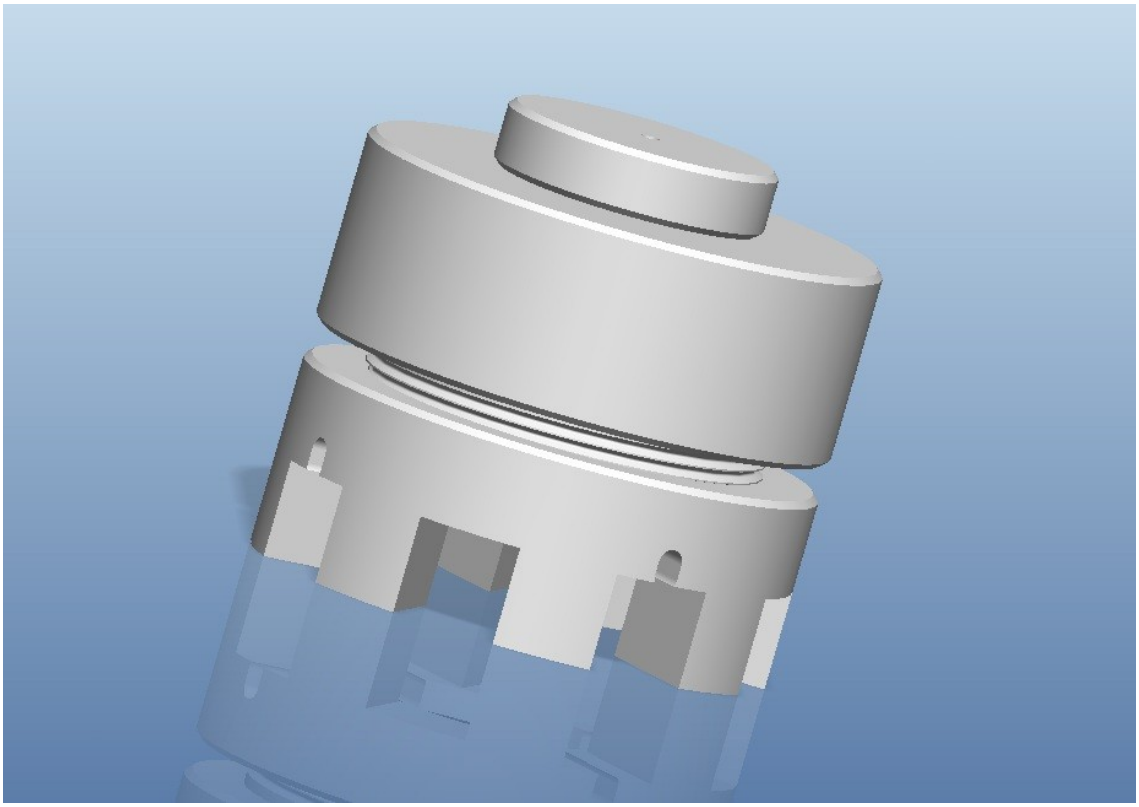

Fig. 3.1.3.2: 3D model of the assembled reactor

The middle part has a one inch hole through all the length of the piece that is the actual mold in which the solution is poured in.
On the bottom from the inside there are the O-ring lodging and going to the outside an air space that aids the thermal insulation.
From one point at the internal end of the air chamber departs one hole that reaches the top of the piece. This hole permits the insertion of a thermocouple that can measure directly the temperature of the silicon wafer.

The cap has one hole through all the length to avoid compression of the fluids (the mold isn't completely filled with the scaffold forming solution) inside the mold during the closing down of the reactor or the decompression due to the low temperature during the chilling.

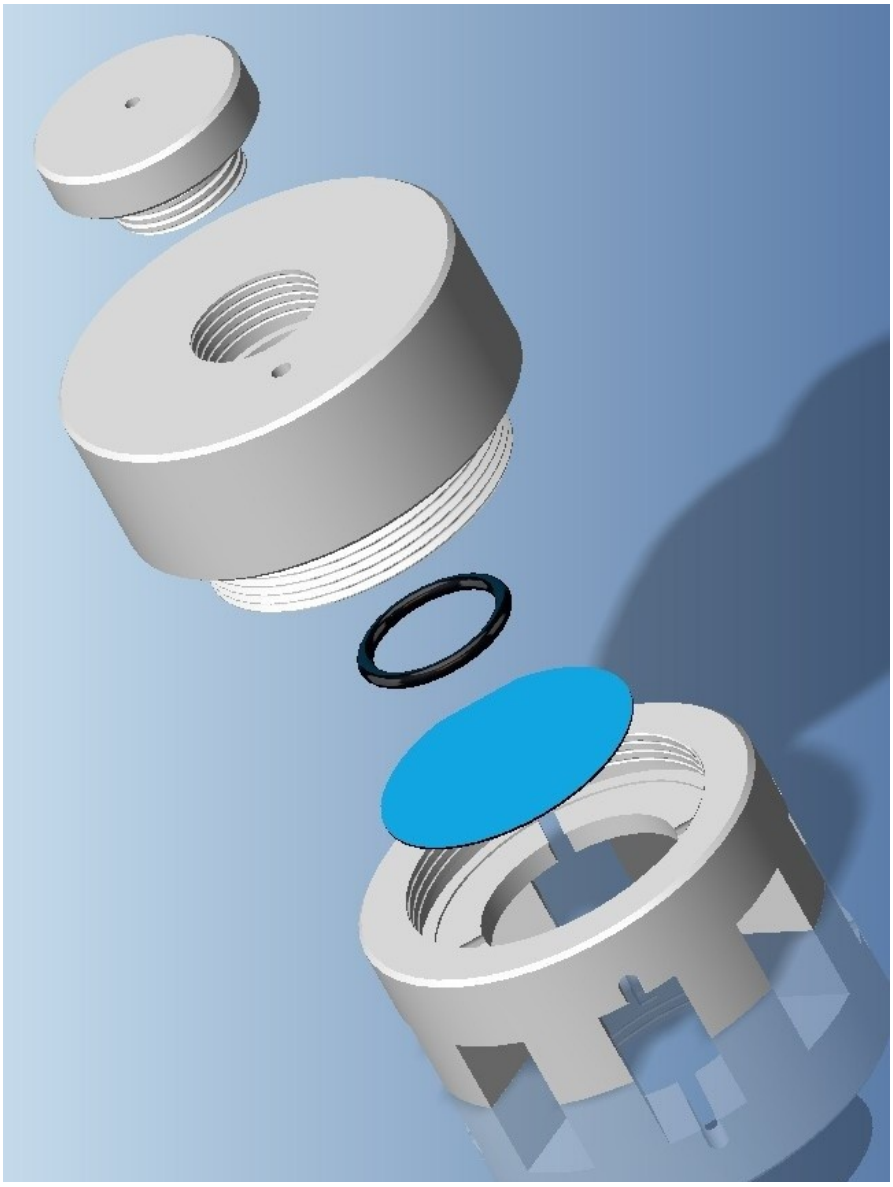

Fig. 3.1.3.3: Exploded view of the 3D model of the reactor

3.1.4 Optimization of the process

In this work several process parameters has been varied to investigate any change in the structure, morphology and mechanical properties of the scaffolds so obtained.
We started from the following set-up and then changed one parameter per time.
After finding the best value of the changed parameter by visual analysis (SEM) of the scaffold structure, this value was adopted in the set-up for the next parameters.

From bibliography, the starting parameter we adopted were:

- Polymer (PLLA) concentration: 4,6 % wt in 1,4-dioxane
- Time of chilling: 4 days
- Temperature of chilling: -50 C° (temperature imposed to the chiller)
- Time of leaching: 4-5 days

The time of chilling has been varied as follows:

- 32 hours
- 28 hours
- 24 hours
- 20 hours
- 16 hours
- 12 hours

After noticing that a good structure could be obtained after 12 hours we also investigate

- 8 hours
- 2,5 hours

The leaching time has been varied as follows:

- 48 hours
- 44 hours
- 40 hours
- 36 hours
- 32 hours
- 28 hours

The chilling temperature was investigated in this range (temperature imposed to the chiller):

- - 70 C°
- - 60 C°
- - 50 C°
- - 40 C°

- - 30 C°
- - 20 C°

As happened many times in science, serendipity came in our help. In fact, during a trial set-up without expectations of any significant results, we obtained an exceptional good structure at a high temperature respect of the above mentioned, thus we decided to focus on the following temperatures:

- - 40 C°
- - 30 C°
- - 20 C°
- - 10 C°

The polymer concentration has been varied as follow:

- 4 %wt
- 3.5 %wt
- 3 %wt
- 2.5 %wt
- 2 %wt

Futhermore we investigate the effect of the mold's shape:

- Small beaker
- Circular
- Square
- Exagonal
- New reactor

3.1.5 Realized scaffolds

The scaffolds realized during this work are listed in Tab.3.1.5.1.

NAME	Material	CONCENTRATION	Mold type	TIPS T	TIPS Time	Leaching Time
T26	PLLA	0.11g in 2,3mL Dioxane	Small Teflon beaker	-26±1°C (Al) (-50 set) - Fatta taratura a tre terminali - Asciugato l'holder di Al	3g	3 days
T27	PLLA	0.11g in 2,3mL Dioxane	Small Teflon beaker	-26±1°C (Al) (-50 set) - Fatta taratura a tre terminali - Asciugato l'holder di Al	3g	3 days
T28	PLLA	0.11g in 2,3mL Dioxane	Small Teflon beaker	-28±1°C (Al) (-50 set) - Fatta taratura a tre terminali - Asciugato l'holder di Al	46h	3,5 days
T29	PLLA/CeO_2	0.11g in 2,3mL Dioxane + 0.01g CeO_2	Small Teflon beaker	-28±1°C (Al) (-50 set) - Fatta taratura a tre terminali - Asciugato l'holder di Al	46h	3,5 days
T30 A round B square C hexag	PLLA	0.17g in 3,3mL Dioxane	New molds of 494 mm^2surface area	-28±1°C (Al) (-50 set) - Fatta taratura a tre terminali - Asciugato l'holder di Al	3,5gg	3 days
TIPS Si	PLLA	0,337g in 7,4 ml Dioxane	Teflon reactor with Si wafer	-58±1°C (Bagno EtOH) (-50 set) - Fatta taratura a un terminale	48h	4 days
T31	PLLA	4ml of 5,1g in 10,9 ml Dioxane solution	New square teflon mold	-29±1°C (Al) (-50 set) - Fatta taratura a tre terminali - Asciugato l'holder di Al	3gg	4 days
T32	PLLA	2,5ml of 5,1g in 10,9 ml Dioxane solution	New circular teflon mold	-29±1°C (Al) (-50 set) - Fatta taratura a tre terminali - Asciugato l'holder di Al	3gg	4 days
T33	PLLA	4ml of 5,1g in 10,9 ml Dioxane solution	Small Teflon beaker	-29±1°C (Al) (-50 set) - Fatta taratura a tre terminali - Asciugato l'holder di Al	3gg	4 days

T34	PLLA/CeO_2	0,15g+0,02g CeO_2 in 3,6ml Dioxane	Small Teflon beaker	-30±1°C (Al) (-50 set) - Fatta taratura a tre terminali - Asciugato l'holder di Al	3,5g	4 days
TIPS Si X 2	PLLA	0,15g in 3,6 ml Dioxane	New Teflon Reactor	9±1°C (Al) (-35 set) - Fatta taratura a due terminali - In livella	1g	4,5 days
T35	PLLA	0,15g in 3,6 ml Dioxane	Small Teflon beaker	-10±1°C (Al) (-25 set) - Fatta taratura a tre terminali - Asciugato l'holder di Al	21h	4 days
T36	PLLA	0,15g in 3,6 ml Dioxane	New circular teflon mold	-10±1°C (Al) (-25 set) - Fatta taratura a tre terminali - Asciugato l'holder di Al	21h	4 days
TIPS Si X 3	PLLA	0,3g in 7,2 ml Dioxane	New Teflon Reactor	10±1°C (Al) (-30 set) - Fatta taratura a due terminali - In livella	16h	3 days
T37	PLLA	0,15g in 3,6 ml Dioxane	Small Teflon beaker	-10±1°C (Al) (-30 set) - Fatta taratura a tre terminali - Asciugato l'holder di Al	16h	4 days
T38	PLLA	0,15g in 3,6 ml Dioxane	Small Teflon beaker	-10±1°C (Al) (-30 set) - Fatta taratura a tre terminali - Asciugato l'holder di Al	20h	4 days
T39	PLLA	0,15g in 3,6 ml Dioxane	Small Teflon beaker	-10±1°C (Al) (-30 set) - Fatta taratura a tre terminali - Asciugato l'holder di Al	24h	4 days
T40	PLLA	0,15g in 3,6 ml Dioxane	Small Teflon beaker	-10±1°C (Al) (-30 set) - Fatta taratura a tre terminali - Asciugato l'holder di Al	12h	4 days
T41	PLLA	0,15g in 3,6 ml Dioxane	Small Teflon beaker	-10±1°C (Al) (-30 set) - Fatta taratura a tre terminali - Asciugato l'holder di Al	28h	4 days
T42	PLLA	0,15g in 3,6 ml Dioxane	Small Teflon beaker	-10±1°C (Al) (-30 set) - Fatta taratura a tre terminali - Asciugato l'holder di Al	32h	4 days
TIPS Si X 4	PLLA	0,3g in 7,2 ml Dioxane	New Teflon Reactor	10±1°C (Al) (-30 set) - Fatta taratura a due terminali - In livella	20h	3 days

T43	PLLA	0,15g in 3,6 ml Dioxane	Small Teflon beaker	-10±1°C (Al) (-30 set) - Fatta taratura a tre terminali - Asciugato l'holder di Al	20h	28h
T44	PLLA	0,15g in 3,6 ml Dioxane	Small Teflon beaker	-10±1°C (Al) (-30 set) - Fatta taratura a tre terminali - Asciugato l'holder di Al	20h	32h
T45	PLLA	0,15g in 3,6 ml Dioxane	Small Teflon beaker	-10±1°C (Al) (-30 set) - Fatta taratura a tre terminali - Asciugato l'holder di Al	8h	4 days
T46	PLLA/CeO_2	0,15g in 3,6ml Dioxane with dispersed CeO_2	Small Teflon beaker	-10±1°C (Al) (-30 set) - Fatta taratura a tre terminali - Asciugato l'holder di Al	24h	5 days
T47 e bis	PLLA	0,13g in 3,6 ml Dioxane	Small Teflon beaker	-10±1°C (Al) (-30 set) - Fatta taratura a tre terminali - Asciugato l'holder di Al	20h	4 days
T48 e bis	PLLA	0,11g in 3,6 ml Dioxane	Small Teflon beaker	-10±1°C (Al) (-30 set) - Fatta taratura a tre terminali - Asciugato l'holder di Al	20h	4 days
T49 e bis	PLLA	0,09g in 3,6 ml Dioxane	Small Teflon beaker	-10±1°C (Al) (-30 set) - Fatta taratura a tre terminali - Asciugato l'holder di Al	20h	4 days
T50 e bis	PLLA	0,07g in 3,6 ml Dioxane	Small Teflon beaker	-10±1°C (Al) (-30 set) - Fatta taratura a tre terminali - Asciugato l'holder di Al	20h	6 days
TIPS Si X 5	PLLA	0,3g in 7,2 ml Dioxane	New Teflon Reactor	10±1°C (Al) (-30 set) - Fatta taratura a due terminali - In livella	20h	3 days
T51 e bis	PLLA	0,15g in 3,6 ml Dioxane	Small Teflon beaker	-10±1°C (Al) (-30 set) - Fatta taratura a tre terminali - Asciugato l'holder di Al	20h	4 days
TIPS Si X 6	PLLA	0,3g in 7,2 ml Dioxane	New Teflon Reactor	10±1°C (Al) (-30 set) - Fatta taratura a due terminali - In livella	20h	3 days
T52 e bis	PLLA	0,15g in 3,6 ml Dioxane	Small Teflon beaker	-5±1°C (Al) (-20 set) - Fatta taratura a tre terminali - Asciugato l'holder di Al	20h	4 days

T53 e bis	PLLA	0,15g in 3,6 ml Dioxane	Small Teflon beaker	0±1°C (Al) (-10 set) - Fatta taratura a tre terminali - Asciugato l'holder di Al	20h	4 days
T54 e bis	PLLA	0,15g in 3,6 ml Dioxane	Small Teflon beaker	-20±1°C (Al) (-40 set) - Fatta taratura a tre terminali - Asciugato l'holder di Al	20h	4 days
T55 e bis	PLLA	0,10g in 3,6 ml Dioxane	Small Teflon beaker	-8±1°C (Al) (-30 set) - Fatta taratura a tre terminali - Asciugato l'holder di Al	20h	4 days
T55' e bis	PLLA	0,10g in 3,6 ml Dioxane	Small Teflon beaker	-10±1°C (Al) (-30 set) - Fatta taratura a due terminali - In livella	20h	4 days
T37' e bis	PLLA	0,15g in 3,6 ml Dioxane	Small Teflon beaker	-10±1°C (Al) (-30 set) - Fatta taratura a due terminali - In livella	16h	4 days
T42' e bis	PLLA	0,15g in 3,6 ml Dioxane	Small Teflon beaker	-10±1°C (Al) (-30 set) - Fatta taratura a due terminali - In livella	32h	4 days
T47' e bis	PLLA	0,15g in 3,6 ml Dioxane	Small Teflon beaker	-10±1°C (Al) (-30 set) - Fatta taratura a due terminali - In livella	20h	4 days
TIPS Si X 7	PLLA/CeO_2	0,3g in 7,2 ml Dioxane with dispersed CeO_2	New Teflon Reactor	-10±1°C (Al) (-30 set) - Fatta taratura a due terminali - In livella	20h	4 days

Tab.3.1.5.1: Realized scaffolds list

3.1.6 Design of lithographic mask

One of the reasons why we chose to use a silicon wafer as the bottom of the mold in the new reactor (§3.1.3) is because of the possibility of developing a lithographic pattern on it.

The structure of the scaffold that we pursue is given by the dissolution of the polymer solvent, after that this is frozen. The solvent crystallize with the mechanism of formation and the shape of dendrites.

With this lithographic pattern we tried to trigger the formation of an organized pattern of dendrites in the chilling sample to obtain a better structure of the scaffold that could be more suitable for cells.

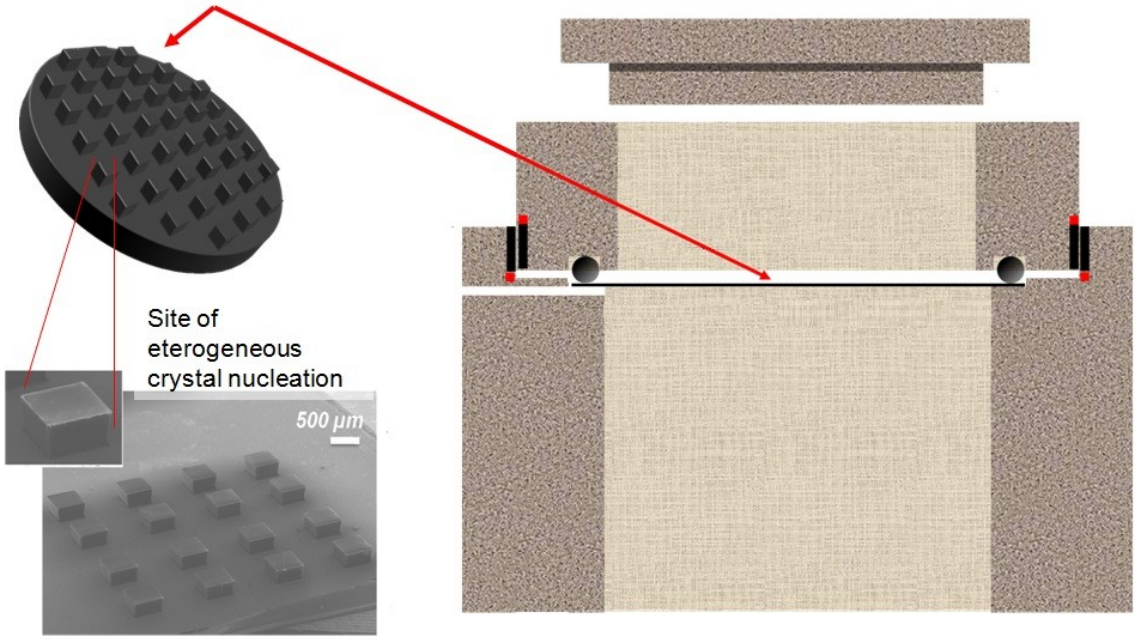

Fig. 3.1.6.1: Scheme of the photolithographic pattern for the reactor

After producing a good amount of scaffolds, the dimensions and distances between near pore channels has been analyzed thus has been decided to realize a photolithographic mask structured as in Fig.3.1.6.2 a) and b).

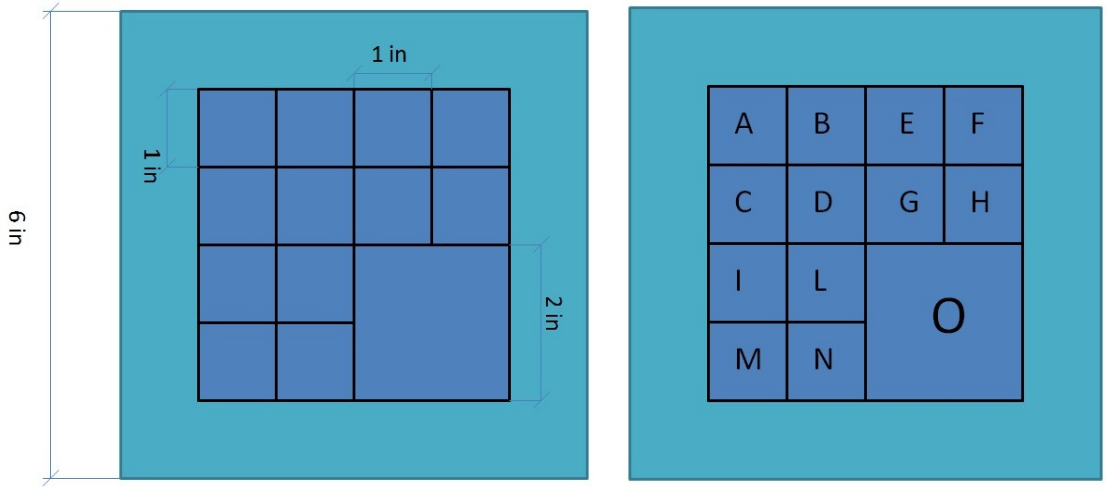

(a) (b)

Fig. 3.1.6.2: Scheme of the photolithographic mask; a) dimensions, b) pattern subdivision

We designed various patterns to obtain square pillars with different size of the square side and different distance between the center of the squares.

Some of the patterns are positive to obtain wells instead of pillars (used photo-resist is negative).
We also designed one pattern with a cross shape to mimic the dendrite shape.

Match between patterns:

- Influence of pillar size:
  - A,B and D
  - L and M
- Influence of the shape: - B and C
- Influence of the spacing:
  - A,I,M and N
  - B and L
- Influence between P/N:
  - A and G
  - B and E
  - F and L
  - D and H

.

The pattern design is explained in Tab.3.1.6.1

Letter	Side [μm]	Spacing [μm] (from center to center)	Positive / Negative	Shape
A	50	250	N	Square
B	100	250	N	Square
C	100	250	N	Cross
D	20	250	N	Square
E	100	250	P	Square
F	100	300	P	Square
G	50	250	P	Square
H	20	250	P	Square
I	50	150	N	Square
L	100	300	N	Square
M	50	300	N	Square
N	50	500	N	Square

Tab. 3.1.6.1: Photolithographic mask design

3.1.7 Realization of the photo mask

A small amount of SU-8 was deposited on top of the silicon wafer. Immediately after the resist has been homogeneously distributed by spin coating technique.
Spin-coating followed this path: from 0 to 3000 rpm in 5 sec, 3000 rpm constant per 30 sec, from 3000 to 5000 rpm in 1 sec, 5000 constant per 5 sec and finally from 5000 to 0 rpm in 5sec. Soft backing was run for 20 min at 45 °C.
The edges of the wafer has been trenched removing the external ring with different thickness. The exposure was held for 70 seconds at 18,8 watt.
Hard backing has been performed at 65 °C for 90 seconds and then at 90 °C for 5 minutes.
Finally, the wafer has been stirred in SU-8 developer for 15 minutes, rinsed in clean SU-8 developer for 60 seconds and dried with compressed air.

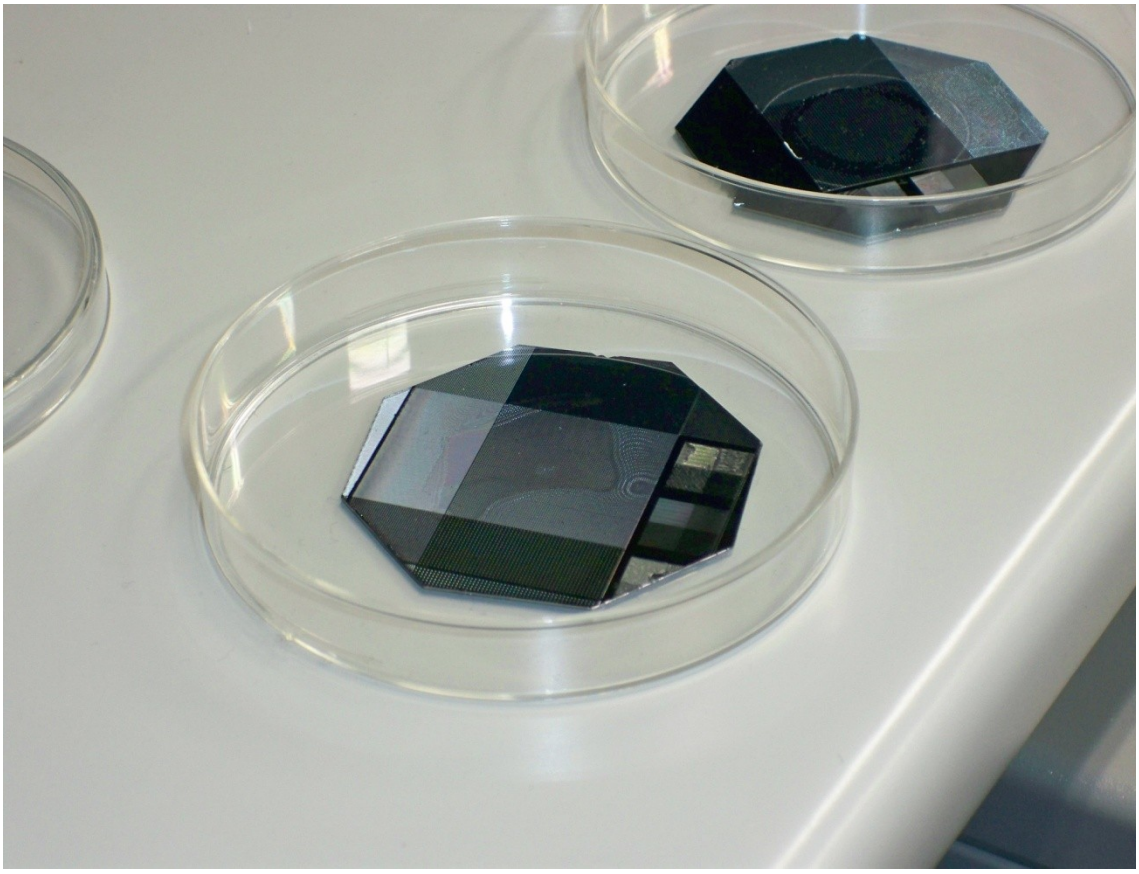

Fig. 3.1.7.1: Picture of trials of pattern N and L

3.2 Scaffolds characterization

3.2.1 Morphology and mechanical characterization

3.2.1.1 Scanning electron microscopy (SEM)

Scaffold morphology was mainly determined by optical and scanning electron microscopy (SEM) observations. The non-biologically treated scaffolds were mounted on aluminum stubs using adhesive conducting carbon tape and platinum sputtered for 40 seconds (EMITECH K500X, United Kingdom), prior to be observed in a field-emission scanning electron microscope (FE-SEM, HITACHI HIGH SU8000, Japan; FE-SEM, HITACHI HIGH S4800, Japan) operating at acceleration voltages of 1 ÷ 10 KV. Once cell seeded, PLLA scaffolds were subdued to cell fixation and dehydration prior to SEM investigation, to avoid damage of the UH vacuum chamber of the microscope. Briefly, cells were fixed by covering the scaffold with glutaraldeide (GA) 2,5% in self made phosphate buffer (PB) 0,1 M at pH 7.2 for 2 h and then washed several times in PB. The construct was further washed in PB and subsequently kept in PB-EtOH solution at increasing EtOH concentrations from 30% to 100%. Once dried in air, the sample was finally ready for metallization.

3.2.1.2 Compression test

Scaffold mechanical properties were investigated by means of compression testing. The main round sample was cut into cubes of 5-6 mm edge, being the pore channels side oriented either along or perpendicular to the sample holder. The cubes were mounted on a EZ-S 500N (SHIMADZU, Japan) universal tensile tester, inside an environmental chamber (CHROMO CHAMBER M-600FN, TAITEC, Japan) set at 37°C and compressed at speed rate of 3 $mm \cdot min^{-1}$. For each test, the tensile strength was normalized to the average sectional area of the relative sample. For each sample, the compression modulus (E) was obtained by averaging the measurements performed in triplicate or quadruplicate, being E derived from the elastic portion of the compression diagram in each measurement. Data plot and fitting were made using Microcal Origin 8.0 software.

Fig. 3.2.1.2.1: Utilized compression test machine

3.2.1.3 Porosity measurements

The procedure used to measure porosity is described in §2.4

3.2.2 Biological validation

The biological validation of the scaffolds was performed by two different techniques. In a first attempt, the cells were seeded onto 3D scaffolds using a novel, vacuum-based technique aimed at obtaining inner layer perfusion, while in a second set of experiments, thin scaffold sections were obtained by cryostat processing and then seeded with the cells. Both procedures allowed the setup of cell cultures up to 7 days.

Fig. 3.2.2.1: Utilized cryostat

3.2.2.1 Sample preparation for cryostat

After removing the top and bottom part by cutting with a sharp blade, to obtain exposed channels on both the surfaces, the scaffold, has been gently ripped along the diameter. Then the sample has been immersed in an aqueous solution with 30% wt of sucrose solution.

Once the scaffold had sunk in the solution, it could be treated to obtain a suitable sample for the cryostat.

A small dewar has been filled with a small quantity of grinded dry ice and hexane. The scaffold has been placed on a small plate ladle with a small quantity of solution and put in contact with the surface of the melting dry ice.

After freezing, the sample has been moved inside of rectangular shape metal ladle and covered with OCT (Optimal Cutting Temperature compound), immersed again in the dry ice and, when frozen, moved on top of the sample holder, previously covered with a layer of OCT, and placed inside the cryostat (Fig.3.2.2.1.1) (LEICA, Germany), kept at the fixed temperature of -20 °C to avoid re-melting of the including agent .

In order to obtain a more stable attachment of the sample to the holder, a small metal cold weight is pressed against the sample during the OCT hardening.
When the sample froze it has been cut in slices of 60 μm of thickness. The slices have been placed on petri-dish or microscope slide for a firs observation.

3.2.2.2 Cell seeding on thin sections

HUVEC and Vybrant-stained hMSC were co-cultured in EBM-2 medium onto poly-styrene dishes or onto TIPS scaffold sections for 7 days. At this timepoint, the cells were washed twice in sterile PBS and fixed with a solution containing paraformaldehyde (PFA, concentration 4% in PBS) for 30 minutes at 4°C.

Subsequently, cell membrane was permeabilized with TRITON X-100 (SIGMA-Aldrich, Concorezzo, Italy) for 2 minutes, washed twice in PBS and incubated with 5% Bovine Serum Albumin (BSA) to avoid unspecific antibody staining.

3.2.2.3 Sample preparation for 3D cell seeding

The scaffold has been cut with a sharp blade removing the top and bottom part exposing the pore channels. Afterwards, it has been washed several times with ethanol, sterilized by UV light for 5 minutes per side and soaked in sterile cell medium at 37°C, 5% CO_2.

3.2.2.4 3D Cell seeding

To achieve complete scaffold colonization, Vybrant-stained hMSC and HUVEC were forced to enter scaffold inner layers using a vacuum-based technique. Cells can access the inner part of the scaffold directly from the axial pores or by sliding through the surface ends of the lateral branches. However, as shown schematically in Fig.3.2.2.4.1, the infiltration process can be very different if performed from the bottom or the top scaffold surface, given the oriented fishbone structure of the pores. Referring to the fishbone cross section, the two possible mechanisms proposed are

visually described in Fig.3.2.2.4.1. When cells are forced within the scaffold from the top side, the surface terminal lamellae act like a multi-funneled structure, whose effect is to convoy the cell flux mainly into the vertical channels (Fig.3.2.2.4.1(a)). When cells are infiltrated from the bottom side (Fig.3.2.2.4.1(b)), the reverse-funnel configuration facilitates cell migration from the backbone channels to the side branches, leading to a more uniform cell distribution within the construct. Therefore, to improve an even cell distribution, the scaffold was positioned with its back face adjacent to the syringe inlet, both during normalization and seeding steps.

3D dTIPS scaffold was positioned in a plastic syringe and locked by mean of PTFE rings.

3D co-culture onto TIPS scaffolds was performed in EBM-2 medium for 7 days. At this timepoint, the cells were washed twice in sterile PBS and fixed with a solution containing paraformaldehyde (PFA, concentration 4% in PBS) for 30 minutes at 4°C.

Subsequently, cell membrane was permeabilized with TRITON X-100 (SIGMA-Aldrich, COncorezzo, Italy) for 2 minutes and incubated with 5% Bovine Serum Albumin (BSA) to avoid unspecific antibody staining.

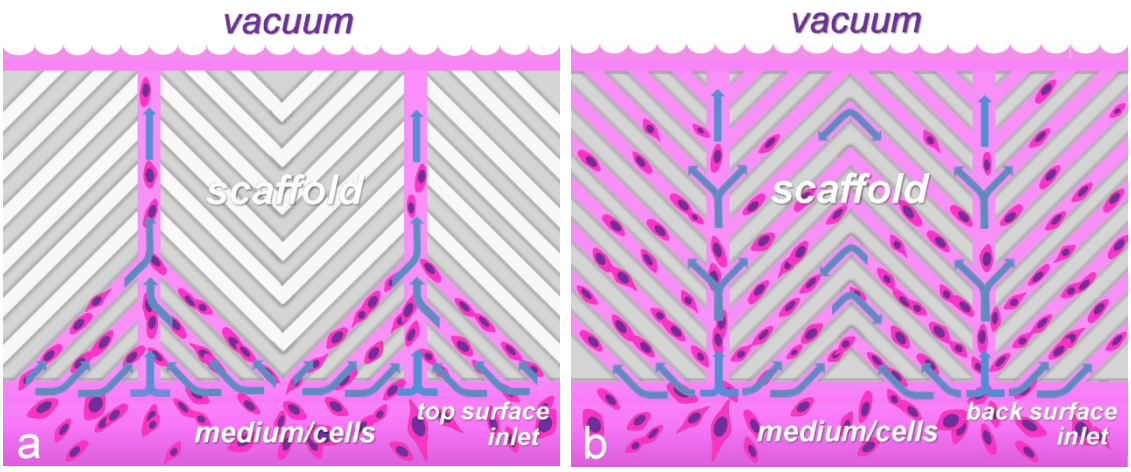

(a) (b)

Fig. 3.2.2.4.1: Schematics of cellular infiltration mechanisms upon the application of a pressure gradient: (a) top surface inlet, (b) back surface inlet.

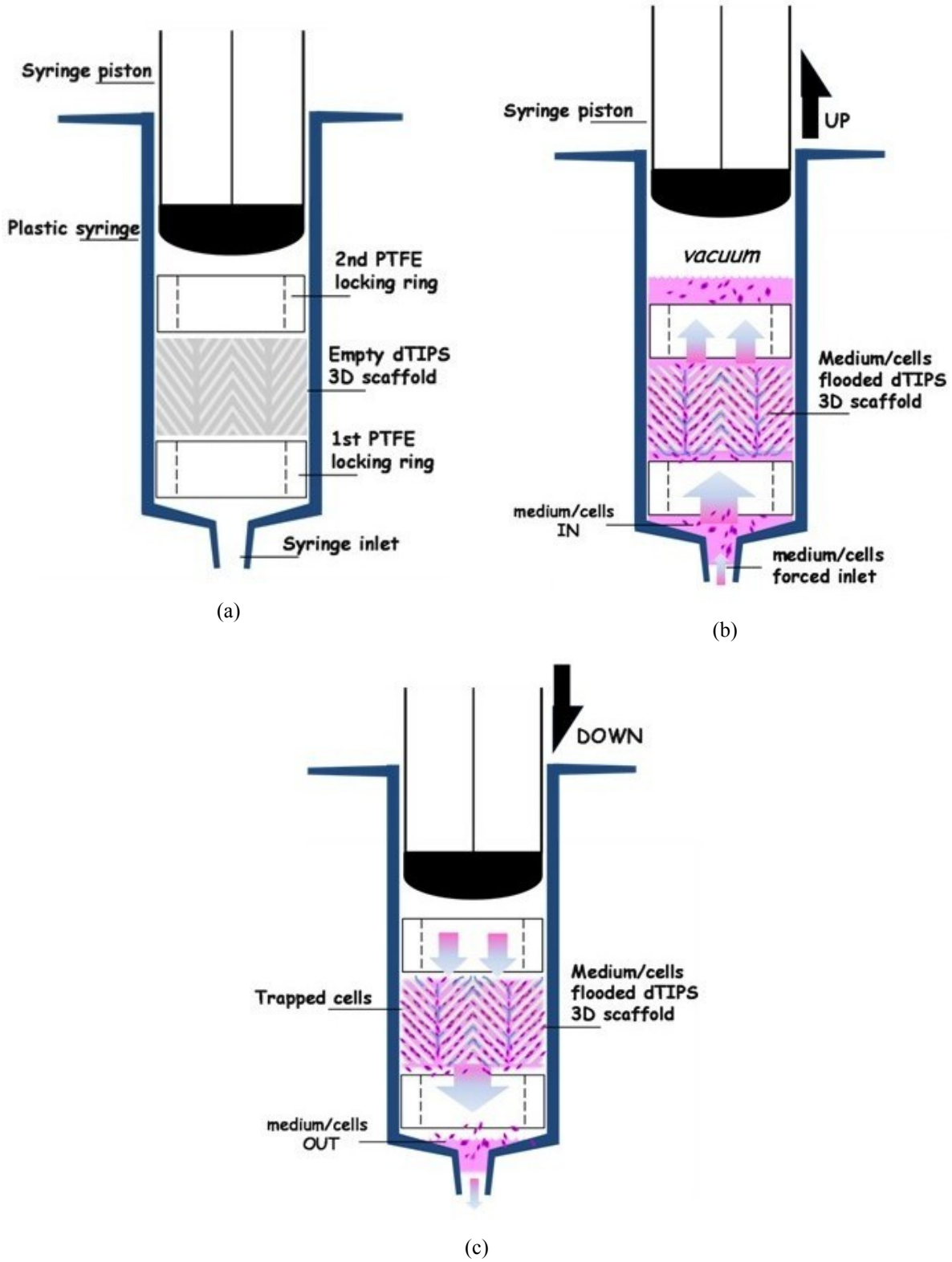

Fig. 3.2.2.4.2: Scheme of the syringe cell seeding procedure: a) set-up; b) aspiration; c) expulsion

In Fig.3.2.2.4.2 is represented the syringe set-up and procedure utilized for the cell seeding.

Fig.3.2.2.4.3 shows a dTIPS scaffold after 7DIV of cells culturing, after extraction from the culture dish (Fig. 3.2.2.4.3(a)) and after immersion in PFA for cell fixation.

(a) (b)

Fig. 3.2.2.4.3: Pictures of the scaffolds after cells seeding a) as extracted from the culture dish and b) soaked in PFA for cell fixation

Dark pink regions visible in both figures over the samples correspond to the cell colonized areas, whose intensity can be related to the cell density within the 3D PLLA scaffolds.

3.2.2.5 Immunofluorescence

The samples were incubated for 2 hours with primary antibodies directed against alpha smooth muscle actin (ASMA) or von Willenbrand Factor (vWF). The first antibody was intended to stain actin filaments, thus highlighting cell morphology, while the latter is directed against a protein (vWF) exclusively expressed in endothelial cells.

After massive washing in PBS, the samples were incubated with appropriate FITC-labelled secondary antibody. Nuclei were counterstained with 4',6'-diamidino-2-phenylindole (DAPI) for 2 minutes. The occurrence of specific signals was visualized under LEICA TCS-5 confocal microscope.

Chapter 4

Results and discussion

4.1 Morphological characterization

4.1.1 Scaffold structure

The processing method was directional TIPS to enhance the ordered configuration in the scaffold porosity. The scaffolds were initially fabricated by dTIPS from 6.4 wt% PLLA/dioxane solutions. The solution was put on a cold plate kept at -40°C, and thus the thermal gradient was applied from the bottom to the top of the solution free surface, in the perpendicular direction.

During the work we varied the process parameters but the structure itself didn't change. What changed were the dimensions of each part of this structure.

The scaffold's macrostructure that can be observed const of a peripheral region, bottom, external borders and sometimes external ring on the surface, of non ordered units of the microstructure and a core region of highly ordered structure.

The disorder of the peripheral region was due to the contact with the walls of the mold.

Forcing the thermal gradient to only occur in the perpendicular direction resulted in the dioxane crystals coordination into densely packed vertical arrays. After the sample reached the thermal equilibrium at -40°C, the dioxane crystals were then dissolved in an EtOH/H_2O bath at -18°C, and their fingerprints were left in the polymeric matrix.

The processing was reliable and reproducible. The resulting porosity was characterized by a long-range ordered hierarchical structure.

Fig.4.1.1.1 shows the SEM micrographs of the morphology of obtained scaffolds.

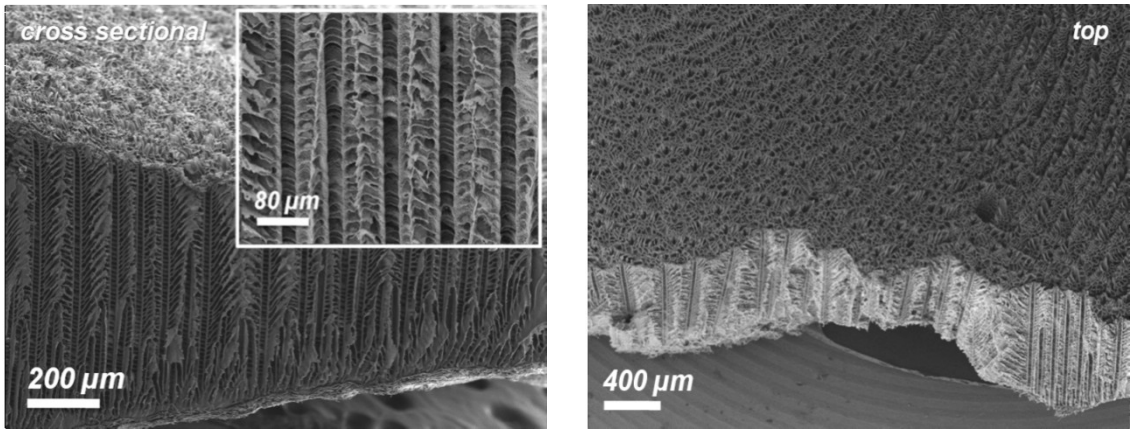

(a) (b)

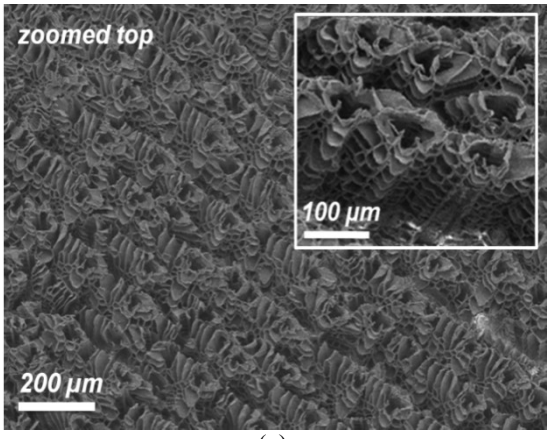

(c)

Fig.4.1.1.1: SEM micrographs of scaffolds obtained by directional TIPS carried out at -40°C onto 6.4% PLLA in 1,4 dioxane solutions: (left to right, starting from the left upper corner) a) cross sectional view; b) top view of a PLLA scaffold prepared by dTIPS, 4,5 cm in diameter and 0.6 mm thick showing the circular pore arrangement observable at the macro-scale; c) top zoomed views of surface morphology resulting from the protrusion of the lamellae on the surface

Starting from the cross sectional view (Fig.4.1.1.1 a)), one can observe an array of straight parallel channels of about 20 µm diameter (inset of Fig.4.1.1.1 a)) going across the entire scaffold thickness. Each channel exhibits side tubular branches of comparable diameter departing from the whole channel length at about 45 to 70 degrees with respect to the channel axis.

As a result, the observed cross sections assume a typical multiple fishbone-like pore arrangement, as depicted in the figure.

The holes in Fig.4.1.1.1 correspond to the top (Fig.4.1.1.1 b) and c)) surfaces channel terminations. As visible, the channel section is characterized by a three-poled stingray-like shaped section.

The pores are arranged in concentrical rows, which confer the scaffold a typical

surface fibrous texture on the 80 μm scale (Fig.4.1.1.1 b)). This peculiar arrangement is nothing but the consequence of the circular symmetry impressed by mold inner walls, which are responsible for triggering the heterogeneous nucleation of the solvent.

Finally, if we observe the fracture line shown in the picture, it is possible to notice how the tail channel density in the cross section varies depending on the fracture plane orientation. In particular, the channels appear more densely packed in fracture planes perpendicular to the pore rows (radial direction) and less dense in those tangent to the row direction.

In the case of directional TIPS, the highly ordered configuration deriving from the processing conditions allowed a rational study of the scaffold morphology. From the combined electronic and optical microscopy analysis of the samples, it was possible to model the scaffold pore architecture and identify the single repetitive pore unit.

The structure as a whole can be assumed as the stack of parallel planar fibers intimately in contact, each one representing an array of dendritic units co penetrating each other (Fig.4.1.1.2 a)).

The single pore dendrite unit is evidenced in the SEM micrograph of Fig.4.1.1.2 b) and schematized by the simplified model of Fig.4.1.1.2 c), as the superposition of a number of polymeric lamellar layers (three, in Fig.4.1.1.2 b)), whose amount depends on the scaffold thickness.

Each section of the pore unit, is constituted by three main lamellae which depart from the stingray sectioned central channel. Two of the lamellae elongate from the stingray wings in the row direction (*y* direction), towards the first neighboring pore unit, while the third one (generally shorter) departs from the stingray tail in the radial direction (*x* direction).

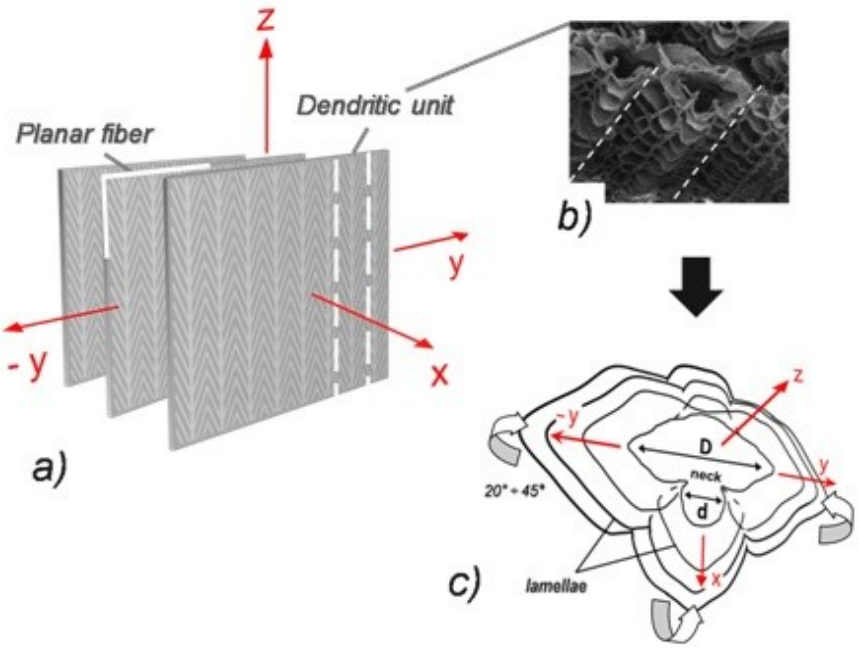

Fig:4.1.1.2: a) Exploded view of the schematics of the scaffold; b) SEM visualization of a surface terminating single PLLA dendritic unit obtained by dTIPS; c) Schematics of a three-layered segment of the unit: growth (z), in-row (y) and row-to-row (x) directions are indicated together with the 20° ÷ 45° lamellar bending.

Referring to Fig.4.1.1.2 c), the parameters *d* and *D* were defined as the diameter of the minor pole of the channel section (stingray tail), and the channel cross-sectional largest dimension (stingray wing-to-wing aperture), respectively.
The diagonal side channels observed in Fig.4.1.1.1 a) correspond to the inter-space between two adjacent lamellae in the vertical direction *z*. In this case their diameter is about 20 µm, thus comparable with *d*, but can decrease to 15 ÷ 18 µm in case of pronounced lamellar bending.

The observation of the cross sections of the dTIPS samples, constantly evidence how, at the micron scale, the fracture of the scaffold tends to occur in correspondence of the necking point of the stingray tail, thus leaving the tail channel well exposed on the section plane. The tail channel diameter corresponds to *d* and can be easily measured.

However, it must be noted that the main channel aperture *D*, which is always about three times larger than *d,* is the effective parameter that must be considered for cell accommodation evaluations.

In Fig.4.1.1.3 are reported some examples of a well ordered structure, in

Fig.4.1.1.4 instead an example of a disordered structure.

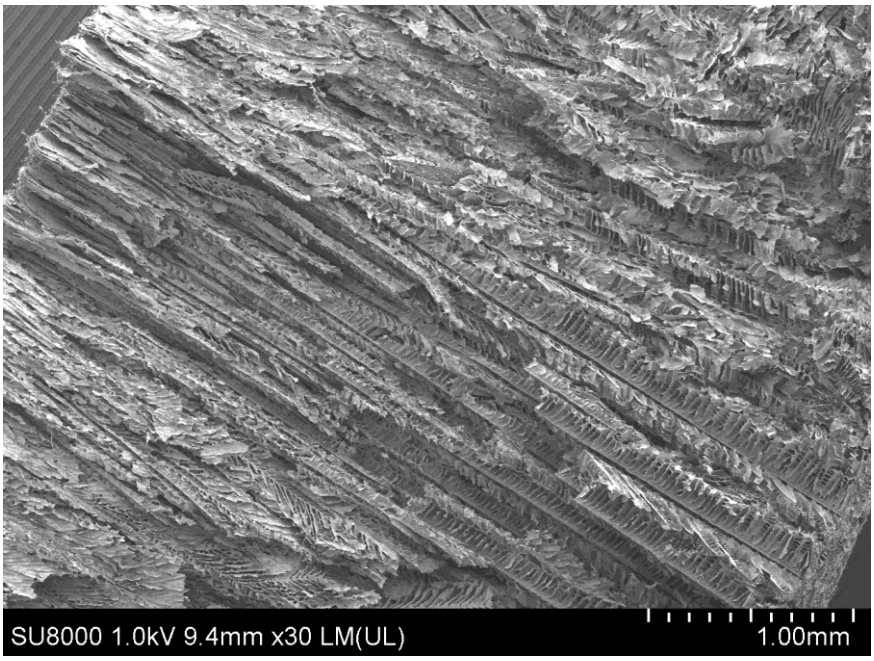

(a)

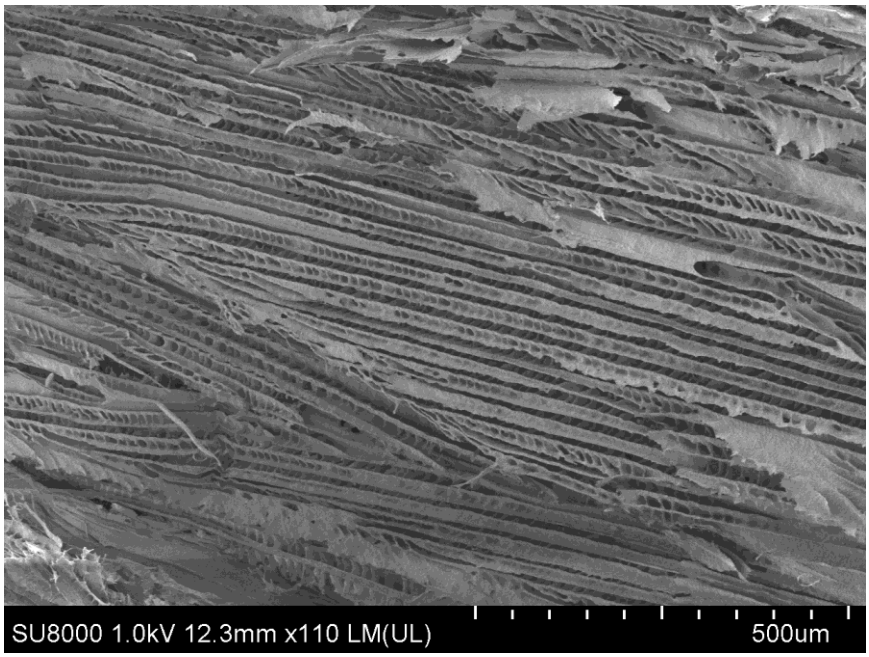

(b)

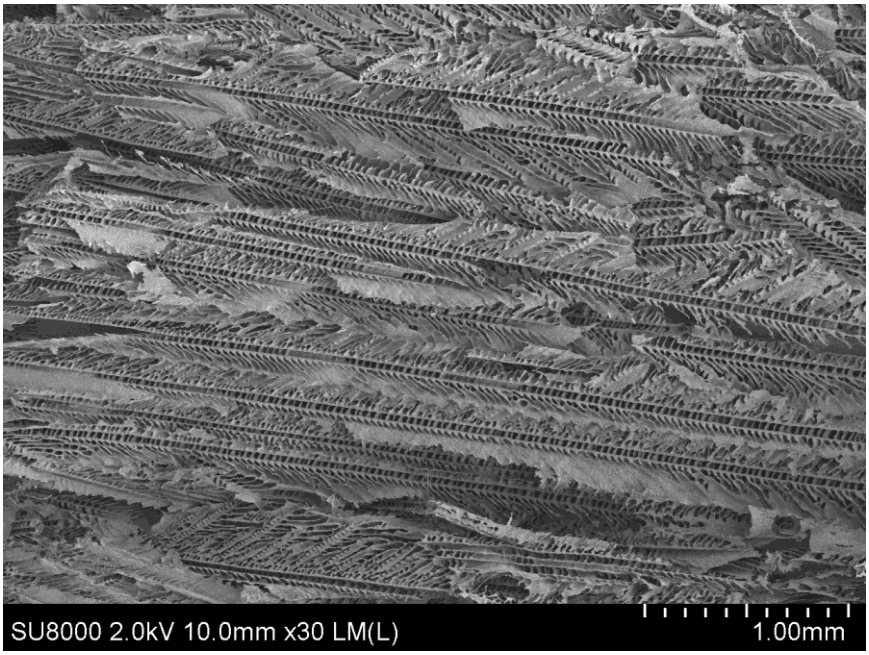

(C)

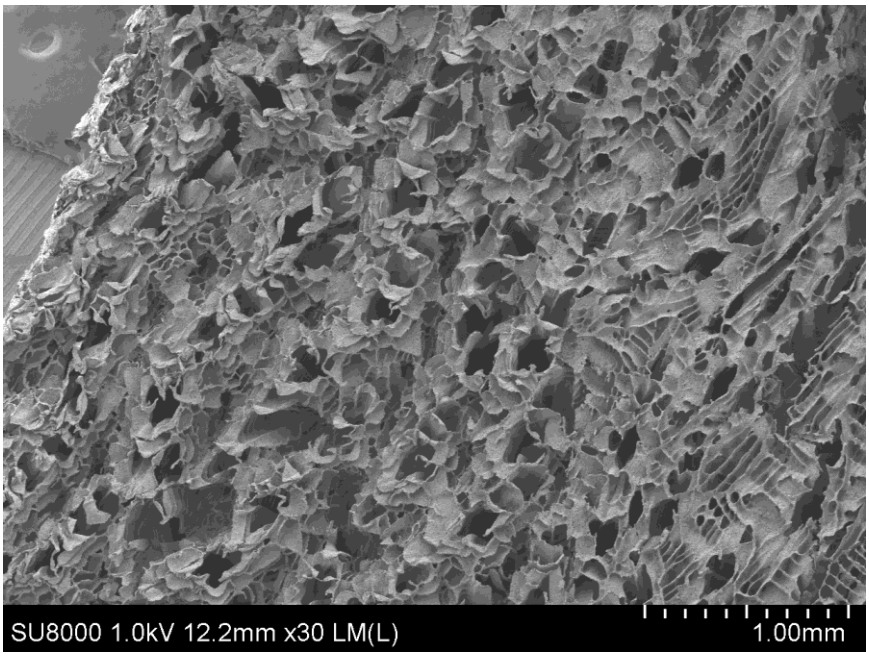

(d)

Fig.4.1.1.3: Examples of well ordered structure of dTIPS scaffolds: a) TIPS 30 cross section; b) TIPS 30 cross section; c) TIPS 39 cross section; d) TIPS Si X 2 surface

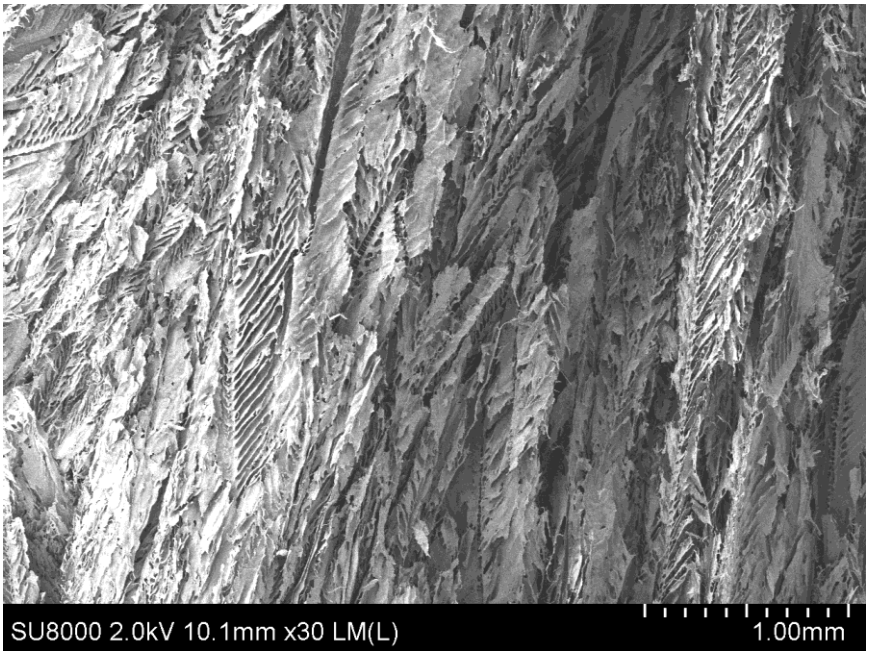

(a)

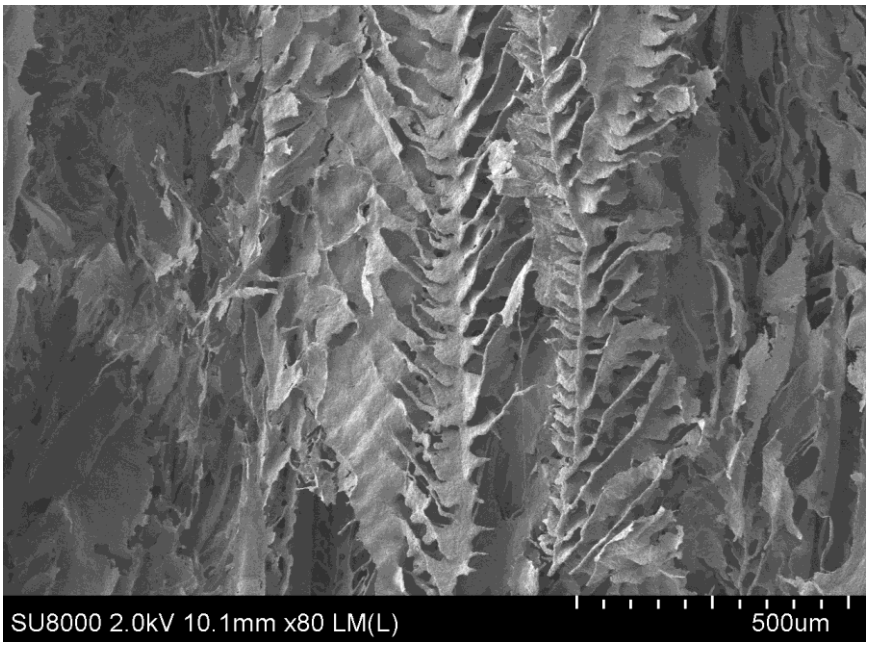

(b)

Fig.4.1.1.4: Examples of non ordered structure of dTIPS scaffolds: a) TIPS 49 cross section; b) TIPS 49 cross section

4.1.2 Porosity measurements

Porosity measurements were conducted as described in §2.4.

The porosity values found for these scaffolds are reported in Tab.4.1.2.1.

TIPS	W_s [g]	W' [g]	W'' [g]	ε_{open} [%]	ε_{tot} [%]	ε_{closed} [%]
T37'	0.03505	0.013	0.4883	94.73345	94.72658	-0.00686
T42'	0.05431	0.0156	0.7328	93.85251	94.56699	0.714477
T47	0.05209	0.017	0.7935	94.81279	95.14945	0.336659
T47'	0.04906	0.0162	0.7877	95.09119	95.38339	0.292208
T48	0.03893	0.0144	0.6332	95.43801	95.43934	0.001333
T49	0.03212	0.0122	0.6648	96.42714	96.37098	-0.05615
T50	0.02447	0.0095	0.462	96.15341	96.03928	-0.11413
T54	0.03645	0.014	0.4927	94.69668	94.57606	-0.12063
T51	0.03065	0.0114	0.4236	94.70281	94.6871	-0.01571
T52	0.0357	0.0136	0.5083	94.92188	94.83268	-0.0892
T53	0.04065	0.0101	0.5644	93.68854	94.70988	1.021341
T55	0.03054	0.0122	0.6441	96.60189	96.43554	-0.16635

Tab.4.1.2.1: Measured values of porosity of selected scaffolds obtained by dTIPS

As shown in Tab.4.1.2.1, values of total porosity settles around 94,5% ÷ 96,5% that is in line with values from other works on TIPS scaffold in bibliography.

Open porosity values are ,almost in every case, bigger than total porosity, that of course is not possible.

This error is due to air micro bubbles trapped under the scaffold during the W' measurements.

This is a clear sign of the really good interconnection of the porosity in the scaffolds and, with a good approximation is possible to affirm that open porosity assets around 97% ÷ 98% of the total porosity.

Therefore close porosity must be the remaining 2% ÷ 3%.

4.2 Mechanical characterization

The mechanical properties of dTIPS scaffolds made during this work have been obtained by mean of compression test.

The scaffolds has been cut into cubes of approximately 5 mm of side and then subjected to compression.

The compression has been actuated both in the direction of the pore channels and in the direction perpendicular to them.

An example of the mechanical behavior of the scaffolds in reported in Fig.4.2.1 and Fig.4.2.2.

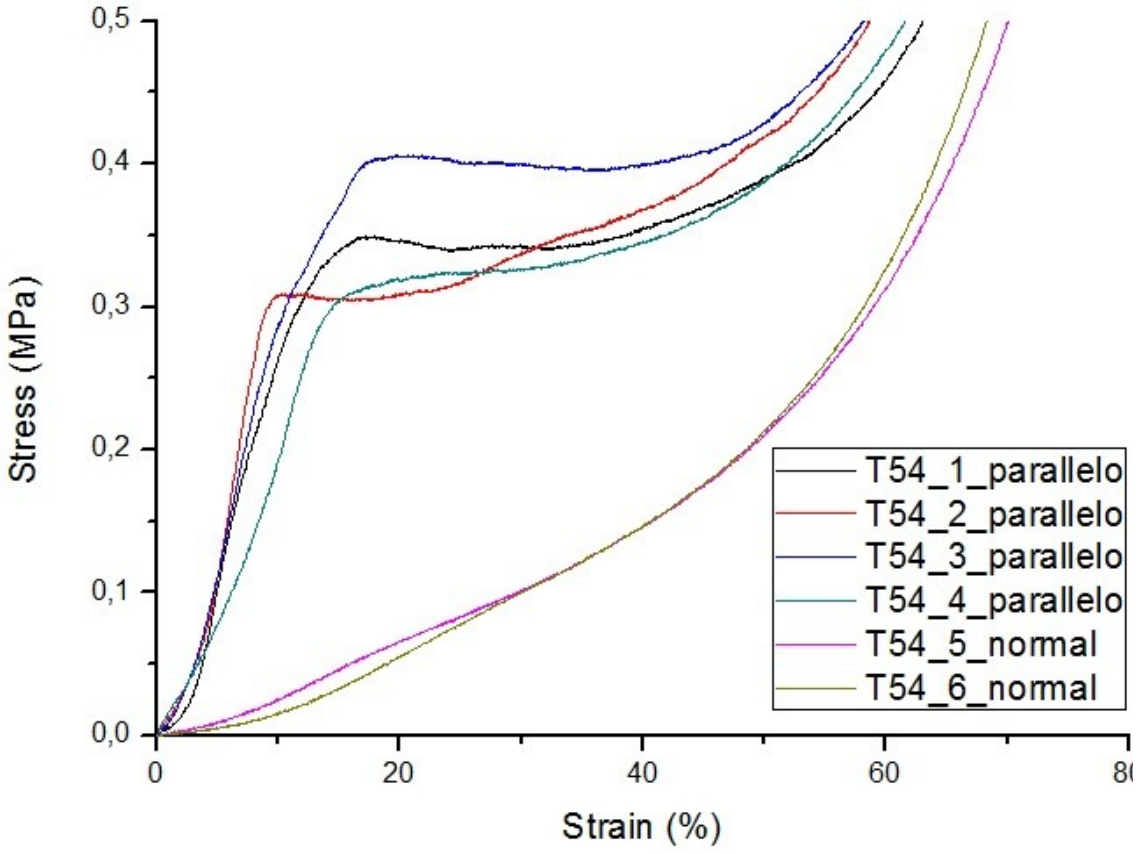

Fig.4.2.1: Stress-strain graphs of TIPS 54 in channel direction and perpendicular to channel direction

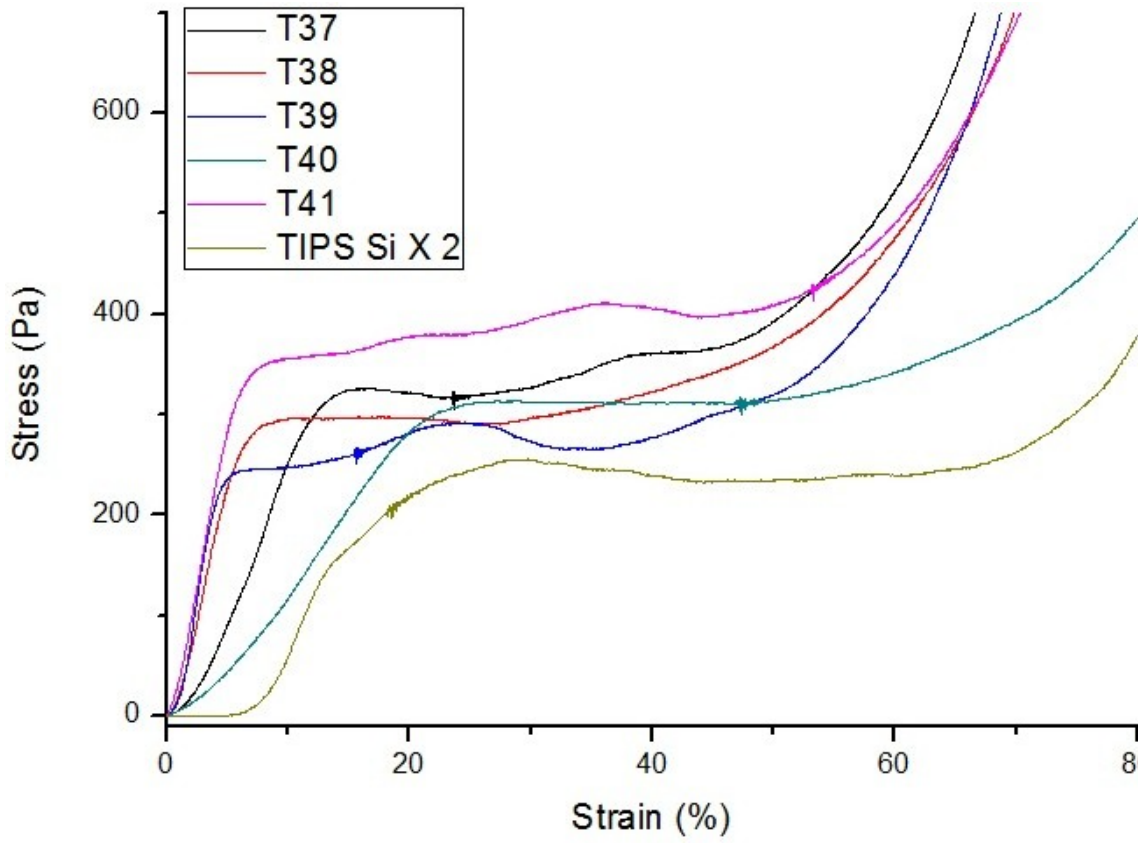

Fig.4.2.2: Stress-strain graphs of TIPS 37, TIPS 38, TIPS 39, TIPS 40, TIPS 41 and TIPS Si X 2 in channel direction

From Stress-strain graphs is possible to notice how the behavior of dTIPS scaffolds aligns with the behavior of cellular materials.
It's quite easy to recognize a first linear elastic deformation, a plateau and the final densification.

Estimations of the Young's modulus have been made possible through the analysis of the Stress-strain curves as shown in Fig.4.2.3.
Multiple samples of the same scaffold have been tested and arithmetical means have been calculated from the obtained values.
Calculated values of dTIPS scaffolds Young's modulus along the channel direction have been reported in Tab.4.2.1.

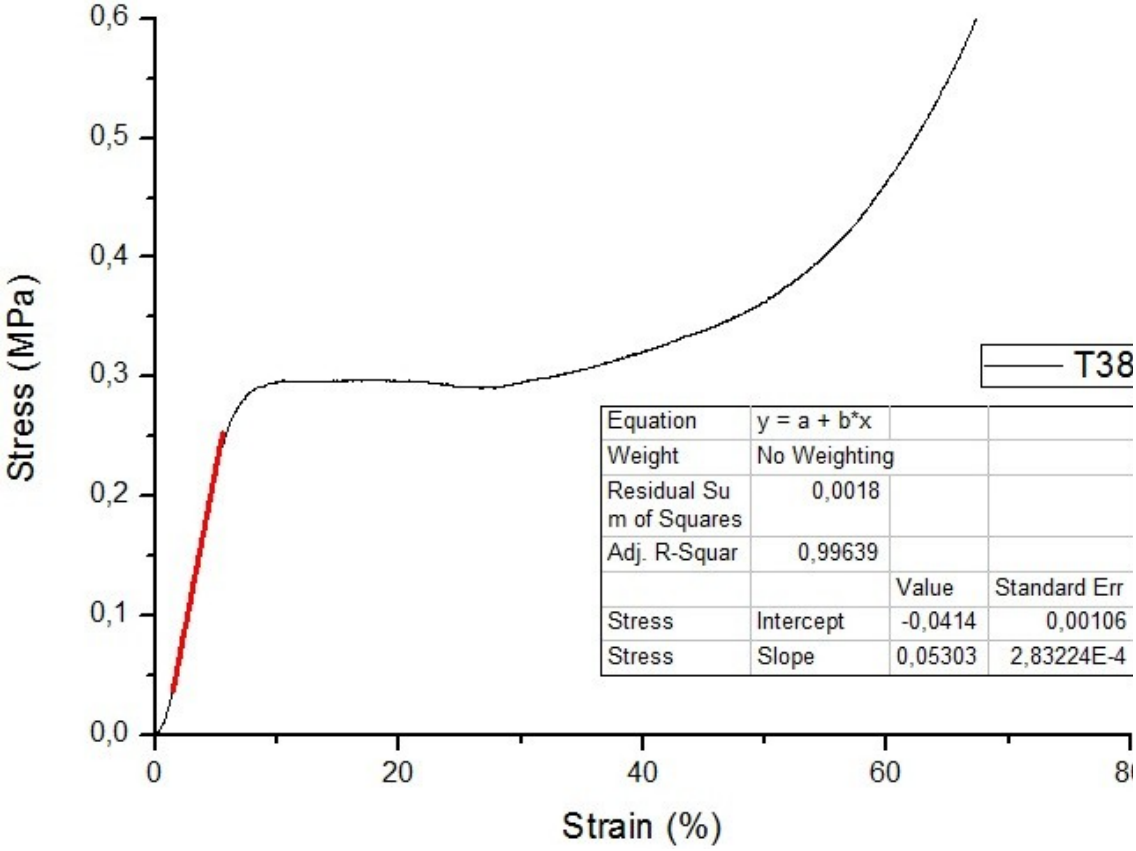

Fig.4.2.3: Linear fitting of the stress-strain curve of TIPS 38 along the direction of the channels

NAME	Young's modulus [MPa]	NAME	Young's modulus [MPa]
T37'	2.93	**T47**	1.99
T38	5.3	**T51**	3
T39	6.79	**T52**	2.5
T40	2.05	**T53**	2.89
T41	6.62	**T54**	3.22
Tsi X2	3.41		

Tab.4.2.1: Calculated values of dTIPS's Young's modulus of selected scaffolds along channel direction

Young's modulus values calculated for dTIPS scaffold assets between values of 2 MPa and 7 MPa. These values are in line with other works on TIPS scaffolds reported in bibliography.

4.3 Influence of process parameters variation

4.3.1 Influence of the chilling temperature

The effect of chilling temperature has been observed by mean of changes in morphology, porosity and mechanical properties.

In Fig.4.3.1.1 the behavior of total porosity in function of the chilling temperature is presented.

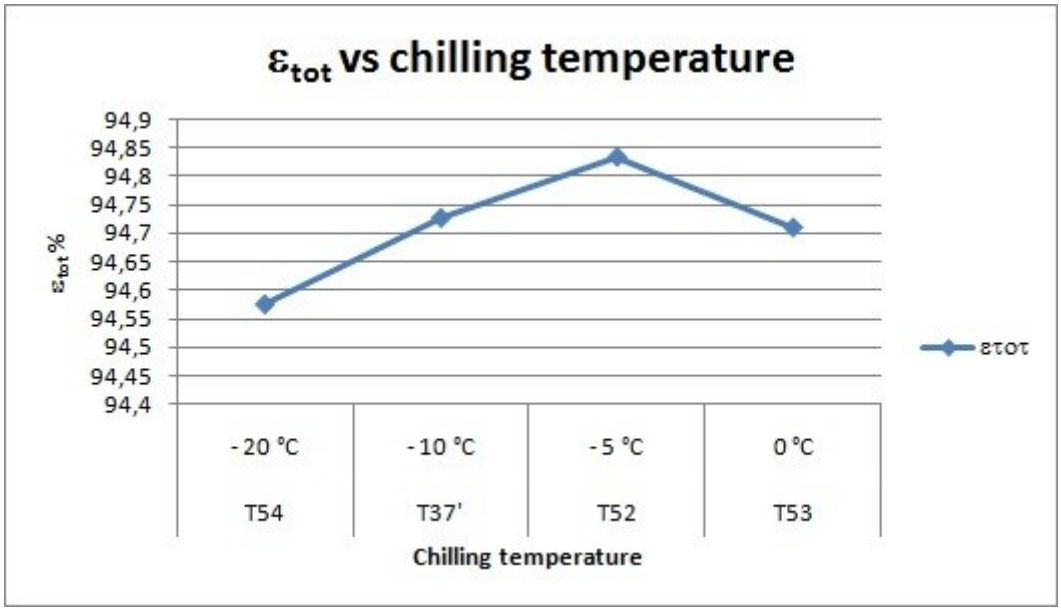

Fig.4.3.1.1: Total porosity trend in function of chilling temperature

As shown in Fig.4.3.1.1, the slight variation of porosity is not enough to be considered significant even if an increase of porosity with of the chilling temperature can be noticed.

As previously mentioned, the mechanism of formation of the porosity results in dendrite-like cavities, which are the fingerprints of the crystallized solvent after leaching.

What can be expected from such mechanism is the formation of a larger microstructure with the increase of the temperature.

This phenomenon is clearly showed in Fig.4.3.1.2 and Fig.4.3.1.3.

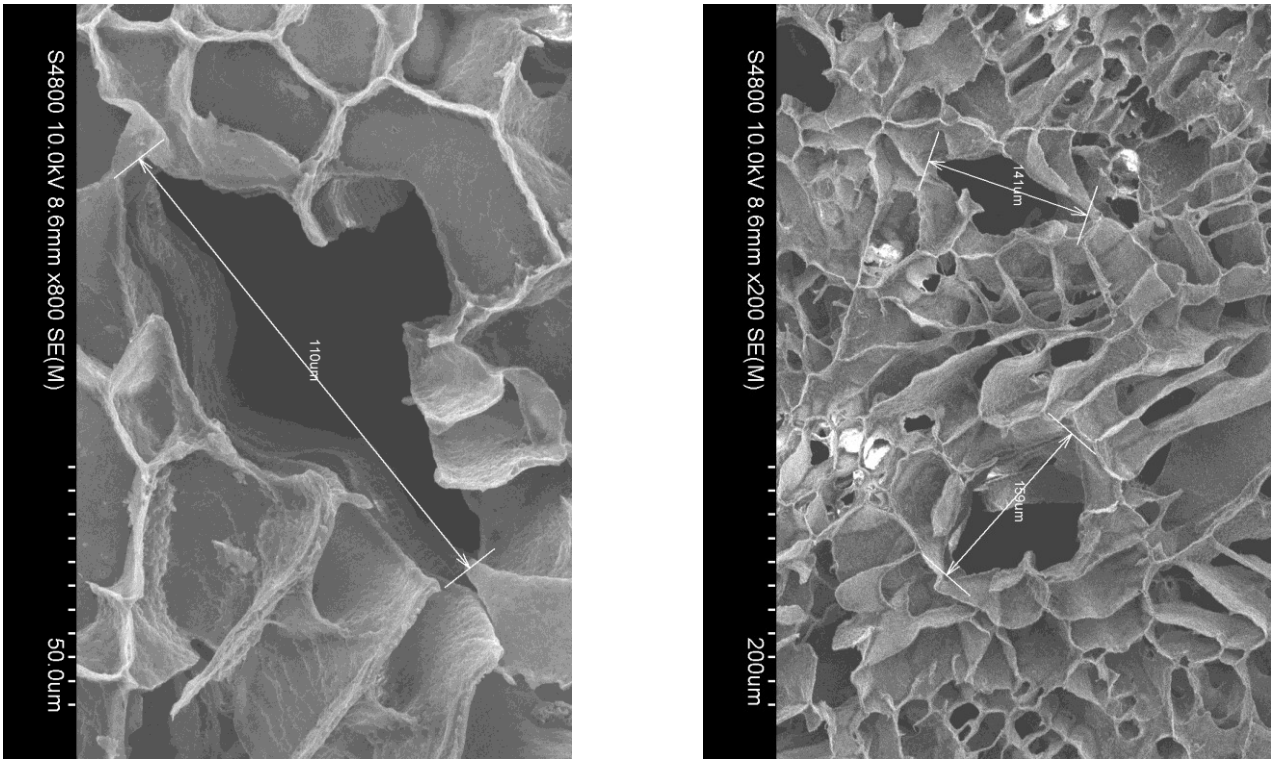

(a)

(b)

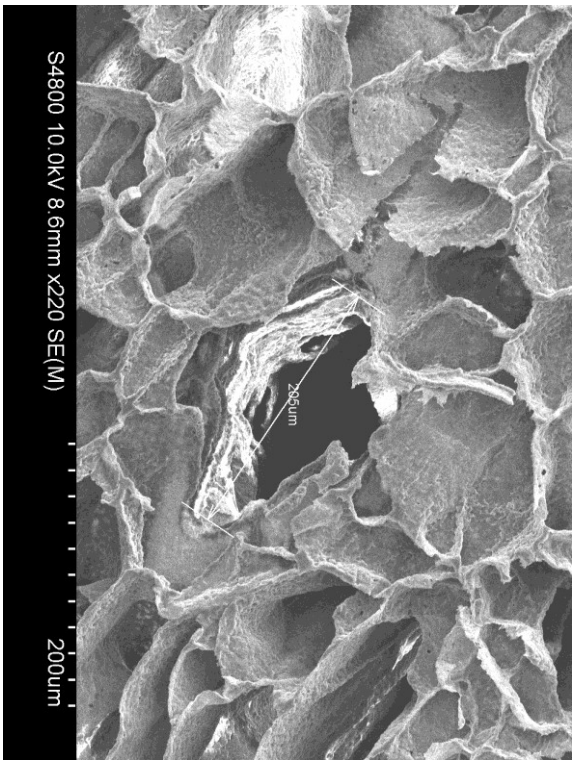

(c)

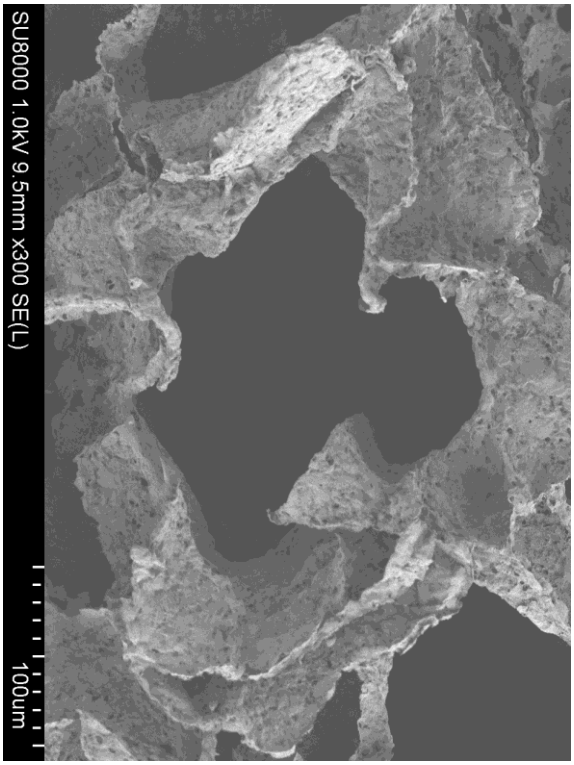

(d)

Fig:4.3.1.2: a) TIPS 54, 110 µm, -20 °C; b) TIPS 52, 150 µm, -5 °C; c) TIPS 53, 200 µm, 0 °C; d) TIPS Si X 2, 250 µm, 9 °C

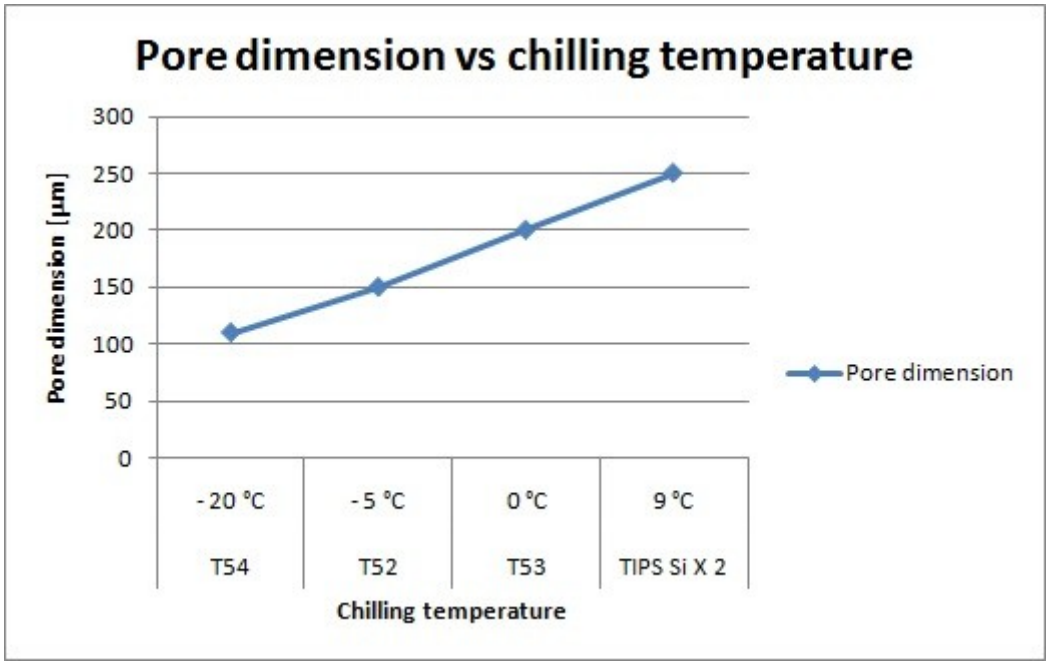

Fig.4.3.1.3: Total porosity trend in function of chilling temperature

As is clearly observable, the dimension of the pore channels increase of almost 150% going from the chilling temperature of -20 °C to 10 °C, that is just below the freezing point of 1,4-dioxane.

In Fig.4.3.1.4, the behavior of the Young's modulus in function of the chilling temperature is shown.

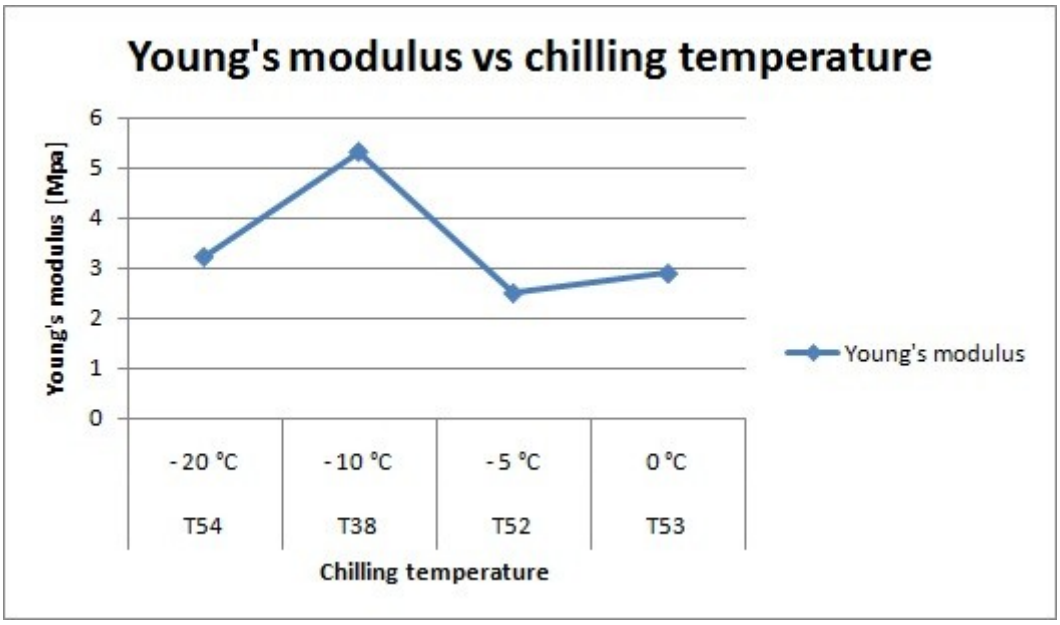

Fig.4.3.1.4: Young's modulus trend in function of chilling temperature

The chilling temperature appears not to have significant influence on scaffolds' mechanical properties or at least it was not possible to find any simple correlation between these two parameters.

4.3.2 Influence of the chilling time

The effect of chilling time has been observed by mean of porosity measurements and mechanical properties.

In Fig.4.3.2.1, the behavior of total porosity in function of the chilling temperature is presented.

As shown in Fig.4.3.2.1, even in this case, variation of porosity as function of the chilling time is slight or not significant within the range considered.

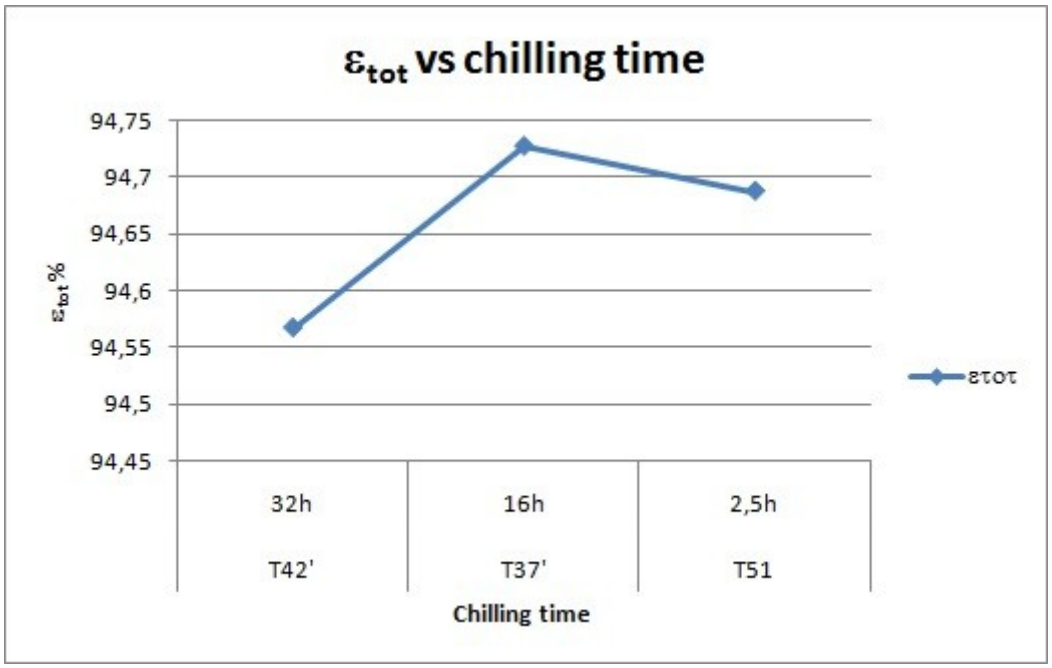

Fig.4.3.2.1: Total porosity trend in function of chilling time

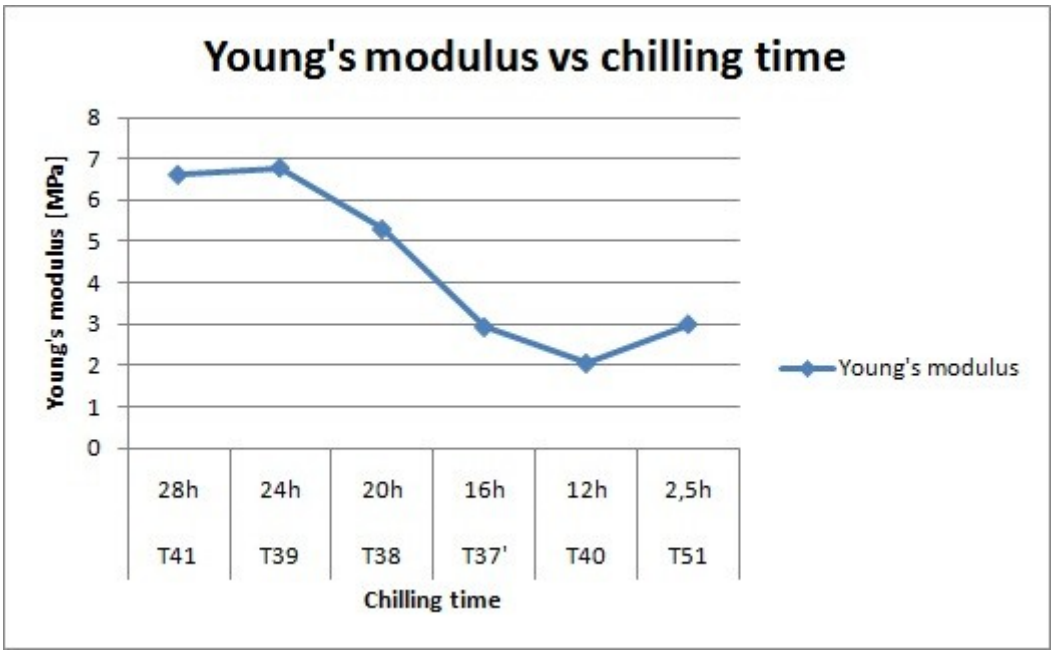

Fig.4.3.2.1: Young's modulus trend in function of chilling time

The variation in the porosity values as a function of the chilling time, was also found to be extremely is low in comparison to other works. Nevertheless, a deep difference in the pore size was observed between the samples obtained after 2,5h.

In Fig.4.3.2.1 is reported the behavior of the Young's modulus in function of a decreasing chilling time.

The values of Young's modulus vary in a range from 2 MPa to 7 MPa in accordance with values in other works on TIPS scaffolds.

A clear increase of the elastic modulus is observed with the increase of the chilling time.

This trend has to be imputed to the longer time at disposition for the expulsion of polymer, inside the solvent solution, during the freezing. The more polymer expelled the more the walls of the channel are micro-porosity free. Moreover, a prolonged expulsion of polymer causes the restriction of the pore lumen, accompanied by a thickening of the pore walls and thus an overall increase of the mechanical strength.

4.3.3 Influence of the leaching time

The optimization of the leaching time parameter resulted very difficult and in the end impossible.

During this work we tried to reduce the original chilling time of 4 days but it quickly appeared impossible to find a repeatable time for good results.

The most influent factor was the mold type utilized. The small beaker and the three geometric new molds (circle, square, hexagon) have a fixed bottom, so the diffusion of the EtOH aqueous solution during the leaching happened only from the top of the mold.

This fact, most of the times, made impossible the extraction of the scaffolds from the molds, extending the leaching time and creating a concentration gradient of dioxane inside the scaffold.

Forcing the extraction when the scaffold was still partially frozen always led to the damaging of the scaffold itself.

As show in Fig.4.3.3.1 this could happen by ripping the frozen part from the defrosted part or, in the worst case, by the re-dissolution of the polymer in the dioxane high

concentration region that led to a shrinkage of the structure and the loss of micro-structural order.

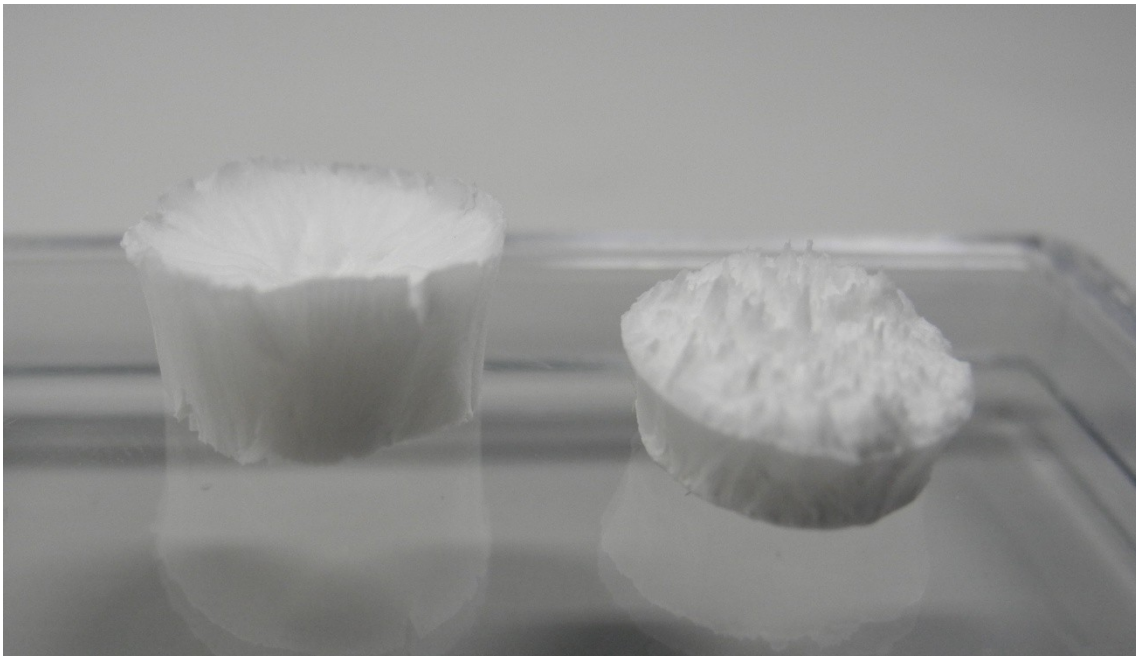

Fig.4.3.3.1: Damaged scaffold after premature extraction from small beaker mold

The leaching time for these two types of molds varied from 6 to 3 days.
With the new reactor, the leaching process is sensibly shorter respect to the other to types.
This fact it's due to the possibility of removing the bottom part of the reactor and so permitting the diffusion of the EtOH aqueous solution from both the top and bottom surfaces.
An average leaching time with the reactor assets around 2 days.

4.3.4 Polymer concentration

The effect of the polymer concentration has been observed by mean of porosity measurements.

In Fig.4.3.4.1 is presented the behavior of total porosity in function of the polymer concentration.

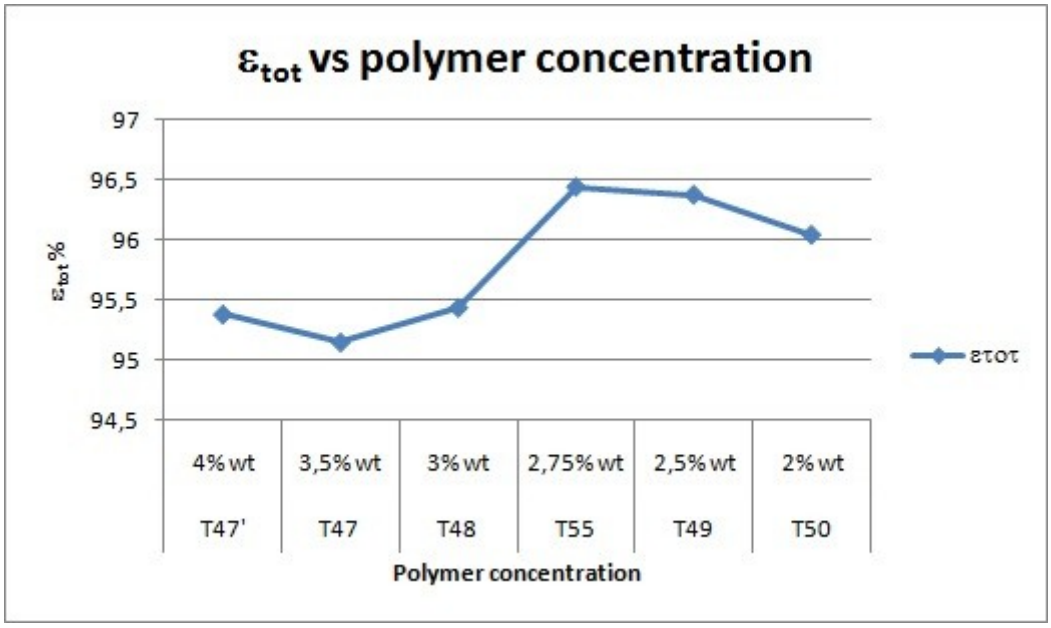

Fig.4.3.4.1: Total porosity trend in function of the polymer concentration

With respect to the PLLA wt% range here investigated, the values are in good accordance with literature values acquired at similar thermal conditions.

The slight differences in the porosity values registered for the different samples (within 0.1%) are to be addressed to the very low concentration range explored in the work as compared to analogous works.

Despite the small values variation is still possible to advise a decreasing trend of the total porosity with the rise of polymer concentration.

This is totally comprehensible if we consider that for the same solution volume, an increase of the amount of polymer implies a reduction of the solvent content, and thus a reduction of the void content after leaching.

4.3.5 Mold geometry

As described in §4.3.3 the mold geometry highly affects the efficiency of the leaching process. Depending on the possibility of opening the bottom of the mold the leaching process is shortened or extended.

Another crucial factor that we observed was the facilitation of the formation of an ordered structure.

What we noticed was that both the circular molds (small beaker and circular mold with increased area), and in less measure the square mold promote the ordered structure formation.

The hexagonal mold instead, showed a low attitude at favoring the formation of any ordered structure.

Fig.4.3.4.1 shows two examples of non ordered structures obtained with the hexagonal mold.

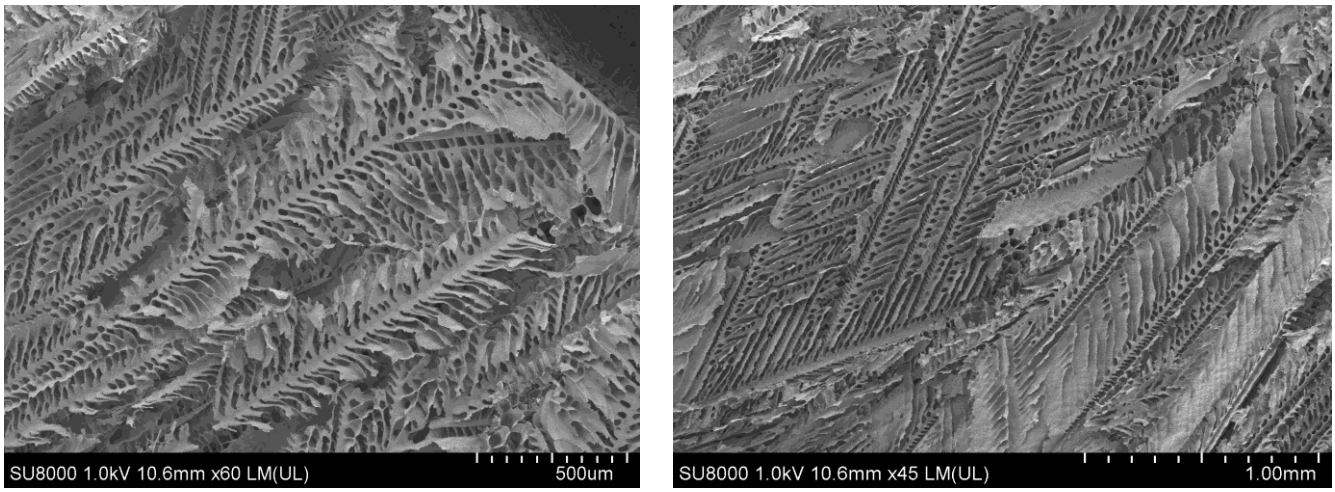

(a) (b)

Fig:4.3.1.2: a) TIPS 30 C cross section; b) TIPS 30 C cross section

The best results have been obtained with the new reactor. Both the possibility of removing the bottom and the improved thermal insulation helped in the obtaining of a very well ordered structure.

4.4 Biological validation

4.4.1 Preparation of hMSC / HUVEC co-culture as stem cell differentiation system in standard poly-styrene dishes

Before setting up three-dimensional co-cultures, human Mesenchymal Stem Cells (hMSC) and human Umbilical Vein Endothelial Cells (HUVEC) were co-cultured in Endothelial Basal Medium 2 (EBM-2) onto standard culture poly-styrene dishes. Preliminary experiments showed that it was indeed possible to distinguish red-labelled hMSC and HUVEC on the basis of alpha smooth muscle actin (αSMA, green), which is expressed in both cell types (Fig.4.4.1.1) and von Willenbrand Factor (vWF, green) which is known as an esclusive endothelial cell marker.

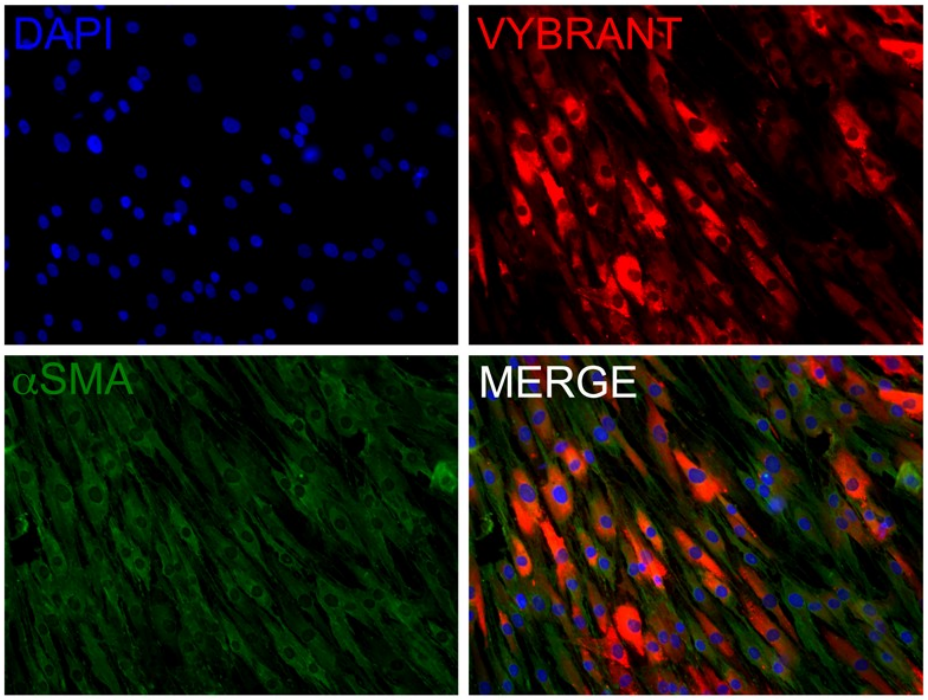

Fig:4.4.1.1: Setup of co-culture differentiation system between hMSC and HUVEC cells: Alpha smooth muscle actin (green) expression in vybrant hMSC (red) and human umbilical vein endothelial cells, co-cultured in standard conditions. Nuclei are counterstained in blue. The picture shows the cytoskeleton arrangement in the two human cell types tested

Seven day co-culture in standard dishes demonstrate that hMSC acquire vWF expression when co-cultured with HUVEC cells in EBM-2 medium (Fig.4.4.1.2).

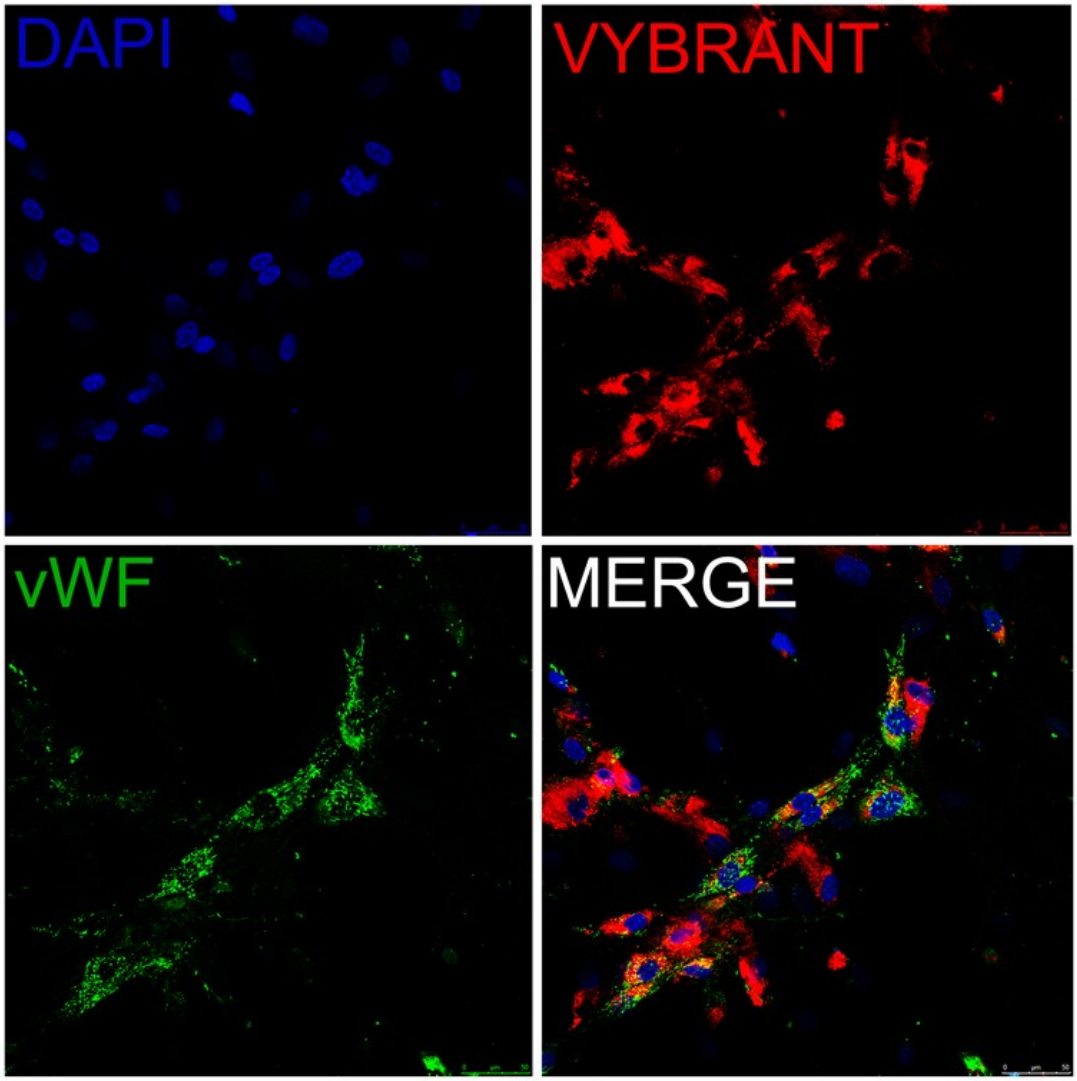

Fig:4.4.1.2: hMSC endothelial differentiation in co-culture system: Expression of endothelial-specific marker von Willenbrand Factor (vWF, green) in human Mesenchymal stem Cells (hMSC, red), co-cultured for 7 days with human umbilical vein endothelial cells (HUVEC) in standard culture conditions. The presence of red cells showing vWF green staining demonstrates stem cell succesfull differentiation towards the endothelial phenotype

4.4.2 3D cell co-culture and stem cell differentiation towards endothelial phenotype

Scaffold thin sections were sterilized by ethanol washings and soaked in Endothelial Basal Medium 2 (EBM-2) for 24 hours. At this time-point, human mesenchymal stem cells (hMSC) were stained with red Vybrant vital dye and mixed with human umbilical vein endothelial cells (HUVEC) in 1:5 ratio.
Therefore, they were co-seeded onto the scaffolds and on thin sections. Scanning electron microscope (SEM) micrographs taken after 7 days showed the ability of human cells to adhere functionally and survive onto the scaffolds and thin sections as demonstrated by the massive secretion of extracellular matrix (ECM) all over the structure (Fig. 4.4.2.1).

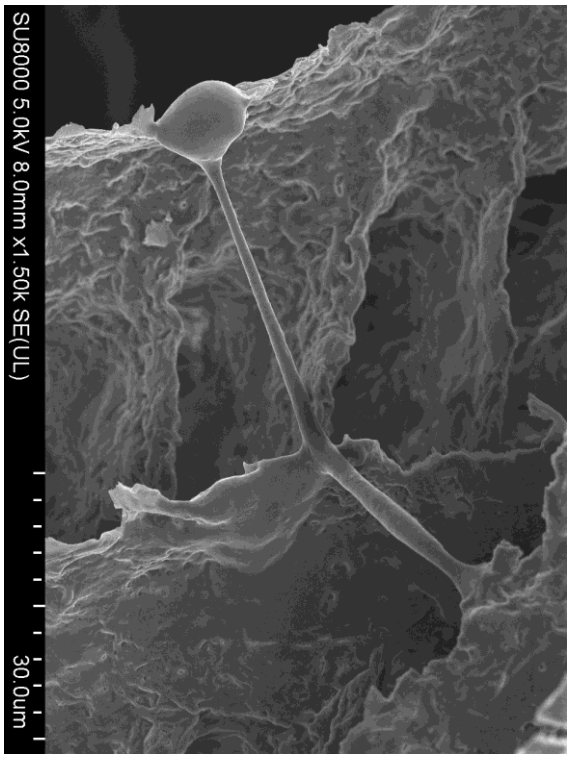

(a)

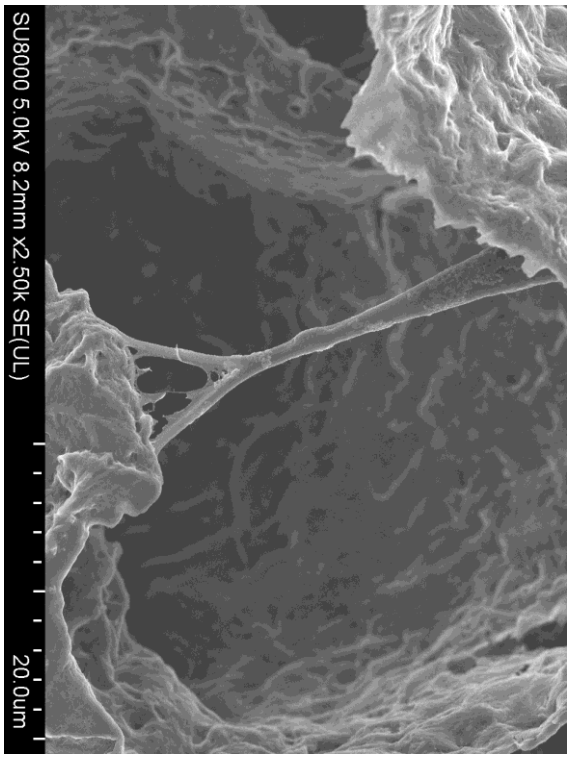

(b)

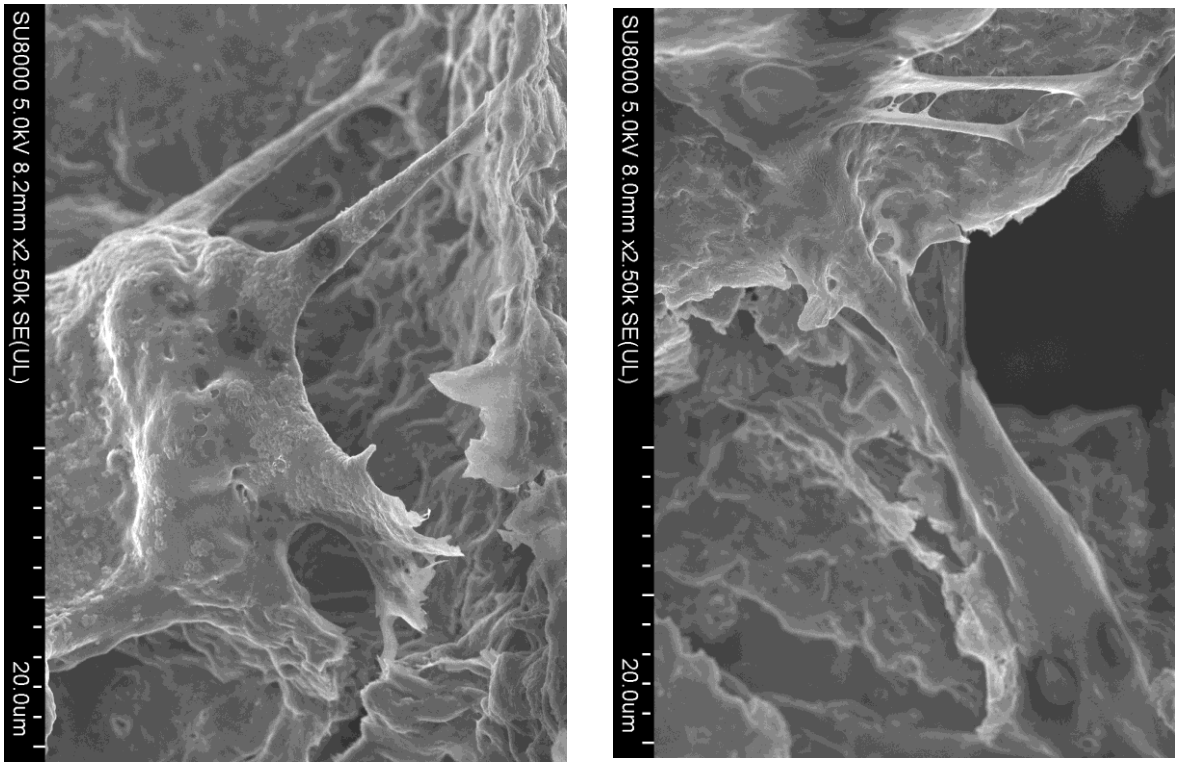

(c) (d)

Fig:4.4.2.1: Human mesenchymal stem cells (hMSC) and human umbilical vein endothelial cells co-cultured for 7 days onto TIPS scaffold thin sections show the ability to adhere functionally, bridge over the pores and grow inside the channels a), b). SEM micrographs display the massive production of extracellular matrix (ECM) c), d).

Nuclei staining demonstrated cell massive colonization of 3D porous structure and their aligninment inside the pores. Immunofluorescence analysis for Vybrant vital dye (Fig.4.4.2.2 red) and von Willenbrand Factor (vWF, green) further demonstrated the successful setup of co-cultures within 3D scaffolds and thin sections (Fig.4.4.2.2). Finally, when deeper examination of 3D co-culture specimens was conducted, human mesenchymal stem cell differentiation towards endothelial phenotype was confirmed on 3D scaffolds and thin sections, as shown by vWF staining (green) in vibrant-labelled cells (red, Fig.4.4.2.3).

As reported in previous investigations on 3D scaffolds, SEM and immunofluorescence analyses are known to underestimate cell presence in the samples. This is mainly due to specimen manipulation and processing. In particular, such problems derive from the severe dehydration required for sample preparation in the case of SEM analysis, while the peeling-off of exposed surface cellular layers is

known to occur when cells are exposed to the repeated washings required for immunofluorescence analysis. Moreover, the gold layer deposition required for SEM analysis causes cell flattening and consequent loss of important cellular features, which also makes it hard to distinguish cells from the underlying polymer substrate.

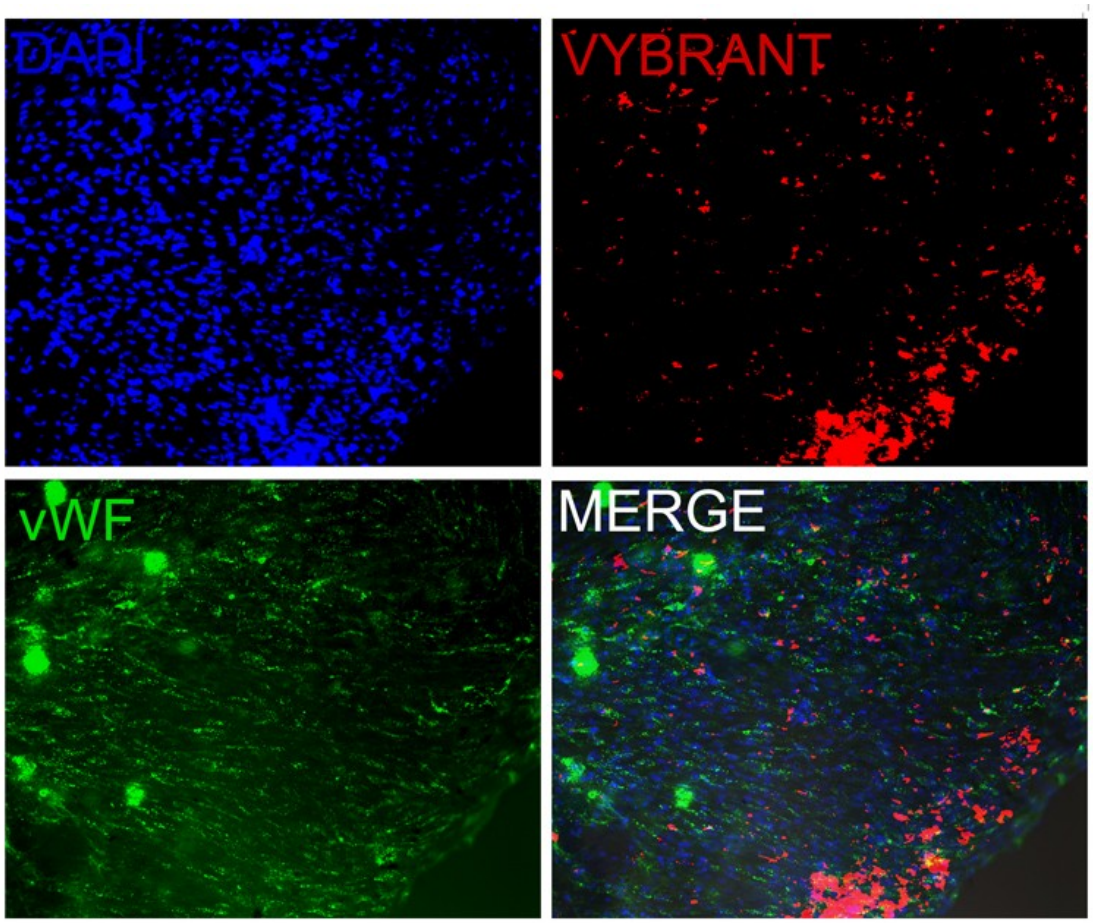

Fig:4.4.2.2: Massive cell colonization of scaffold thin sections: Low magnification image of scaffold thin section seeded for 7 days with human mesenchymal stem cells (hMSC, red) and human umbilical vein endothelial cells (HUVEC). Von Willenbrand Factor (vWF) protein staining (green) in red cells accounts for successful stem cell differentiation towards endothelial phenotype

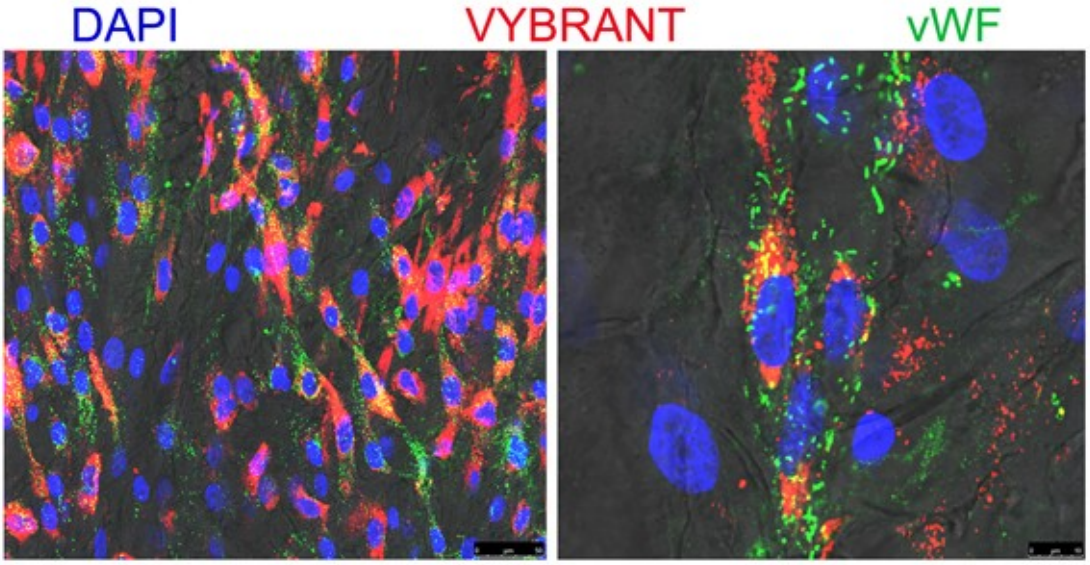

Fig:4.4.2.3: hMSC differentiate towards endothelial phenotype when co-cultured for 7 days onto TIPS thin sections with HUVEC cells: High magnification images showing scaffold thin section seeded for 7 days with human mesenchymal stem cells (hMSC, red) and human umbilical vein endothelial cells (HUVEC). Von Willenbrand Factor (vWF) protein staining (green) in red cells accounts for successful stem cell differentiation towards endothelial phenotype

Chapter 5

Conclusions

5.1 Conclusions

With this work we demonstrated that it is possible to tailor the pore architecture of 3D polymer scaffold made by dTIPS.

Morphologic and geometric characteristics of such scaffolds are in the optimal range for promoting the adhesion and growth of a wide field of cells type.

These scaffolds show a mean overall porosity value of 95% and a grade of pore interconnection over 90%.

So far, experimental data show that small pore dimensions are obtained with the maximum cooling time, the lowest cooling temperature and the highest polymer concentration, in the range of investigated values.

Maximum pore diameters instead, are obtained applying a short cooling time, keeping the cooling temperature right under the freezing point of the dioxane and lowering the polymer concentration.

Young's modulus evaluated from compression test of scaffold samples vary in the range of 1 to 8 MPa in according to similar works in bibliography.

An increasing of the elastic modulus has been observed with the increase of the cooling time.

Biological validation has been tested by mean of cell seeding on scaffold's thin sections and directly on tridimensional sections up to 5 mm.

After 7 DIV (days in vitro) of culture, a massive colonization has been detected on the thin sections and the tridimensional sections both.

5.2 Prospectives

The principal aim of these scaffolds is the realization of a vascular framework inside a regenerated tissue.

To obtain this goal, future research will try to obtain a vascularized tissue, stacking tissues obtained with scaffold thin sections, one on top of each other.

More tests will be performed, trying to trigger the nucleation of dendrites, utilizing the reactor and the elaborated silicon wafer.

References

[1] R. Langer, J. P. Vacanti *Tissue engineering*, Science (1993), 260, 920-6

[2] S. Mitragotri, J. Lahann *Physical approaches to biomaterial design*, Nature Mater. (2009), 8, 15-23

[3] L. E. Freed, G. Vunjak-Novakovic, R. J. Biron, D. B. Eagles, D. C. Lesnoy, S. K. Barlow, R. Langer *Biodegradable polymer scaffolds for tissue engineering*, Bio-Technol. (1994), 12, 689-93

[4] K. Nolan, Y. Millet, C. Ricordi, C. L. Stabler *Tissue engineering and biomaterials in regenerative medicine*, Cell Transplant. (2008), 17, 41-243

[5] A. N. Patel, W. Sherman *Cardiac stem cell therapy from bench to bedside*, Cell Transplant. (2007), 16, 875-8

[6] A. Irintchev, M. Langer, M. Zweyer, R. Theisen, A. Wernig *Functional improvement of damaged adult mouse muscle by implantation of primary myoblasts*. J. Physiol. (1997), 500, 775–85

[7] C. Yeo, A. Mathur *Autologous bone marrow-derived stem cells for ischemic heart failure: REGENERATE-IHD trial*, Regen. Med. (2009), 4, 119-27

[8] M. Siepe, M. N. Giraud, M. Pavlovic, C. Receputoa, F. Beyersdorf, P. Menasché, T. Carrel, H. T. Tevaearai *Myoblast-seeded biodegradable scaffolds to prevent post–myocardial infarction evolution toward heart failure*, J. Thorac. Cardiovasc, Surg. (2006), 132, 124-31

[9] T. Hadlock, J. Elisseeff, R. Langer, J. Vacanti, M. Cheney *A tissue engineered conduit for peripheral nerve regeneration*, Biomaterials (1999), 20, 1109-15

[10] E. Tognana, A. Borrione, C. De Luca, A. Pavesio *Hyalograft® C: hyaluronan-based scaffolds in tissue-engineered cartilage*, Cells Tissues Organs (2007), 186, 97-103

[11] C. B. Weinberg, E. Bell *A blood vessel model constructed from collagen and cultured vascular cells*, *Science (198*6), 231, 397-400

[12] A. Fort, N. Fort, C. Ricordi, C. L. Stabler *Biohybrid devices and encapsulation technologies for engineering a bioartificial pancreas*, Cell Transplant. (2008), 17, 997-1003

[13] M. J. Yaszemski, D. L. Wise *Tissue engineering and novel delivery systems*, Edition 2, *CRC Press* (2004), ISBN 0824747860, 9780824747862

[14] D. F. Mosher. *A role for fibronectin in self-repair after ischemic injury*, Nat. Med. (2001), 7, 324-30

[15] L. G. Griffith, M. A. Swartz. *Capturing complex 3D tissue physiology in vitro*, Nat. Rev. Mol. Cell. Biol. (2006), 7, 211-24

[16] T. Ziegler, R. M. Nerem. *Tissue engineering a blood vessel: regulation of vascular biology by mechanical stresses*, J. Cell. Biochem. (1994), 56, 204-9

[17] G. C. Engelmayr, Jr., M. Cheng, C. J. Bettinger, J. T. Borenstein, R. Langer, L. E. *Freed. Accordion-like honeycombs for tissue engineering of cardiac anisotropy*, Nature Mater. (2008) 7, 1003-10

[18] T. Okano, N. Yamada, M. Okuhara, H. Sakai, Y. Sakurai. *Mechanism of cell detachment from temperature-modulated, hydrophilic–hydrophobic polymer surfaces*, Biomaterials (1995), 16, 297-303

[19] K. Nishida, M. Yamato, Y. Hayashida, K. Watanabe, K. Yamamoto, E. Adachi, S. Nagai, A. Kikuchi, N. Maeda, H. Watanabe, T. Okano, Y. Tano. *Corneal reconstruction with tissue-engineered cell sheets composed of autologous oral mucosal epithelium*, N. Eng. J. Med. (2004), 351, 1187-96

[20] T. Shimizu, M. Yamato, A. Kikuchi, T. Okano. *Cell sheet engineering for myocardial tissue reconstruction*. Biomaterials (2003), 24, 2309-16

[21] T. Shimizu, M. Yamato, Y. Isoi, T. Akutsu, T. Setomaru, K. Abe, A. Kikuchi, M. Umezu, T. Okano. *Fabrication of pulsatile cardiac tissue grafts using a novel 3-dimensional cell sheet manipulation technique and temperature-responsive cell culture surfaces*, Circ. Res. (2002), 90, e40-e48

[22] G. Orive, R. M. Hernandez, A. Rodriguez Gascon, R. Calafiore, T. M. Chang, P. de Vos, G. Hortelano, D. Hunkeler, I. Lacik, J. L. Pedraz. *History. Challenges and perspectives of cell microencapsulation*, Trends Biotechnol. (2004), 22, 87-92

[23] H. Uludag, P. de Vos, P. A. Tresco. *Technology of mammalian cell encapsulation*, Adv. Drug. Deliv. Rev. (2000), 42, 29-64

[24] R. P. Lanza, J. L. Hayes, W. L. Chick. *Encapsulated cell technology*, Nat. Biotechnol. (1996), 14, 1107-11

[25] B. P. Chan, T. Y. Hui, C. W. Yeung, J. Li, I. Mo, G. C. F. Chan. *Self-assembled collagen–human mesenchymal stem cell microspheres for regenerative medicine*, Biomaterials (2007), 28, 4652–66

[26] R. L. Knight, H. E. Wilcox, S. A. Korossis, J. Fisher, E. Ingham. *The use of acellular matrices for the tissue engineering of cardiac valves*, Proc. Inst. Mech. Eng. (2008), 222, 129-143

[27] G. H. Borschel, Y. C. Huang, S. Calve, E. M. Arruda, J. B. Lynch, D. E. Dow, W. M. Kuzon, R. G. Dennis, D. L. Brown. *Tissue engineering of recellularized small-diameter vascular grafts*, Tissue Eng. (2005), 11, 778-86

[28] S. Hall. *Axonal regeneration through acellular muscle grafts*, J. Anat. (1997), 190, 57-71

[29] J. H. Ingram, S. Korossis, G. Howling, J. Fisher, E. Ingham. *The use of ultrasonication to aid recellularization of acellular natural tissue scaffolds for use in anterior cruciate ligament reconstruction*, Tissue Eng. (2007), 13, 1561-72

[30] S. F. Badylak. *Xenogeneic extracellular matrix as a scaffold for tissue reconstruction*, Transpl. Immunol. 12, (2004), 367-77

[31] M. H. Zheng, J. Chen, Y. Kirilak, C. Willers, J. Xu, D. Wood. *Porcine small intestine submucosa (SIS) is not an acellular collagenous matrix and contains porcine DNA: possible implications in human implantation*, J. Biomed. Mater. Res. B Appl. Biomater. (2005), 73, 61-7

[32] H. Chajra, C. F. Rousseau, D. Cortial, M. C. Ronzière, D. Herbage, F. Mallein-Gerin, A. M. Freyria. *Collagen-based biomaterials and cartilage engineering. Application to osteochondral defects*, Biomed. Mater. *Eng.* (2008), 18, 33-45

[33] A. Shah, J. Brugnano, S. Sun, A Vase, E. Orwin. *The development of a tissue-engineered cornea: biomaterials and culture methods*, Pediatr. Res. (2008), 63, 535-44

[34] S. Masuda, T. Shimizu, M. Yamato, T. Okano. *Cell sheet engineering for heart tissue repair*, Adv. Drug Deliv. *Rev.* (2008), 60, 277-85

[35] J. Elisseeff, C. Puleo, F. Yang, B. Sharma. *Advances in skeletal tissue engineering with hydrogels*, Orthod. Craniofac. Res. (2005), 8, 150-61

[36] L. Draghi, S. Resta, M. G. Pirozzolo, M. C. Tanzi. *Microspheres leaching for scaffold porosity control*, J. Mat. Sci.: Mat. Med. (2005), 16, 1093-97

[37] A. S. Rowlands, S. A. Lim, D. Martin, J. J. Cooper-White. *Polyurethane /poly(lactic-co-glycolic) acid composite scaffolds fabricated by thermally induced phase separation*, Biomaterials (2007), 28, 2109-21

[38] Y. M. Lima, H. J. Gwona, J. Shina, J. Pyo, Y. C. Nho. *Preparation of porous poly(-caprolactone) scaffolds by gas foaming process and in vitro/in vivo degradation behavior using γ-ray irradiation*, J. Ind. Eng. Chem. (2008), 14, 436-41

[39] S. Yang, K.-F. Leong, Z. Du, C.-K. Chua. *The design of scaffolds for use in tissue engineering. Part II. Rapid prototyping techniques*, Tissue Eng. (2002), 8, 1-11

[40] G. Vozzi, C. Flaim, A. Ahluwalia, S. Bhatia. *Fabrication of PLGA scaffold using soft lithography and microsyringe deposition*, Biomaterials (2003), 24, 2533-40

[41] Y. Mia, Y. Chana, D. Traua, P. Huang, E. Chenc. *Micromolding of PDMS scaffolds and microwells for tissue culture and cell patterning: A new method of microfabrication by the self-assembled micropatterns of diblock copolymer micelles*, Polymer (2006), 47, 5124-30

[42] J. T. Borenstein, E. J. Weinberg, B. K. Orrick, C. Sundback, M. R. Kaazempur-Mofrad, J. P. Vacanti. *Microfabrication of three-dimensional engineered scaffolds*, Tissue Eng. (2007), 13, 1837-44

[43] E. Figallo, M. Flaibani, B. Zavan, G. Abatangelo, N. Elvassore. *Micropatterned biopolymer 3d scaffold for static and dynamic culture of human fibroblasts*, Biotech. Prog. (2008), 23, **210-16**

[44] S. Arumuganathar, S. N. Jayasinghe. *Pressure-assisted spinning: a versatile and economical, direct fibre to scaffold spinning methodology*, Macromol. Rapid Commun. (2007), 28, 1491-96

[45] D. Li, Y. Xia. *Electrospinnig of nanofibers: reinventing the wheel?*, Adv. Mater. (2004), 16, 1159-70

[46] V. Lassalle, M. L. Ferreira. *PLA nano- and microparticles for drug delivery: an overview of the methods of preparation*, Macromol. Biosci. (2007), 7, 767-83

[47] F. Peng, J. R. Olson, M. T. Shaw, M. Wei. *Influence of pretreatment on the surface characteristics of PLLA fibers and subsequent hydroxyapatite coating*, J. Biomed. Mater. Res. B: Appl. Biomater. (2008), 88, 220-29

[48] G. Ciardelli, V. Chiono, C. Cristallini, N. Barbani, A. Ahluwalia, G. Vozzi, A. Previti, G. Tantussi, P. Giusti. *Innovative tissue engineering structures through advanced manufacturing technologies*, J. Mat. Sci.: Mat. Med. (2004), 15, 305-10

[49] A. U. Daniels, M. K. O. Chang, K. P. Andriano, J. Heller. *Mechanical properties of biodegradable polymers and composites proposed for internal fixation of bone*, J. Appl. Biomat. (1990), 1, 57-78

[50] J. Kohn, R. Langer. Bioresorbable and Bioerodible Materials. In: B. D. Ratner, A. S. Hoffman, F. J. Schoen, J. E. Lemons (eds). *Biomaterials science: an introduction to materials in medicine*, New York, Academic Press (1996), 64-72

[51] J. C. Middleton, A. J. Tipton. *Synthetic biodegradable polymers as medical devices*, Med. Plast. Biomat. (1998), 5, 30-9

[52] W. S. Pietrzak, D. R. Sarver, M. L. Verstynen. *Bioabsorbable fixation devices: status for the craniomaxillofacial surgeon*, J. Craniofacial. Surg. (1997), 8, 87-91

[53] R. B. Elliott, L. Escobar, P. L. J. Tan, M. Muzina, S. Zwain, C. Buchanan. *Live encapsulated porcine islets from a type 1 diabetic patient 9.5 yr after xenotransplantation*, Xenotransplantation (2007), 14, 157-61

[54] L. Turnpenny, C. M. Spalluto, R. M. Perrett, M. O'Shea, K. P. Hanley, I. T. Cameron, D. I. Wilson, N. A. Hanley. *Evaluating human embryonic germ cells: concord and conflict as pluripotent stem cells*, Stem Cells (2006), 24, 212-20

[55] K. Hans R. Schöler. The potential of stem cells: an inventory. In: N. Knoepffler, D. Schipanski, S. L. Sorgner. *Humanbiotechnology as social challenge*, Ashgate Publishing, Ltd. (2007), 28. ISBN 0754657558

[56] A. Vats, R. C. Bielby, N. S. Tolley, R. Nerem, J. M. Polak. *Stem cells*, Lancet (2005), 366, 592-602

[57] Y. J. Geng. *Molecular mechanism for cardiovascular stem cell apoptosis and growth in the hearts with atherosclerotic coronary disease and ischemic heart disease*, Ann. N. Y. Acad. Sci. (2003), 687-97

[58] W. J. Larsen. *Human Embryology* - 3rd Edition, Churchill Livingstone, Elsevier Science Health Science div, Saint Louis, MO (2001), paperback

[59] R. Y. Tsai. *Plasticity, niches, and the use of stem cells,* Dev. Cell. (2002), 2, 707-12

[60] I. Kehat, D. Kenyagin-Karsenti, M. Snir, H. Segev, M. Amit, A. Gepstein, E. Livne, O. Binah, J. Itskovitz-Eldor, L. Gepstein. *Human embryonic stem cells can differentiate into myocytes with structural and functional properties of cardiomyocytes*, *J.* Clin. Invest. (2001), 108, 407-14

[61] J. A. Thomson, J. Itskovitz-Eldor, S. S. Shapiro, M. A. Waknitz, J. J. Swiergiel, V. S. Marshall, J. M. Jones. *Embryonic Stem cell lines derived from human blastocysts*, Science (1998), 282, 1145-47

[62] M. F. Pittenger, B. J. Martin. *Mesenchimal stem cells and their potential as cardiac therapeutics*, Circ Res. (2004), 95, 9-20

[63] D. Seliktar, R. A. Black, R. P. Vito, R. M. Nerem. *Dynamic mechanical conditioning of collagen gel blood vessel constructs induces remodeling in vitro*, Ann. Biomed. Eng. (2000), 28, 351-62

[64] J. Leor, Y. Amsalem, S. Cohen. Cells, *scaffolds, and molecules for myocardial tissue engineering*, Pharmacol. Therapeut. (2005), 105, 151-63

[65] W. H. Zimmermann, I. Melnychenko, T. Eschenhagen. *Engineered heart tissue for regeneration of diseased hearts*, Biomaterials (2004), 25, 1639–47

[66] P. Akhyari, P.W. Fedak, R.D. Weisel, T.Y. Lee, S. Verma, D.A. Mickle, R. K. Li. *Mechanical stretch regimen enhances the formation of bioengineered autologous cardiac muscle grafts*, Circulation (2002), 106, 137-42

[67] C. K. Colton, *Implantable biohybrid artificial organs*, Cell. Transplant. (1995), 4, 415-36

[68] U. S. Food and Drug Administration. *Human tissue intended for transplantation* (1997), 21, CFR 1270

[69] U. S. Food and Drug Administration. *Proposed approach to regulation of cellular and tissue-based products: availability and public meeting*, Fed. Regist. (1997), 62, 9721-2

[70] U. S. Food and Drug Administration. *Guidance for industry: guidance for human somatic cell therapy and gene therapy*. Fed. Regist. (1998), 63, 36413

[71] U. S. Food and Drug Administration. *Guidance for industry: precautionary methods to reduce the possible risk of transmission of zoonoses by blood and blood products from xenotransplantation product recipients and their contacts*. Fed. Regist. (1999), 64, 73562-3

[72] U. S. Food and Drug Administration. *Medical device classification procedures: determination of safety and effectiveness* (2000), 21, CFR 860.7

[73] American Society for Testing and Materials. *Standard specification for virgin poly(L-lactic acid) resine for surgical implants* (1999). In: American Society for Testing and Materials. 1999 annual book of ASTM standards, *ASTM*, Conshocken, PA (1999), 1440-42

[74] J. R. Morgan, M. L. Yarmush. *Tissue engineering methods and protocols* (1999), Totowa, NJ, Humana Press

[75] H. Petite, V. Viateau, W. Bensaïd, A. Meunier, C. Pollak, M. Bourguignon, K. Oudina, L. Sedel, G. Guillemin. *Tissue-engineered bone regeneration*, Nat. Biotech. (2000), 18, 959-63

[76] Y. Cao, J. P. Vacanti, K. T. Paige, J. Upton, C. A. Vacanti. *Transplantation of chondrocytes utilizing a polymer-cell construct to produce tissue-engineered cartilage in the shape of a human ear*, Plast. Reconstruct. Surg. (1997), 100, 297-302

[77] K. Nishida, M. Yamato, Y. Hayashida, K. Watanabe, N. Maeda, H. Watanabe, K. Yamamoto, S. Nagai, A. Akihiko, Y. Tano, T. Okano. *Functional bioengineered corneal epithelial sheet grafts from corneal stem cells expanded ex vivo on a temperature-responsive cell culture surface*, Transplantation, (2004), 77, 379-85

[78] M. N. Banta, R. S. Kirsner. *Modulating diseased skin with tissue engineering: actinic purpura treated with Apligraf®*, Dermatol. Surg. (2002), 28, 1103-6

[79] R. W. Sands, D. J. Mooney. *Polymers to direct cell fate by controlling the microenvironment*, Curr. Opin. Biotechnol. (2007), 18, 448-53

[80] L. A. Solchaga, E. Tognana, K. Penick, H. Baskaran, V. M. Goldberg, A. I. Caplan, J. F. Welter. *A rapid seeding technique for the assembly of large cell/scaffold composite constructs*, Tissue Eng. (2006), 12, 1851-63

[81] H. C. H. Ko, B. K. Milthorpe, C. D. McFarland. *Engineering thick tissues - the vascularisation problem*, Eur. Cell. Mater. (2007), 14, 1-19

[82] Z. Ge, L. J. Suggs. *Matrices and scaffolds for drug delivery in vascular tissue engineering*, Adv. Drug Deliv. Rev. (2007), 59, 360-73

[83] E. Traversa, B. Mecheri, C. Mandoli, S. Soliman, A. Rinaldi, S. Licoccia, G. Forte, F. Pagliari, S. Pagliari, F. Carotenuto, M. Minieri, P. Di Nardo. *Tuning hierarchical architecture of 3D polymeric scaffolds for cardiac tissue engineering*, J. Experim. Nanosci. (2008), 3, 97-110

[84] Y. S. Nam, J. J. Yoon, T. G. Park. *A novel fabrication method for macroporous scaffolds using gas foaming salt as porogen additive*, J. Biomed. Mater. Res. (2000), *53*, 1-7

[85] Y. Gong, Q. Zhou, C. Gao, J. Shen. *In vitro and in vivo degradability and cytocompatibility of poly(l-lactic acid) scaffold fabricated by a gelatin particle leaching method*, Acta Biomater. (2007), 3, 531-40

[86] J. M. Corey, C. C. Gertz, B. S. Wang, L. K. Birrell, S. L. Johnson, D. C. Martin, E. L. Feldman. *The design of electrospun PLLA nanofiber scaffolds compatible with serum-free growth of primary motor and sensory neurons*, Acta Biomater. (2008), 4, 863-75

[87] A. Ndreu, L. Nikkola, H. Ylikauppila, N. Ashammakhi, V. Hasirci. *Electrospun biodegradable nanofibrous mats for tissue engineering*, Nanomed. (2008), 3, 45-60

[88] T. Tanaka, D. R. Lloyd. *Formation of poly(-lactic acid) microfiltration membranes via thermally induced phase separation*, J. Membrane Sci. (2004), 238, 65-73

[89] F. Yang, X. Qu, W. Cui, J. Bei, F. Yu, S. Lu, S. Wang. *Manufacturing and morphology structure of polylactide-type microtubules orientation-structured*

scaffolds, Biomaterials (2006), 27, 4923-33

[90] A.S. Rowlands, S.A. Lima, D. Martin, J.J. Cooper-White. *Polyurethane/poly(lactic-co-glycolic) acid composite scaffolds fabricated by thermally induced phase separation*, Biomaterials (2007), 28, 2109-21

[91] J. Blaker, J. Knowles, R. Day. *Novel fabrication techniques to produce microspheres by thermally induced phase separation for tissue engineering and drug delivery*, Acta Biomater. (2008), 4, 264-72

[92] Ch. Schugens, V. Maquet, C. Grandfils, R. Jerome, Ph. Teyssie. *Biodegradable and macroporous polylactide implants for cell transplantation: I. Preparation of macroporous polylactide supports by solidliquid phase separation*, Polymer (1996), 37, 1027-38

[93] X. Hu, H. Shen, F. Yang, J. Bei, S. Wang. *Preparation and cell affinity of microtubular orientation-structured PLGA(70/30) blood vessel scaffold*, Biomaterials (2008), 29, 3128-36

[94] P. X. Ma, R. Zhang. *Microtubular architecture of biodegradable polymer scaffolds*, J. Biomed. Mater. Res. (2001), 56, 469-77

[95] G. Wei, P. X. Ma. *Structure and properties of nano-hydroxyapatite/ polymer composite scaffolds for bone tissue engineering*, Biomaterials (2004), 25, 4749-57

[96] Goldstein, J. (2003) *Scanning electron microscopy and x-ray microanalysis*. Kluwer Adacemic/Plenum Pulbishers, 689 p.

[97] Reimer, L. (1998) *Scanning electron microscopy : physics of image formation and microanalysis*. Springer, 527 p.

[98] Egerton, R. F. (2005) *Physical principles of electron microscopy : an introduction to TEM, SEM, and AEM*. Springer, 202.

[99] Clarke, A. R. (2002) *Microscopy techniques for materials science*. CRC Press (electronic resource)

[100] L. G. Cima, J. P. Vacanti, C. Vacanti, D. Ingber, D. Mooney, R. Langer. *Tissue engineering by cell transplantation using degradable polymer substrates*, J. Biomech. Eng. (1991), 113, 143-51

[101] J. M. Karp, R. Langer. *Development and therapeutic applications of advanced biomaterials*, Curr. Opin. Biotechnol. (2007), 18, 454-59

[102] D. Goupil. Sutures. In: B. D. Ratner, A. S. Hoffman, F. J. Schoen, J. E. Lemons, (eds). *Biomaterials science: an introduction to materials in medicine*, New York, Academic Press (1996), 356-60

[103] L. E. Euliss, J. A. DuPont, S. Gratton, J. DeSimone. *Imparting size, shape, and composition control of materials for nanomedicine*, Chem. Soc. Rev. (2006), 35, 1095-104

[104] K. R. Milner, C. A. Siedlecki. *Submicron poly(l-lactic acid) pillars affect fibroblast adhesion and proliferation,* J. Biomed. Mater. Res. A (2007), 82, 80-91

[105] D. K. Gilding. *Degradation of polymers: mechnisms and implications for biomedical applications*. In: D. F. Williams, (eds). Biocompatibility of clinical implant materials, Boca Raton, FL, *CRC* Press (1981), 2, 43-65

[106] K. A. Beningo, Y. L. Wang. *Flexible substrata for the detection of cellular traction forces*, Trends Cell Biol. (2002), 12, 79-84

[107] A. A. Ignatius, L. E. Claes. *In vitro biocompatibility of bioresorbable polymers: Poly(L,DL-lactide) and poly(L-lactide-co-glycolide)*, Biomaterials (1996), 17, 831-39

[108] K. Ghosh, D. E. Ingber. *Micromechanical control of cell and tissue development: implications for tissue engineering*, Adv. Drug Deliv. Rev. (2007), 59, 104

1306-18

[109] B.S. Kim, A. Putnam, T. J. Kulik, D.J. Mooney. *Optimizing seeding and culture methods to engineer smooth muscle tissue on biodegradable polymer matrices*, Biotechnol. Bioeng. (1998), 57, 46-54

[110] S. H. Yang, C. K. Hsu, K. C. Wang, S. M. Hou, F. H. Lin. *Tricalcium phosphate and glutaraldehyde crosslinked gelatin incorporating bone morphogenetic protein-viable scaffold for bone tissue engineering*, J. Biomed. Mater. Res. B Appl. Biomater. (2005), 74, 468-75

[111] J. C. Middleton, A. J. Tipton. *Synthetic biodegradable polymers as orthopedic devices*, Biomaterials (2000), 21, 2335-46

[112] T. H. Barrows. *Degradable Implant materials: a review of synthetic absorbable polymers and their applications*, Clin. Mat. (1986), 1, 233-57

[113] A. Matsumoto, T. Kitazawa, J. Murata, Y. Horikiri, H. Yamahara. *A novel preparation method for PLGA microspheres using non-halogenated solvents*, J. Control. Release (2008), 129, 223-7

[114] A. Jaklenec, E. Wan, M. E. Murray, E. Mathiowitz. *Novel scaffolds fabricated from protein-loaded microspheres for tissue engineering*, Biomaterials (2008), 29, 185-92

[115] C. M. Agrawal, G. G. Niederauer, D. M. Micallef, K. A. Athanasiou. *The use of PLA-PGA polymers in orthopedics*. In: D. L. Wise, D. J. Trantolo, D. E. Altobelli, M. J. Yaszemski, J. D. Greser, E. R. Schwartz, (eds). Encyclopedic handbook of biomaterials and bioengineering Part A. Materials, vol. 2, New York, *Marcel Dekker* (1995), 1055-89

[116] J. E. Bergsma, W. C. de Bruijn, F. R. Rozema, R. R. M. Bos, G. Boering. *Late degradation tissue response to poly(L-lactide) bone plates and screws*, Biomaterials (1995), 16, 25-31

[117] D. K. Gilding, A. M. Reed. *Biodegradable polymers for use in surgery - polyglycolic/poly(lactic acid) homo- and copolymers*, Polymer (1979), 20, 1459-84

[118] F. A. Barber. *Resorbable fixation devices: a product guide*, Orthopedic Special Edition (1998), 4, 1111-17

[119] W. P. Werschler. *Advanced injection techniques of poly-L-lactic acid: a case-based presentation*, Dermatol. Ther. (2007), Suppl 1, 16-9

[120] Orthopedic Biomaterials, The World Market, 2nd Edition, *Kalorama Information* (2007)

[121] O. G. Lewis, W. Fabisial. Sutures. In: Kirk-Othmer encyclopedia of chemical technology, 4th ed., New York, *Wiley* (1997)

[122] R.A. Miller, J. M. Brady, D. E. Cutright. *Degradation rates of oral resorbable implants (polylactes and polyglycolates): Rate modification with changes in PLA/PGA copolymer ratios*, J. Biomed. Mater. Res. (1977), 11, 711-19

[123] C. S. Cojocaru, J.M. Padovani, T. Wade, C. Mandoli, Jaskierowicz, J. E. Wegrowe, A. Fontcuberta i Morral, D. Pribat. *Conformal anodic oxidation of aluminium thin films*, Nano Letters (2005), 5, 675-80

[124] E. Mele, F. Di Benedetto, L. Persano, D. Pisignano, R. Cingolani. *Combined capillary force and step and flash lithography*, Nanotechnology (2005), 16, 391-95

Acknowledgements

This thesis is far from being just the result of a scientific investigation. Nor it can be reduced to a single-man effort. Instead, it encloses the contribution of innumerable persons, who directly or not, purposely or unconsciously, have represented a stimulus in every possible way.

First of all, I wish to express my gratitude to my advisor, prof. Enrico Traversa, together with the National Institute for Material Science and the International Center for Materials Nanoarchitectonics, for giving me the opportunity to join his research group in Japan and to carry out my research in a friendly environment.

Everlasting gratitude and affection goes to Dr. Corrado Mandoli who, with endless patience, helped and taught me during the six months internship period.

To Dr. Takashi Minowa for welcoming me to his lab and to the world of biology.

To Dr. Giancarlo Forte who saved me and Corrado from exterminating every single living form in our samples, and contributed significantly in this work.

To Yasuji “the runnig cube” Masuda, for being the best and fastest turner/milling/”I can do everything”-man in NIMS and for the patience with which he didn’t behead me and Corrado. His help was life-saving.

To Dr. Hidehiko Tanaka and all the administrative MANA office for their kind help.

To Rumiko Enjoji, for her help with bureaucracy, her friendship and for listening me trying to speak Japanese.

A special thanks to the Italian researchers sadly known in these horrible days as “the 10 of Tsukuba” for all the experiences we made together in and out of work ambient. In particular to Enrico Cenni, Dr. Marco Fronzi and Claudia Carmignano.

To the many gaijin, researchers or not, that I met in Japan and with which I shared good moments.

My journey to this point starts way before these six months in Japan. Therefore is impossible for me not to mention all the people I met and lived together in these five years in Padua.

To all the people from university residences, in particular from Ederle. A special mention goes to one of my best friends Agostino and to one of the most important persons I've met, Sara.

To my classmates Agnese, Davide, Laura and Michela for being an irreplaceable sustain during this adventure.

I also want to thank all my friends from Verona for all the nights and days spent together in these years.

Finally I wish to thank my roots, my strength, my model. In one word, my family. Without you I would never be able to be here today. Your support, your understanding are invaluable to me

This is the end of a cycle and, with any luck, the beginning of a new one.

April 15th, 2011 Fabio Turella